

Orientational order and glassy states in networks of semiflexible polymers

Dissertation

zur Erlangung des Doktorgrades
der Mathematisch-Naturwissenschaftlichen Fakultäten
der Georg-August-Universität zu Göttingen

vorgelegt von

Martin Kiemes

aus Lebach

Göttingen 2010

D7

Referent: Prof. Dr. Annette Zippelius

Korreferent: Prof. Dr. Reiner Kree

Tag der mündlichen Prüfung: 23.11.2010

Abstract

Motivated by the structure of networks of cross-linked cytoskeletal biopolymers, the orientationally ordered phases in networks of randomly cross-linked semiflexible polymers are studied in two dimensions. We consider permanent cross-links prescribing a finite angle, and treat them as quenched disorder in a semi-microscopic replica field theory. Starting from a fluid of single polymers and small polymer clusters (sol), and increasing the cross-link density, a continuous gelation transition occurs. In the resulting gel, the semiflexible chains display either long-range orientational order or are frozen in random directions. The phase behavior is categorized depending on the value of the crossing angle, the degree of thermal fluctuations about the crossing angle, the cross-link concentration, and the stiffness of the polymers. A crossing angle $\theta \sim 2\pi/M$ leads to long-range M -fold orientational order, e.g. a hexatic phase for $\theta = 60^\circ$ or a tetratic phase for $\theta = 90^\circ$. The critical cross-link density depends on the bending stiffness of the polymers and the cross-link geometry; the higher the stiffness and the lower M , the lower the critical number of cross-links. In-between the sol and the long-range ordered state, we always observe a gel which is a statistically isotropic amorphous solid (SIAS). The SIAS is characterized by random positional and random orientational localization of the participating polymers.

Contents

1	Introduction	1
2	The Model	6
2.1	The single polymer	6
2.2	Cross-links	8
2.3	The network and its configurations	10
2.4	Excluded volume interaction	11
3	The formalism	12
3.1	Performing the disorder average	13
3.2	Decomposing replica space	15
3.3	Towards a statistical field theory	16
3.4	Mean-field approximation	18
3.5	Trivial solution and variational approach	19
4	Analysis of the model	21
4.1	Physical expectations	21
4.2	Discussion of the sol phase	24
4.2.1	Stability of the ORS and HRS	25
4.2.2	Stability 1RS	27
4.3	Discussion of the gel phase	28
4.3.1	Ansatz for the amorphous solid state	29
4.3.2	The Sol-Gel transition	33
5	Hard cross-links	35
5.1	M-fold long-range order	35
5.2	Statistically isotropic amorphous solid	42
5.3	Phase diagram	44
5.4	M-fold order: alternative Ansatz	47
5.4.1	About the order parameter	47
5.4.2	Discussion of the free energy	48
5.4.3	Transition SIAS - 2-fold	50
5.4.4	Transition SIAS-M-fold, $M \geq 3$	53

5.4.5	Discussion	56
6	Soft cross-links	58
6.1	Long-range ordered case	58
6.2	Statistically isotropic amorphous solid	65
6.3	Phase diagram	66
7	Summary, discussion and outlook	67
A	Evaluating expectation values	71
A.1	The WLC propagator	71
A.2	Rules for expectation values	72
A.3	Correlators	74
B	Calculations M-fold I	76
B.1	Gaussian	76
B.2	Log-trace part	78
B.3	Evaluation of the expectation values	79
C	Calculations SIAS	85
C.1	Gaussian part	85
C.2	Log-trace part	86
D	Calculations M-fold II	87
D.1	Gaussian part	87
D.2	Log-trace part	88
D.3	Lowest order contribution to ΔF	90
E	Hubbard-Stratonovich and mean-field approximation	94
	Bibliography	97
	Acknowledgements	101
	Lebenslauf	103

Chapter 1

Introduction

Modern polymer science was initiated in the 1920s by the work of Herrmann Staudinger and Wallace Carothers [48]. Although polymer materials, for example rubber which was vulcanized first in 1839 by Charles Goodyear [24], had been known and used since the 19th century, they were thought of as colloids held together by some mysterious force. It was Staudinger who proposed in 1922 the concept of macromolecules, an idea that gave rise to much controversy in the beginning, but he was later awarded the Nobel Prize. Carothers, on the other hand, demonstrated during this decade, that polymers can be synthesized from their constituent monomers. Since then, the theoretical understanding of polymers and the knowledge about polymer synthesis have evolved dramatically, and synthetic polymer materials, for example nylon, polyethylene and silicone, have become indispensable in the modern world.

During the last twenty years physics has seen a dramatic increase in interest towards biological systems, triggered by advancing experimental insight into the microscopic structures and processes of living matter. Along with this development, *biopolymers* came into the focus of physicists: a substantial part of research in this area is devoted to the study of the cell's cytoskeleton. It is a highly complex, constantly reorganizing structure which plays a crucial role in many functions as the maintenance of cell shape, cell motility, resistance to mechanical stress or transport processes within the cell [2, 32]. Many physicists are concerned with the organization principles and mechanical properties of the network. There are three types of biopolymers involved, each forming a subnetwork contributing specific functionalities: microtubules, intermediate filaments and filamentous actin (F-actin). The microtubules are long, hollow cylinders with a diameter of about $25nm$. They are made of the protein tubulin and are very rigid objects. Amongst other things, this network acts as a route for motor proteins that in turn are involved in transport processes within the cell. The intermediate filaments have a diameter of $8 - 10nm$; this lies in-between that of filamentous actin and the microtubules. In contrast to monomeric tubulin and monomeric actin which are globular, the various

types of intermediate filament monomers are elongated fibrous molecules. It seems that a major function of cytoplasmic intermediate filaments is to resist mechanical stresses. Finally, the actin filaments consist of monomers that are arranged into the form of a tight double stranded helix that appears on electron micrographs as a thread of about $8nm$ width. Their orientational persistence length is comparable to the average contour length and so, they are said to be “semiflexible”, i.e. their bending elasticity lies in a regime between the behavior of random coils and rigid rods.

Actin filaments sit predominantly in the cell cortex where they are arranged into various structures: grouped into a meshwork they support the cell membrane, but they are also involved in the formation of various cell protrusions; in tube-like elongated structures like Microvilli and Filopodia, for example, actin filaments are found to form bundled structures [5, 46], whereas in Lamellipodia (sheet-like protrusions) the polymers are found to be grouped into an essentially two-dimensional branched network [46, 51].

This fascinating structural polymorphism of actin networks is mediated by an abundance of actin binding proteins (ABPs) [58, 46, 3, 16]. ABPs are responsible for assembly and disassembly of filamentous actin; there are cytoskeletal linkers that provide the connection to the other subnetworks and to the cell membrane, ABPs that stiffen actin filaments, and ABPs that promote the assembly of actin filaments into higher order structures by bundling, branching or cross-linking them. Bundling proteins, such as fimbrin or α -actinin, arrange the filaments parallel or antiparallel whereas the branching protein ARP 2/3 and the cross-linker filamin favor finite angles of 70° or 90° respectively and give rise to network structures.

There is a number of statistical physics theories focussing on the aspect of structure formation in actin networks. Concentrating mostly on the interplay of filaments and cross-linkers in an equilibrium environment, their results and predictions are compared to a growing number of *in vitro* experiments and computer simulations on actin networks. Quite generally, this “bottom-up” approach, i.e. starting from simple purified system and progressively adding more and more features and mechanisms, is hoped to give rise to new ideas and concepts that may help to understand the tremendous complexity of the living cell [6].

In [63] and [62], Zilman and Safran theoretically study the emergence of networks from solutions of self-assembling chains, junctions and ends. In terms of ABPs, their setup corresponds to an *in vitro* study of self-assembling (“living”) actin filaments, cross-linking and capping proteins. Within a very generic framework and without specifying any particular interactions, they derive in the random mixing approximation [19] a phase diagram that predicts *inter alia* a percolation transition from sol to gel state. In addition to the gelation transition, the formation of bundles is addressed too. The transition from

an isotropic network to a bundled state is proposed to be driven by entropy. Although the translational and rotational entropy of the rods is diminished by bundling, the entropy of the cross-linkers increases due to the fact that they can be placed anywhere along the parallel polymer strands. Their results on gelation are in accordance with *in vitro* experiments by Tempel *et al.* [53] who consider solutions of actin filaments that are reversibly cross-linked by the bundling protein α -actinin.

A different approach has been applied by Benetatos and Zippelius [9]. Instead of using treadmilling actin filaments like Zilman and Safran, they consider networks of fixed-length semiflexible polymers assembled into networks by *permanent* cross-linkers that align the filaments parallel or antiparallel. Upon increasing the cross-link concentration they find a continuous gelation transition from a fluid phase to a gel, where a finite fraction of the polymers are localized at random positions. For sufficiently stiff polymers, the gelation transition is accompanied by a continuous orientational transition from an isotropic state in the fluid phase to nematic ordering in the gel phase. For lower polymer stiffness, the nematic phase is preceded by an isotropic orientational glass and requires a higher cross-link density to come about. Note that due to the use of the wormlike chain model [31, 50] for the description of the filaments it is possible to investigate how the appearance of long-range orientational order depends on the polymer stiffness.

Bruinsma *et al.* devote several publications to the study of solutions of actin filaments and reversible cross-linkers. Their work is more focused on explaining the structural polymorphism of actin/cross-linker systems with respect to orientationally ordered phases than on the aspect of network structure and the gelation transition. Actin filaments are modeled as very long cylindrical rods with a finite diameter carrying a high negative line charge that is partially screened by counterions of the solution. As for the cross-links, they explore both the possibility of ABPs [11] and of polyvalent ions [13] that might act as cross-linking agents [52, 25]. They apply a generalization of Onsager’s theory [43] and incorporate the effect of cross-linkers as well as the electrostatic forces and the steric effects between the filaments in an effective rod-rod interaction. Due to the competitive interactions of the model, their theory provides a rich phase diagram. Besides isotropic, nematic and bundled phases, they predict also the appearance of exotic phases like the “cubatic” and “tetratic” phase that combine long-range orientational order with positional disorder. The cubatic phase, for instance, features cubic orientational order. It has been proposed by Nelson and Toner on theoretical grounds [38] and found in Monte Carlo computer simulation of “hard cut spheres” by Veerman and Frenkel [57].

Lastly, Kierfeld *et al.* [29] restrict their focus on bundle formation and the unbinding transition of essentially parallel filaments that are confined to

a tube-shaped compartment. The filaments are modeled as semiflexible and interact with a hard core repulsion. The cross-links are reversible and, in contrast to the other approaches discussed so far, are modeled as extended objects. By means of analytical calculations and Monte Carlo simulations they find that a critical cross-linker density is required for the formation of bundles and upon approaching this threshold from above the unbinding happens in a single, discontinuous transition. These results agree qualitatively with *in vitro* experiments of different groups [53, 18] on networks of actin filaments cross-linked by the reversible bundler α -actinin.

The goal of this thesis is to study the generic requirements for the appearance of orientationally ordered phases à la Bruinsma *et al.* within the theoretical framework proposed by Benetatos and Zippelius. In contrast to Benetatos and Zippelius, we will not only consider bundling cross-linkers, but allow for finite angle crossings that may or may not give rise to orientationally ordered structures.

The theory of Benetatos and Zippelius is based on an approach initially developed in order to describe soft random solids, such as rubber [21]. From a semi-microscopic model of cross-linked macromolecules, a mean-field theory is derived. It describes the vulcanization transition and gives a detailed picture of the structure of the resulting amorphous solid phase by accounting even for spatial heterogeneities in terms of a distribution of localization lengths of the individual monomers. The results have been confirmed by molecular dynamics simulations by Barsky and Plischke [4, 45]. The approach of Benetatos and Zippelius provides information about not only spatial but also orientational localization within the gel phase. Consequently, we hope that within our approach we will be able to gather detailed information about the network structure and may provide additional insights into the system that cannot be obtained by an Onsager-like theory.

Furthermore, we believe that an approach featuring permanent cross-links will provide complementary information with respect to the other studies that are based on reversible cross-links; permanent cross-linkers describe the physics on timescales that are significantly shorter than the typical association-dissociation time of a cross-linker in experiment. For example, consider an experiment where the shear modulus of a network is measured. If the shearing takes place very slowly, the cross-linkers have time to release stress by rearranging themselves into new positions and a reversible cross-linker description should be applied. But if, on the other hand, the sample is sheared quite quickly, so that the cross-linkers essentially stay at their positions, they should be modeled as permanent cross-links.

In our opinion, this work is going to contribute new and complementary information to the field of biopolymer networks. Its scope comprises not only

the description of the gelation transition, but also a structural analysis of the resulting amorphous solid phase. Based on a semi-microscopic model, it is a classical statistical mechanics approach that may provide a foundation to other more phenomenological approaches.

Chapter 2

The Model

We consider a large rectangular two-dimensional volume V which contains N identical semiflexible polymers that are assembled by permanent cross-links into random networks. In the following sections, we want to present the modeling details of the individual ingredients.

2.1 The single polymer

Actin filaments have a persistence length $L_p \sim 17\mu\text{m}$ [44, 20]. Their contour length lying typically in the range $L \sim 1 - 20\mu\text{m}$ [20], they are semiflexible, i.e. their behavior lies between that of rigid rods and random coils. The corresponding canonical model is the **wormlike chain model** (WLC) that was first introduced by Kratky and Porod [31]. We adopt the elegant approach of Saitô, Takahashi and Yunoki [50] and represent the polymer by a continuous differentiable space curve $\mathbf{r}(s)$ of total length L . The polymer is assumed to be locally not extensible and the length of the tangential vector $\mathbf{t}(s) := d\mathbf{r}/ds$ is restricted to equal 1 (see Fig. 2.1). The corresponding Hamiltonian is given by

$$\mathcal{H}_{WLC} = \frac{\kappa}{2} \int_0^L ds \left(\frac{d\mathbf{t}(s)}{ds} \right)^2 \quad (2.1)$$

where the parameter κ determines the stiffness of the polymer. For simplicity we set $k_B T \equiv 1$ throughout the thesis. As a consequence, the Hamiltonian needs to be dimensionless and the constant κ has the dimension of a length. We call this characteristic length scale of the WLC model the **persistence length** L_p and defined it by $L_p := 2\kappa$ for reasons to become clear right away: We compute the two-point correlation function by means of the WLC propagator (A.4):

$$\langle \mathbf{t}(0)\mathbf{t}(s) \rangle = \exp\left(-\frac{s}{2\kappa}\right) \quad (2.2)$$

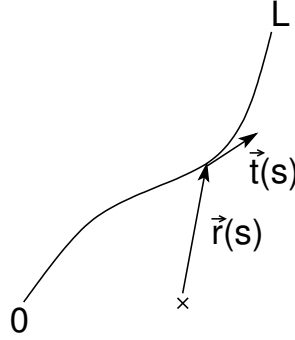


Figure 2.1: Sketch of a semiflexible polymer with position vector $\mathbf{r}(s)$ and tangential vector $\mathbf{t}(s)$.

We see that the quantity L_p sets the length scale of the exponential decay and hence, it is a measure for the persistence of the orientational correlations along the polymer contour. Note that for arbitrary dimension D the persistence length is related to κ by

$$L_p = 2\kappa / (D - 1)k_B T \quad (2.3)$$

where D denotes the dimensionality of the system [30].

The Hamiltonian \mathcal{H}_{WLC} is invariant with respect to interchanging head and tail of the filaments, i.e. the energy is unchanged under reparametrizations of the contour of one polymer i by $\{\mathbf{r}_i(s) \rightarrow \mathbf{r}_i(L - s), \forall s \in [0, L]\}$. F-actin, however, is a polar filament [49]. The WLC Hamiltonian is not sensitive to such a polarity, but the cross-links may or may not differentiate between the two states of the filament, as discussed in the next section.

Let us shortly have a look on the conformational characteristics of the WLC model and consider the dependence of the **radius of gyration** \mathbf{R}_g on the persistence length L_p . The radius of gyration is defined by

$$\begin{aligned} R_g^2 &:= \frac{1}{2L^2} \int_0^L ds_1 ds_2 \langle (\mathbf{r}(s_1) - \mathbf{r}(s_2))^2 \rangle \\ &= \frac{1}{2L^2} \int_0^L ds_1 ds_2 \int_{s_2}^{s_1} d\tau d\tau' \langle \mathbf{t}(\tau) \mathbf{t}(\tau') \rangle \end{aligned} \quad (2.4)$$

and we can evaluate the correlation function by means of the WLC propagator

(A.4):

$$\begin{aligned}
 R_g^2 &= \frac{1}{2L^2} \int_0^L ds_1 ds_2 \int_{s_2}^{s_1} d\tau d\tau' e^{-\frac{1}{L_p}|\tau-\tau'|} \\
 &= \frac{1}{3}L^2 \left(\frac{L_p}{L} - 3 \left(\frac{L_p}{L} \right)^2 + 6 \left(\frac{L_p}{L} \right)^3 - 6 \left(\frac{L_p}{L} \right)^4 + 6 \left(\frac{L_p}{L} \right)^4 e^{-\frac{L}{L_p}} \right) .
 \end{aligned} \tag{2.5}$$

In the limit of very flexible chains, i.e. for $\frac{L_p}{L} \ll 1$, the R_g is given by

$$R_g^2 \sim \frac{1}{3}L_p L . \tag{2.6}$$

The radius of gyration scales thus only as $R_g \propto \sqrt{L}$ in the polymer length. In the limit of high bending rigidity, i.e. $\frac{L_p}{L} \gg 1$, we find the approximate expression

$$R_g^2 \sim \frac{L^2}{12} - \frac{L^2}{60}L/L_p + \mathcal{O}(1/L_p^3) \tag{2.7}$$

that approaches linearly the result for stiff rods. The behavior of the WLC model lies thus between these two limiting cases.

2.2 Cross-links

In our theory, we model the cross-linking proteins as **chemical cross-links** that are establishing *permanent* connections between the polymers. Of course, in reality the biological cross-links are dynamical objects and incessantly break up and reattach elsewhere in the network. Using in this context permanent cross-links amounts to assuming that in the real system there is a separation of timescales: the changes in the network topology must take place on timescales that are by far longer than the typical relaxation time of the system. Note that there are other theories where the cross-links are treated as thermal variables as for example in [13, 11]. Such an approach is sometimes called “annealed approximation” and polymers and cross-links are treated on the same level. However, within such a framework it is for example not possible to obtain the elastic moduli of a system due to cross-linking (letting aside effects originating from entanglement) because if a strain is applied, the cross-links are free to rearrange immediately in order to relax the stress within the network.

We characterize a cross-link by indicating the polymers involved and the positions where they are attached to each other, i.e. by indicating the set of indices $\{i, s; j, s'\}$ (see Fig. 2.2). Once, a cross-link has been established it imposes not only that the two participating polymers stick together but also that their relative orientation is fixed to some prescribed angle θ .

We are going to consider two different types of cross-links. First of all, cross-links that “see” the filaments polarity that we call **sensitive** and second,

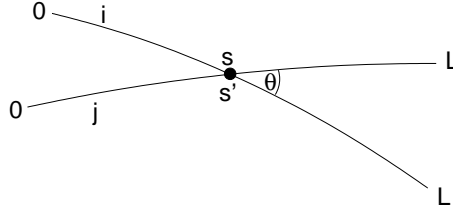


Figure 2.2: Sensitive cross-link.

cross-links that do not, called **unsensitive**. For the sensitive cross-link the statement “Polymer i is attached to polymer j at positions s and s' and they comprise an angle θ ” corresponds uniquely to the situation depicted in Fig. 2.2. In the case of unsensitive cross-links on the other hand, there are four

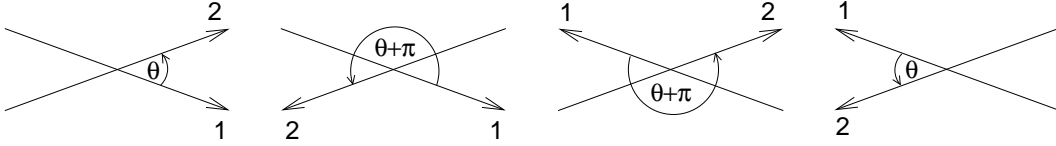


Figure 2.3: Unsensitive cross-link.

equivalent situations that are obtained by interchanging head and tail of the polymers as shown in Fig. 2.3. Consequently, the choice of a system with unsensitive cross-linkers corresponds to having cross-linker with angles both θ and $\theta + \pi$.

Mathematically, the cross-links with their positional and orientational constraints may be expressed by effective pair potentials $v(\mathbf{r}_i(s) - \mathbf{r}_j(s')) + w(\psi_i(s) - \psi_j(s') - \theta)$. For the spatial potential v we choose for simplicity a delta function. We believe that a more realistically shaped cross-linking potential that allows for thermal fluctuations, as for instance a gaussian potential, will not lead to a qualitatively different physical behavior. As for the orientational constraints we will consider two different choices: First, we will consider a delta function as the simplest way to implement the orientational constraint, i.e.

$$\Delta(\psi - \psi', \theta) = \delta(\psi - \psi' - \theta) \quad (2.8)$$

where we normalize the delta function such that $\int \frac{d\varphi}{2\pi} \delta(\varphi) = 1$. It is however much more realistic to use a cross-linking potential that allows for thermal fluctuations around the preferred direction. The cross-linking proteins themselves are also extended structures that will lead to fluctuations of the relative positions and orientations of the interconnected filaments [28, 58]. A simple

model for these “soft” orientational constraints is given by

$$\Delta(\psi - \psi', \theta) = \frac{1}{I_0(\gamma)} e^{\gamma \cos(\psi - \psi' - \theta)} \quad . \quad (2.9)$$

The parameter γ is controlling the variance of the thermal fluctuations of the angle. The bigger γ the more focused are the x-links. More precisely, $\gamma = 10$ corresponds to a standard deviation of around 6° and $\gamma = 40$ corresponds to 3° . It is clear that in the limit $\gamma \rightarrow \infty$ we recover the simple delta function model of “hard” cross-links. In the following we will first explore the behavior of the simpler case of hard cross-links and discuss then the changes that arise when allowing for softness.

2.3 The network and its configurations

A network consisting of N polymers and M cross-links is characterized by the set of indices $\mathcal{C}_M := \{(i_e, s_e; j_e, s'_e), e = 1 \dots M\}$ specifying the positions of all the cross-links. In order to derive a suitable weighting function $\mathcal{P}(\mathcal{C}_M)$ for the different networks configurations we follow the elegant strategy due to Deam and Edwards [14]. Consider the distribution function in our case:

$$\mathcal{P}(\mathcal{C}_M) \propto \frac{1}{M!} \left(\frac{\mu^2 V}{N} \right)^M \text{Tr} \left\{ \prod_{e=1}^M \delta(\mathbf{r}_{i_e}(s_e) - \mathbf{r}_{j_e}(s'_e)) e^{-\mathcal{H}} \right\} \quad . \quad (2.10)$$

The number of cross-links in the system is controlled by a quasi-Poissonian distribution. The mean number of cross-links per polymer $\langle M \rangle / N$ is approximately of order μ^2 as can be shown by proceeding analogously to [47]. In the following, we will call the parameter μ^2 simply the “cross-link density”.

It is in the second contribution on the right hand where the features of the cross-linking process are incorporated: the trace operator denotes the sum over the configurations of the polymers, but only those configurations contribute to the sum that fulfill the constraints imposed by the delta functions. For each configuration the question is: “If we take this snapshot of the system and cross-link all pairs of polymers that are close to each other, does the resulting network correspond to the network characterized by \mathcal{C}_M ?” If the answer is yes, this configuration contributes to $\mathcal{P}(\mathcal{C}_M)$ the corresponding Boltzmann weight $e^{-\mathcal{H}}$, if not, the configuration does not contribute. So, it is assumed that the network formation takes place *simultaneously* and *instantaneously*. Note that there are cross-linking processes where these assumptions hold true, but they apply not necessarily to any system. For a detailed discussion of the Deam-Edwards distribution see [12].

While we define the distribution of cross-links in complete analogy with the original DE approach, the effect of the cross-linking on the network is different:

a cross-link is established if two polymers overlap irrespective of their relative orientation, but it then *reorients* the participating polymers according to its preferential angle θ . In this sense, our DE distribution introduces an additional ordering mechanism.

In contrast to that, one could also use a distribution where a cross-link is introduced if the polymers not only overlap in the melt, but if they have also the correct relative orientation as indicated by the crossing-angle θ . In a previous work dealing with a 3d system of parallel or antiparallel cross-linked networks of semiflexible polymers [9] the authors found that apparently this generalization of the original DE distribution is not sufficient to give rise to long-range orientational order. They applied the modified version instead and found a phase transition to an orientationally long-range ordered phase.

2.4 Excluded volume interaction

An uncross-linked melt of polymers constitutes a homogeneous and isotropic liquid system. Adding more and more cross-linkers to the system that interconnect the polymers to larger and larger clusters, a macroscopic cluster will eventually occur that comprises a finite fraction of the polymers. In order to prevent periodic density fluctuations to appear in the system, we need to introduce additionally the following excluded volume interaction in order to balance the effective attraction induced by the cross-links:

$$\mathcal{H}_{ev} = \frac{N^2}{2V} \sum_{\mathbf{k} \neq 0} \sum_{m \in \mathbb{Z}} \lambda_{|\mathbf{k}|,m}^2 |\rho_{\mathbf{k},m}|^2 \quad (2.11)$$

with

$$\rho_{\mathbf{k},m} := \frac{1}{N} \sum_{i=1}^N \frac{1}{L} \int_0^L ds e^{i\mathbf{k}\mathbf{r}_i(s)} e^{im\psi_i(s)} \quad . \quad (2.12)$$

$\rho_{\mathbf{k},m}$ is the Fourier transformation of the positional-orientational density

$$\rho(\mathbf{x}, \varphi) := \frac{1}{N} \sum_{i=1}^N \frac{1}{L} \int_0^L ds \delta(\mathbf{x} - \mathbf{r}_i(s)) \delta(\varphi - \psi_i(s)) \quad . \quad (2.13)$$

Here, $\mathbf{t}_i(s) = (\cos \psi_i(s), \sin \psi_i(s))$ denotes the orientation of monomer s on polymer i . The coefficients $\lambda_{|\mathbf{k}|,m}^2$ depend only on the absolute value of the vector \mathbf{k} in order to preserve the rotational symmetry of the system. They are later chosen large enough to provide stability with respect to density modulations. For details, see section 4.2.2 .

Chapter 3

The formalism

Our system belongs to the class of **disordered systems**, i.e. systems where permanent random constraints are present that reduce the set of accessible configurations. Here, disorder is brought into the system by the permanent cross-links that assemble the polymers into a network. Their randomness is expressed by a distribution $\mathcal{P}(\mathcal{C})$ that attributes to every possible network configuration \mathcal{C} a probability.

We assume that the free energy of our system is **self-averaging**, i.e. we assume that if the system is sufficiently large essentially all the configurations \mathcal{C} give rise to a similar free energy. Consequently, it is possible to study our model by analyzing not the free energy for one “typical” network configuration \mathcal{C} , which is actually an impossible task for a large system, but by investigating rather the disorder averaged free energy:

$$[F] = \int d\mathcal{C} \mathcal{P}(\mathcal{C}) F_{\mathcal{C}} \quad . \quad (3.1)$$

The standard method for dealing with disordered systems is the **replica method** [17, 42]. In order to avoid calculating the disorder average of $\ln Z$ which is in general a daunting task, one computes the disorder averaged partition function $[Z^n]$ of n identical non-interacting copies of the original system with the same disorder configuration

$$[Z^n] = \int d\mathcal{C} \mathcal{P}(\mathcal{C}) \prod_{\alpha=1}^n Z_{\mathcal{C}}^{(\alpha)} \quad . \quad (3.2)$$

Once this quantity has been computed, $[F]$ can be extracted from $[Z^n]$ by means of

$$[F] = \lim_{n \rightarrow 0} -\ln[Z^n]/n \quad . \quad (3.3)$$

In the following sections we present how we arrive from the original microscopic theory to a mean-field description that will be the basis of our investigations. In particular, we want to highlight the simplifications and approximations that we apply on the way.

3.1 Performing the disorder average

Writing equation (3.2) explicitly for our model we obtain

$$\begin{aligned}
 [Z^n] \propto & \sum_{M=0}^{\infty} \frac{1}{M!} \left(\frac{\mu^2 V}{2Ny} \right)^{MM} \prod_{e=1}^M \left(\sum_{i_e, j_e=1}^N \int_{s_e, s'_e} \sum_{\sigma_e} \right) \left\langle \prod_{e=1}^M \delta(\mathbf{r}_{i_e}(s_e) - \mathbf{r}_{j_e}(s'_e)) \right\rangle \times \\
 & \times \prod_{\alpha=1}^n \left\langle \prod_{e=1}^M \left\{ \delta(\mathbf{r}_{i_e}^{\alpha}(s_e) - \mathbf{r}_{j_e}^{\alpha}(s'_e)) \delta(\psi_{i_e}^{\alpha}(s_e) - \psi_{j_e}^{\alpha}(s'_e) - \theta_{\sigma_e}) \right\} \right\rangle^{\mathcal{H}} \quad (3.4)
 \end{aligned}$$

where $\mathbf{r}_i^{\alpha}(s)$ and $\psi_i^{\alpha}(s)$ denote the position vector and angle of orientation of segment s belonging to polymer i inside the α -replica. Moreover, we used the abbreviation

$$\int_s \equiv (1/L) \int_0^L ds \quad .$$

For sensitive cross-links, θ_{σ} equals always the crossing-angle θ . Therefore, we can omit the summation over σ , and the corresponding normalization constant y equals 1. On the other hand, in the case of unsensitive cross-links θ_{σ} may take one of the two values $\theta_1 = \theta$ and $\theta_2 = \theta + \pi$, and so $y = 2$.

Comparing (3.4) to the general expression (3.2), the first line corresponds to the disorder average over the different network configurations ruled by the Deam-Edwards distribution that we introduced in section 2.3. The second line corresponds to the n -fold product of the constraint partition functions $Z_C^{(\alpha)}$.

As can be seen, the expectation value in the first line has the form of a constraint partition function too, the only difference being that the delta functions do not fix the relative orientations, but only attach the polymers to each other. In this sense, the Deam-Edwards distribution gives rise to an additional cross-linking replica to which we attribute the index 0. However, this ‘‘cross-linking replica’’ has different constraints than the ‘‘thermal replicas’’ and, hence, it may display different physical behavior.

Introducing the shorthand notations

$$\begin{aligned}
 \hat{\mathbf{r}} & \equiv (\mathbf{r}^0, \mathbf{r}^1, \dots, \mathbf{r}^n) \quad \text{and} \quad \check{m} \equiv (m^1, \dots, m^n) \quad , \quad (3.5) \\
 \delta(\hat{\mathbf{r}}) & \equiv \prod_{\alpha=0}^n \delta(\mathbf{r}^{\alpha}) \quad \text{and} \quad \delta(\check{\varphi}) \equiv \prod_{\alpha=1}^n \delta(\varphi^{\alpha})
 \end{aligned}$$

it is possible to write (3.4) in a more compact form as

$$\begin{aligned}
 [Z^n] \propto & \sum_{M=0}^{\infty} \frac{1}{M!} \left(\frac{\mu^2 V}{2Ny} \right)^{MM} \prod_{e=1}^M \left(\sum_{i_e, j_e=1}^N \int_{s_e, s'_e} \sum_{\sigma_e} \right) \quad (3.6) \\
 & \left\langle \prod_{e=1}^M \left\{ \delta(\hat{\mathbf{r}}_{i_e}(s_e) - \hat{\mathbf{r}}_{j_e}(s'_e)) \prod_{\alpha=1}^n \delta(\psi_{i_e}^{\alpha}(s_e) - \psi_{j_e}^{\alpha}(s'_e) - \theta_{\sigma_e}) \right\} \right\rangle_{n+1}^{\mathcal{H}} .
 \end{aligned}$$

The formula factorizes in the cross-link index e and it is possible to perform the sum over the number of cross-links M , leading to an exponential function

$$\begin{aligned}
 [Z^n] &\propto \left\langle \sum_{M=0}^{\infty} \frac{1}{M!} \left(\frac{\mu^2 V}{2N} \right)^M \times \right. \\
 &\quad \times \left. \left(\sum_{i,j=1}^N \int_{s,s'} \delta(\hat{\mathbf{r}}_i(s) - \hat{\mathbf{r}}_j(s')) \frac{1}{y} \sum_{\sigma} \prod_{\alpha=1}^n \delta(\psi_i^{\alpha}(s) - \psi_j^{\alpha}(s') - \theta_{\sigma}) \right)^M \right\rangle_{n+1}^{\mathcal{H}} \\
 &= \left\langle \exp \left(\frac{\mu^2 V}{2N} \sum_{i,j=1}^N \int_{s,s'} \delta(\hat{\mathbf{r}}_i(s) - \hat{\mathbf{r}}_j(s')) \Delta(\check{\psi}_i(s) - \check{\psi}_j(s'), \theta) \right) \right\rangle_{n+1}^{\mathcal{H}}.
 \end{aligned} \tag{3.7}$$

For sensitive cross-links the function Δ is defined as

$$\Delta_s(\check{\psi}, \theta) \equiv \prod_{\alpha=1}^n \delta(\psi^{\alpha} - \theta) \tag{3.8}$$

and in the insensitive case it is defined as

$$\Delta_u(\check{\psi}, \theta) \equiv \frac{1}{2} \left\{ \prod_{\alpha=1}^n \delta(\psi^{\alpha} - \theta) + \prod_{\alpha=1}^n \delta(\psi^{\alpha} - (\theta + \pi)) \right\}. \tag{3.9}$$

Expressing the delta functions and Δ in Fourier space we can rewrite our formula in terms of the new quantity

$$Q(\hat{\mathbf{k}}, \check{m}) = \frac{1}{N} \sum_{i=1}^N \int_s e^{i\hat{\mathbf{k}}\hat{\mathbf{r}}_i(s)} e^{i\check{m}\check{\psi}_i(s)}. \tag{3.10}$$

This is the Fourier transform of

$$Q(\hat{\mathbf{x}}, \check{\varphi}) = \frac{1}{N} \sum_{i=1}^N \int_s \delta(\hat{\mathbf{x}} - \hat{\mathbf{r}}_i(s)) \delta(\check{\varphi} - \check{\varphi}_i(s)) \tag{3.11}$$

which is simply the joint probability distribution of positions and orientations of the polymer segments in all the replicas. $Q(\hat{\mathbf{k}}, \check{m})$ thus carries essential information about the system. The replicated partition function now reads simply

$$[Z^n] \propto \left\langle \exp \left(\frac{\mu^2 N}{2V^n} \sum_{\hat{\mathbf{k}}, \check{m}} \Delta_{\check{m}} |Q(\hat{\mathbf{k}}, \check{m})|^2 \right) \right\rangle_{n+1}^{\mathcal{H}}. \tag{3.12}$$

Because of the symmetry $|Q(\hat{\mathbf{k}}, \check{m})|^2 = |Q(-\hat{\mathbf{k}}, -\check{m})|^2$ it is only the real part of $\Delta_{\check{m}}$ that contributes and thus we redefine the sensitive kernel Δ_s accordingly as

$$\Delta_{s,\check{m}} = \cos \left(\sum_{\alpha} m^{\alpha} \theta \right). \tag{3.13}$$

For insensitive cross-links $\Delta_{u,\check{m}}$ equals zero if the sum $\sum_{\alpha=1}^n m^{\alpha}$ is not even, but otherwise takes the values of the sensitive kernel in (3.13).

3.2 Decomposing replica space

The thermal average $\langle \dots \rangle^{\mathcal{H}}$ is taken with respect to the wormlike chain Hamiltonians $\mathcal{H}_{WLC}^{\alpha}$ and the excluded volume interaction $\mathcal{H}_{ev}^{\alpha}$. We now write the excluded volume contribution explicitly and find

$$[Z^n] \propto \left\langle \exp \left(\frac{\mu^2 N}{2V^n} \sum_{\hat{\mathbf{k}}, \check{m}} \Delta_{\check{m}} |Q(\hat{\mathbf{k}}, \check{m})|^2 - \frac{\lambda^2 N^2}{2V} \sum_{\alpha=0}^n \sum_{\mathbf{k} \neq 0} \sum_m |\rho^{\alpha}(\mathbf{k}, m)|^2 \right) \right\rangle_{n+1}^{\mathcal{H}_{WLC}}.$$

In section 2.4 the parameter λ^2 was introduced in its most general form depending on $|\mathbf{k}|$ and m , but as it turns out a constant is sufficient for our purpose and allows in the following for a more compact notation.

We split up the fields $\Omega(\hat{\mathbf{k}}, \check{m})$ into three subsets dependent on the value of the $(n+1)$ -fold replicated vector $\hat{\mathbf{k}}$:

- the 0-replica sector (0RS) consisting only of the fields $\Omega(\hat{\mathbf{0}}, \check{m})$, \check{m} being arbitrary;
- the 1-replica sector (1RS) including all Ω with $\hat{\mathbf{k}} = (\mathbf{0}, \dots, \mathbf{k}^{\alpha}, \dots, \mathbf{0})$ where $\mathbf{k}^{\alpha} \neq 0$, denoted by $\tilde{\Omega}^{\alpha}(\mathbf{k}, \check{m})$;
- the higher-replica sector (HRS) containing all Ω dependent on vectors $\hat{\mathbf{k}}$, such that wave vectors in at least two replicas are non-zero, i.e. there are $\alpha \neq \beta \in \{0, 1, \dots, n\}$ with $\mathbf{k}^{\alpha} \neq 0$ and $\mathbf{k}^{\beta} \neq 0$.

0RS- and HRS-fields can be treated on the same footing and we denote the sum over 0RS- and HRS- $\hat{\mathbf{k}}$ by $\overline{\sum_{\hat{\mathbf{k}}}$. For the 1RS we introduce $\tilde{\sum}_{\mathbf{k}} \equiv \sum_{\mathbf{k} \neq \mathbf{0}}$.

The reason for splitting up the original field $\Omega(\hat{\mathbf{k}}, \check{m})$ is that the 1RS fields represent density fluctuations in our system. In fact, we are above all interested in the physics of the HRS and so, in order to simplify the analysis, we introduced the excluded volume interaction of section 2.4 which enables us to control and suppress the density fluctuations. The corresponding additional terms appear logically only in the 1RS part of the free energy and therefore the 0RS/HRS- and 1RS contributions have to be treated separately.

Combining Δ with the coefficient of the excluded volume contribution we obtain the new 1RS-kernel

$$\tilde{\Delta}_{\check{m}}^{\alpha} = \frac{\lambda^2 N}{2V} \prod_{\beta \neq \alpha=1}^n \delta_{m\beta, 0} - \frac{\mu^2}{2V^n} \Delta_{\check{m}} \quad . \quad (3.14)$$

Furthermore, we introduce $\tilde{Q}^{\alpha}(\mathbf{k}, \check{m})$ as a shorthand notation for

$$\tilde{Q}^{\alpha}(\mathbf{k}, \check{m}) \equiv Q(\{\mathbf{0}, \dots, \mathbf{k}^{\alpha}, \dots, \mathbf{0}\}, \check{m}) \quad (3.15)$$

and $[Z^n]$ now reads

$$\begin{aligned}
 [Z^n] \propto & \left\langle \exp \left(-N \sum_{\alpha=0}^n \sum_{\mathbf{k}, \tilde{m}} \tilde{\Delta}_{\tilde{m}}^{\alpha} |\tilde{Q}^{\alpha}(\mathbf{k}, \tilde{m})|^2 \right) \times \right. & (3.16) \\
 & \left. \times \exp \left(\frac{\mu^2 N}{2V^n} \sum_{\hat{\mathbf{k}}, \tilde{m}} \Delta_{\tilde{m}} |Q(\hat{\mathbf{k}}, \tilde{m})|^2 \right) \right\rangle_{n+1}^{\mathcal{H}_{WLC}}.
 \end{aligned}$$

At this stage, a few comments are in order. With equation (3.16) we have written the disorder averaged replicated partition function in a very elegant and compact way, but we are still dealing with a highly complicated interacting system. On the other hand, after the disorder average over all possible network configurations the polymers have become equivalent, which enables us to apply the mean-field approximation. In order to do so, we will reformulate our theory in terms of a single polymer in a fluctuating field and then obtain the mean-field approximation replacing the fluctuating field by its saddle-point value.

3.3 Towards a statistical field theory

In (3.16) the polymer interactions are hidden in the square terms $|\tilde{Q}^{\alpha}|^2$ and $|Q|^2$. In order to decouple the polymers we apply a **Hubbard-Stratonovich transformation** (HS). Because the transformation is carried out for each component $\tilde{Q}^{\alpha}(\mathbf{k}, \tilde{m})$ and $Q(\hat{\mathbf{k}}, \tilde{m})$ separately, we can simplify things by presenting the calculation for a single component only. For that purpose we introduce

$$Q := \frac{1}{N} \sum_{i=1}^N \int_s e^{i\mathbf{k}\mathbf{r}_i(s)} e^{im\psi_i(s)} \quad (3.17)$$

and, denoting by a the coefficient of component Q in the exponent, the HS transformation reads then

$$\begin{aligned}
 [Z^n] &= \left\langle \exp(Na|Q|^2) \right\rangle & (3.18) \\
 &= \frac{bN}{\pi} \int d\Re\Omega \, d\Im\Omega \left\langle \exp \left(-bN|\Omega|^2 + 2N\sqrt{ab} \Re\{\Omega Q\} \right) \right\rangle.
 \end{aligned}$$

The parameter b needs to be positive in order to ensure convergence of the integral, but apart from that it is arbitrary. The benefit of applying a HS transformation is that Q now appears *linearly* inside the exponential function. This allows us to transform the original theory of N interacting particles into

an effective theory of a single particle in a fluctuating field:

$$\begin{aligned}
 [Z^n] &= \frac{bN}{\pi} \int d\Re\Omega \, d\Im\Omega \, e^{-bN|\Omega|^2} \times \\
 &\quad \times \prod_{i=1}^N \left\langle \exp \left(2\sqrt{ab} \Re \left\{ \Omega \int_s e^{i\mathbf{k}\mathbf{r}_i(s)} e^{im\psi_i(s)} \right\} \right) \right\rangle \\
 &= \frac{bN}{\pi} \int d\Re\Omega \, d\Im\Omega \, e^{-bN|\Omega|^2} \times \\
 &\quad \times \left\langle \exp \left(2\sqrt{ab} \Re \left\{ \Omega \int_s e^{i\mathbf{k}\mathbf{r}(s)} e^{im\psi(s)} \right\} \right) \right\rangle^N \\
 &=: \frac{bN}{\pi} \int d\Re\Omega \, d\Im\Omega \, \exp(-N\mathcal{H}_{eff}) \quad .
 \end{aligned} \tag{3.19}$$

Here, we introduced the **effective Hamiltonian**,

$$\mathcal{H}_{eff} = b|\Omega|^2 - \ln \left\langle \exp \left(2\sqrt{ab} \Re \left\{ \Omega \int_s e^{i\mathbf{k}\mathbf{r}(s)} e^{im\psi(s)} \right\} \right) \right\rangle. \tag{3.20}$$

Let us now turn to the full expression (3.16). After the HS transformation $[Z^n]$ can be written as

$$[Z^n] \propto \int \mathcal{D}\{\tilde{\Omega}^\alpha, \Omega\} \exp \left(-N\mathcal{H}_{eff}(\{\tilde{\Omega}^\alpha, \Omega\}) \right) \quad , \tag{3.21}$$

where the integrals over $\tilde{\Omega}^\alpha$ and Ω are meant to be integrations over real and imaginary parts separately. The effective Hamiltonian \mathcal{H}_{eff} is given by

$$\begin{aligned}
 \mathcal{H}_{eff}(\{\tilde{\Omega}^\alpha\}, \Omega) &= \sum_{\alpha=0}^n \sum_{\mathbf{k}} \sum_{\tilde{m}} |\tilde{\Omega}^\alpha(\mathbf{k}, \tilde{m})|^2 + \frac{\mu^2}{2V^n} \sum_{\hat{\mathbf{k}}} \sum_{\tilde{m}} |\Omega(\hat{\mathbf{k}}, \tilde{m})|^2 \\
 &\quad - \ln \left\langle \exp \left(2i \sum_{\alpha=0}^n \sum_{\mathbf{k}} \sum_{\tilde{m}} \sqrt{\tilde{\Delta}_{\tilde{m}}} \Re \left(\tilde{\Omega}^\alpha \int_s e^{-i\mathbf{k}^\alpha \mathbf{r}^\alpha(s)} e^{-im\tilde{\psi}(s)} \right) \right. \right. \\
 &\quad \left. \left. + \frac{\mu^2}{V^n} \sum_{\hat{\mathbf{k}}} \sum_{\tilde{m}} \sqrt{\Delta_{\tilde{m}}} \Re \left(\Omega \int_s e^{-i\hat{\mathbf{k}}\mathbf{r}(s)} e^{-im\tilde{\psi}(s)} \right) \right) \right\rangle_{n+1}^{\mathcal{H}_{WLC}}.
 \end{aligned} \tag{3.22}$$

The HS transformation was performed such that convergence of the integrals in (3.21) is guaranteed by a positive coefficient in front of the square terms $|\tilde{\Omega}^\alpha|^2$ and $|\Omega|^2$ in the effective Hamiltonian. The straightforward choice for the transformation, i.e. $b = a$ speaking in terms of the simplified example (3.18), cannot be applied here because of the indefiniteness of $\tilde{\Delta}^\alpha$ and Δ .

Note that we have to take care of the symmetries of \tilde{Q}^α and Q , i.e. the relations

$$Q(\hat{\mathbf{k}}, \tilde{m}) = Q^*(-\hat{\mathbf{k}}, -\tilde{m}) \quad \text{and} \quad \tilde{Q}^\alpha(\mathbf{k}, \tilde{m}) = \tilde{Q}^{\alpha*}(-\mathbf{k}, -\tilde{m}) \tag{3.23}$$

need to be reflected by their corresponding fields $\Omega(\hat{\mathbf{k}}, \check{m})$ and $\tilde{\Omega}^\alpha(\mathbf{k}, \check{m})$. As a consequence of this symmetry, it was possible to omit in (3.22) the real part operators \Re that we used in (3.20) in order to have a compact notation of the HS transformation involving a complex field.

To summarize, we have shown that our original microscopic theory is equivalent to a field theory given by (3.21) and (3.22). Instead of a sum over the configurations of the polymers, we now have the integrations over the fluctuating fields $\tilde{\Omega}^\alpha$ and Ω , and the original Hamiltonian and the disorder averaged cross-link constraints have been replaced by the effective Hamiltonian \mathcal{H}_{eff} .

3.4 Mean-field approximation

So far, no approximations have been made and the statistical field theory that we have derived in the preceding section is still very complicated. In order to simplify things, we are now going to apply the **saddle-point approximation** [7] and replace the integral (3.21) by its maximal contribution. A necessary condition for saddle-point fields $\tilde{\Omega}_{SP}^\alpha$ and Ω_{SP} to correspond to the minimal value of the effective Hamiltonian is stationarity of \mathcal{H}_{eff} with respect to small variations of the fields:

$$\begin{aligned} \frac{\partial \mathcal{H}_{eff}}{\partial \Re \tilde{\Omega}^\alpha(\mathbf{k}_0, \check{m}_0)} = 0 \quad , \quad \frac{\partial \mathcal{H}_{eff}}{\partial \Im \tilde{\Omega}^\alpha(\mathbf{k}_0, \check{m}_0)} = 0, \\ \frac{\partial \mathcal{H}_{eff}}{\partial \Re \Omega(\hat{\mathbf{k}}_0, \check{m}_0)} = 0 \quad \text{and} \quad \frac{\partial \mathcal{H}_{eff}}{\partial \Im \Omega(\hat{\mathbf{k}}_0, \check{m}_0)} = 0. \end{aligned}$$

Combining real and imaginary parts in order to have a more compact notation the saddle-point equations read explicitly

$$\tilde{\Omega}^\alpha(\mathbf{k}, \check{m}) = i\sqrt{\tilde{\Delta}} \frac{1}{\langle \dots \rangle} \int_s \left\langle e^{-i\mathbf{k}^\alpha \mathbf{r}^\alpha(s)} e^{-i\check{m}\check{\psi}(s)} e^{\mathcal{W}(\{\tilde{\Omega}^\alpha\}, \Omega)} \right\rangle_{n+1}^{\mathcal{H}_{WLC}} \quad (3.24)$$

and

$$\Omega(\hat{\mathbf{k}}, \check{m}) = \sqrt{\Delta} \frac{1}{\langle \dots \rangle} \int_s \left\langle e^{-i\hat{\mathbf{k}}\mathbf{r}(s)} e^{-i\check{m}\check{\psi}(s)} e^{\mathcal{W}(\{\tilde{\Omega}^\alpha\}, \Omega)} \right\rangle_{n+1}^{\mathcal{H}_{WLC}} . \quad (3.25)$$

The function \mathcal{W} is given by

$$\begin{aligned} \mathcal{W}(\{\tilde{\Omega}^\alpha\}, \Omega) := & 2i \sum_{\alpha=0}^n \sum_{\check{m}} \sum_{\mathbf{k}} \sqrt{\tilde{\Delta}} \Re \left(\tilde{\Omega}^\alpha \int_s e^{-i\mathbf{k}^\alpha \mathbf{r}^\alpha(s)} e^{-i\check{m}\check{\psi}(s)} \right) \\ & + \frac{\mu^2}{V^n} \sum_{\hat{\mathbf{k}}} \sum_{\check{m}} \sqrt{\Delta} \Re \left(\Omega \int_s e^{-i\hat{\mathbf{k}}\mathbf{r}(s)} e^{-i\check{m}\check{\psi}(s)} \right) . \end{aligned} \quad (3.26)$$

Once we have found the solution of the saddle-point equations, we can insert the saddle-point values of the fields into the effective Hamiltonian. We then obtain the approximation

$$-\ln[Z^n] \sim N\mathcal{H}_{eff}(\{\tilde{\Omega}_{SP}^\alpha, \Omega_{SP}\}) \quad , \quad (3.27)$$

showing that the effective Hamiltonian evaluated for the saddle-point values of the fields is, in fact, a free energy. In the following we will call this the **replica free energy** \mathcal{F} :

$$\mathcal{F}(\{\tilde{\Omega}_{SP}^\alpha, \Omega_{SP}\}) := \mathcal{H}_{eff}(\{\tilde{\Omega}_{SP}^\alpha, \Omega_{SP}\}) \quad . \quad (3.28)$$

3.5 Trivial solution and variational approach

What are the solutions of the stationarity equations (3.24) and (3.25)? Unfortunately, they turn out to be very complicated self-consistency equations and we are only able to calculate rigorously the solution

$$\tilde{\Omega}^\alpha(\mathbf{k}, \tilde{m}) = 0 \quad \text{and} \quad \Omega(\hat{\mathbf{k}}, \tilde{m}) = \delta_{\hat{\mathbf{k}}, \hat{\mathbf{0}}} \delta_{\tilde{m}, \hat{\mathbf{0}}} \quad . \quad (3.29)$$

As we will see in section 4.2, this solution corresponds to a fluid phase and we will show that it is stable up to cross-link densities of $\mu^2 = 1$.

For cross-link densities above that threshold we are going to use a variational approach to figure out what the corresponding physical situation is. The basic idea is to derive trial Ansätze for the ORS/HRS field $\Omega(\hat{\mathbf{k}}, \tilde{m})^1$, insert them into the replica free energy \mathcal{F} , and minimize the resulting physical free energy F with respect to the variational parameters. The variational parameters are related to physical order parameters that indicate the emergence of the phase under consideration. Therefore, a finite value of the resulting variational parameters corresponds to the presence of the related physical phase.

In order to come up with an Ansatz for the fields Ω , we first need to clarify their physical significance. To this end, it is convenient to express our theory on saddle-point level in terms of new fields $\Omega'(\hat{\mathbf{k}}, \tilde{m})$ and $\tilde{\Omega}'^\alpha(\mathbf{k}, \tilde{m})$ that we introduce by

$$\Re\Omega'(\hat{\mathbf{k}}, \tilde{m}) := \Delta_{\tilde{m}}^{-1/2} \Re\Omega(\hat{\mathbf{k}}, \tilde{m}) \quad (3.30)$$

$$\Im\Omega'(\hat{\mathbf{k}}, \tilde{m}) := \Delta_{\tilde{m}}^{-1/2} \Im\Omega(\hat{\mathbf{k}}, \tilde{m}) \quad (3.31)$$

and

$$\Re\tilde{\Omega}'^\alpha(\mathbf{k}, \tilde{m}) := \tilde{\Delta}_{\tilde{m}}^{-1/2} \Re\tilde{\Omega}^\alpha(\mathbf{k}, \tilde{m}) \quad (3.32)$$

$$\Im\tilde{\Omega}'^\alpha(\mathbf{k}, \tilde{m}) := \tilde{\Delta}_{\tilde{m}}^{-1/2} \Im\tilde{\Omega}^\alpha(\mathbf{k}, \tilde{m}) \quad (3.33)$$

¹In 4.2.2 we choose the excluded volume interaction such that the 1RS fields $\tilde{\Omega}^\alpha$ equal zero even for cross-link densities above $\mu^2 = 1$.

Details on this transformation are given in Appendix E. The corresponding free energy reads

$$\begin{aligned}
 & \mathcal{F}'(\{\tilde{\Omega}^\alpha\}, \Omega) \tag{3.34} \\
 = & \sum_{\alpha=0}^n \sum_{\tilde{\mathbf{k}}} \sum_{\tilde{m}} \tilde{\Delta}_{\tilde{m}} |\tilde{\Omega}^\alpha(\mathbf{k}, \tilde{m})|^2 + \frac{\mu^2}{2V^n} \overline{\sum_{\hat{\mathbf{k}}} \sum_{\tilde{m}} \Delta_{\tilde{m}} |\Omega(\hat{\mathbf{k}}, \tilde{m})|^2} \\
 & - \ln \left\langle \exp \left(2i \sum_{\alpha=0}^n \sum_{\tilde{\mathbf{k}}} \sum_{\tilde{m}} \tilde{\Delta}_{\tilde{m}} \Re \left(\tilde{\Omega}^\alpha \int_s e^{-i\mathbf{k}^\alpha \mathbf{r}^\alpha(s)} e^{-i\tilde{m}\check{\psi}(s)} \right) \right. \right. \\
 & \left. \left. + \frac{\mu^2}{V^n} \overline{\sum_{\hat{\mathbf{k}}} \sum_{\tilde{m}} \Delta_{\tilde{m}} \Re \left(\Omega \int_s e^{-i\hat{\mathbf{k}} \mathbf{r}(s)} e^{-i\tilde{m}\check{\psi}(s)} \right)} \right) \right\rangle_{n+1}^{\mathcal{H}_{WLC}}.
 \end{aligned}$$

Inserting the solutions of the corresponding saddle-point equations into (3.34) we will obtain the same free energy as before.

The advantage of this transformation is that for the new fields Ω'_{SP} there is a relation that attributes them a clear physical meaning:

$$\Omega'_{SP}(\hat{\mathbf{k}}, \tilde{m}) \sim \left[\frac{1}{N} \sum_{i=1}^N \int_s \left\langle e^{i\hat{\mathbf{k}} \mathbf{r}_i(s)} e^{i\tilde{m}\check{\psi}_i(s)} \right\rangle \right] \tag{3.35}$$

$$\tilde{\Omega}'_{SP}(\mathbf{k}, \tilde{m}) \sim \left[\frac{1}{N} \sum_{i=1}^N \int_s \left\langle e^{i\mathbf{k} \mathbf{r}_i^\alpha(s)} e^{i\tilde{m}\check{\psi}_i(s)} \right\rangle \right] \tag{3.36}$$

The fields now are related to disorder averaged expectation values of a physical observable. Here, we have written the \sim -symbol to indicate the use of the saddle-point approximation.

Chapter 4

Analysis of the model

4.1 Physical expectations

In this section, we discuss the expected behavior of our system and its dependence on the different model parameters, namely the cross-link density μ^2 , the polymer stiffness κ and the cross-linking angle θ .

First of all, upon gradually increasing the number of cross-links we expect a transition¹ from a **sol** phase, i.e. a fluid system consisting of single polymers and finite polymer clusters, to a **gel** where a macroscopic localized network has been formed. This transition has already been found for a variety of gelling systems where the formation of the random network is governed by a Deam-Edwards distribution. In [27] networks are considered consisting of polymers that are modeled as flexible, semiflexible and perfectly rigid filaments, and interconnections are formed by cross- or end-links. Moreover, in [23, 54] random networks of covalently bonded p-beine are considered and in [55] point particles are arranged into a networks by harmonic springs.

It is generically found that the sol-gel transition takes place at a critical cross-link density of $\mu^2 = 1$. Moreover, within the macroscopic cluster, the cross-linked objects are localized at random positions with a homogeneous distribution over the volume. This corresponds to the presence of **macroscopic translational invariance** (MTI) in the system. MTI means the following: because of the localization of the polymers within the macroscopic cluster, translational invariance is broken *microscopically*. However, there are no *macroscopic* features that allow one to notice an eventual shift of the system. MTI is a generic ingredient of all phases that we are going to consider.

With respect to our model it is, above all, the *orientational* structure

¹In this context we are not talking about a common thermodynamical phase transition: because of the permanent cross-links, we need to prepare a completely new network configuration every time that we change one of the parameters that influence the cross-linking process, i.e. when changing μ^2 or κ .

within the macroscopic cluster that we are interested in. Orientational order may emerge due to the orientational constraints of the cross-links.

Consider the idealized situation of a system built from stiff rods and from the perfectly strict orientational constraints (2.8). In the case of *sensitive* cross-links we start from one polymer and attach a second polymer to it such that they intersect with the prescribed crossing angle θ . If we repeat this

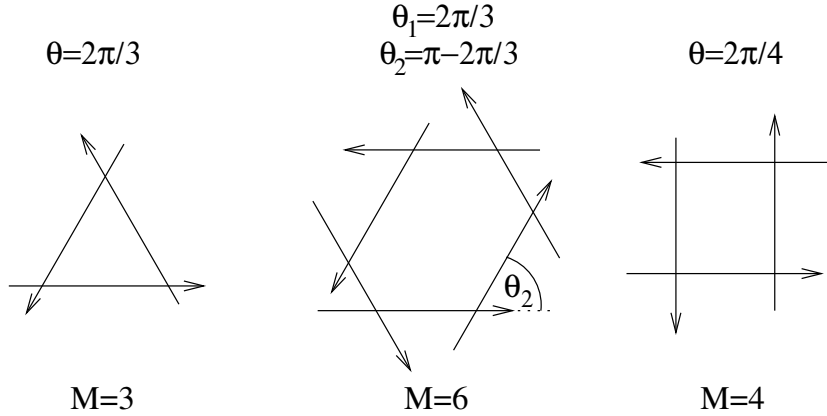


Figure 4.1: How the cross-links promote M -fold rotational symmetry. The first two pictures show the situations for $\theta = \frac{2\pi}{3}$ for sensitive and unsensitive cross-links. The picture on the right corresponds to $\theta = \frac{\pi}{2}$; here there is no difference between sensitive and unsensitive cross-links.

procedure successively by adding a third polymer to the second one and so on, and if θ equals an integer fraction of 2π , i.e. $\theta = \frac{2\pi}{M}$, we will recover the original direction after a full 2π -rotation. The cross-links thus suggest discrete M -fold rotational order in this idealized situation. This is easily generalized to the situation where θ is a rational multiple of 2π . The difference is that we will get back to the original direction only after several 2π -rotations. If, on the other hand, θ is an *irrational* multiple of 2π we will never again reach the original direction, but we get arbitrarily close to every angle. The corresponding symmetry thus is full isotropy.

In the case of *unsensitive* cross-links, it turns out that there is a difference between crossing-angles $\theta = \frac{2\pi}{M}$ with M being an odd number, and crossing-angles where M is an even number. For unsensitive cross-links, there are two possible cross-linking angles: besides $\theta_1 = \frac{2\pi}{M}$ there is also the second possibility of $\theta_2 = \pi - \frac{2\pi}{M}$ (see Fig. 2.3). This angle can be rewritten as $\theta_2 = \frac{M-2}{2M} \times 2\pi$. If M is odd this expression indicates that this second cross-linking angle gives rise to $2M$ -fold order in the system because $M - 2$ and $2M$ have no common prime factors. If M is even, nominator and denominator share a factor of 2 that cancels and we are back at an angle that gives rise to

M -fold order.

Given a cross-linking angle θ that corresponds to a discrete rotational symmetry, it will depend on the orientational correlation length of the semiflexible polymers, i.e. their bending stiffness, and the network structure if this symmetry may or may not be promoted throughout the system. Such an orientationally ordered phase is exotic insofar that it combines long-range orientational order with positional disorder. Note that for instance the tetratic phase that corresponds to $M = 4$ in our system has already been found in computer simulations of liquid crystal systems [15, 59] as well as in experiments [61, 37]. Sketches of gels with long-range four-fold order ($\theta = 90^\circ$) or long-range three-fold or six-fold order respectively ($\theta = 120^\circ / 60^\circ$) are shown in Fig. 4.2 and Fig. 4.3.

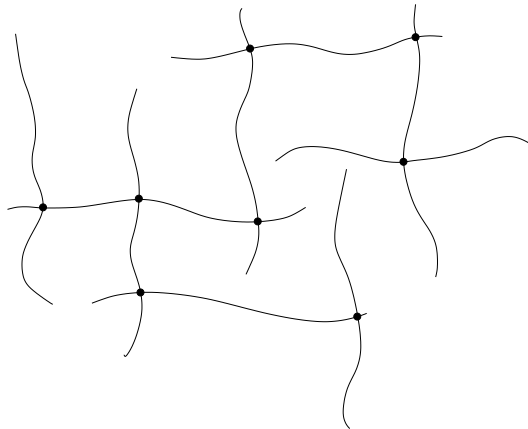


Figure 4.2: Sketch of the tetratic phase ($M=4$).

If a long-range discrete orientationally ordered state cannot be established, either because of the crossing angle or because of the before-mentioned reasons, there is always the possibility of an orientational glass. Here, the tangential vectors of the polymer segments are frozen in random directions in analogy to the low temperature phase of a spin glass [36, 1, 10]. We call such a state a statistically isotropic amorphous solid (SIAS). In analogy to the definition of MTI, there are no macroscopic features in the SIAS phase that would allow one to tell that a rotation of the system has happened, and we call this symmetry **macroscopic rotational invariance** (MRI) accordingly. For the long-range ordered case, on the other hand, isotropy is broken macroscopically and only a discrete rotational symmetry survives.

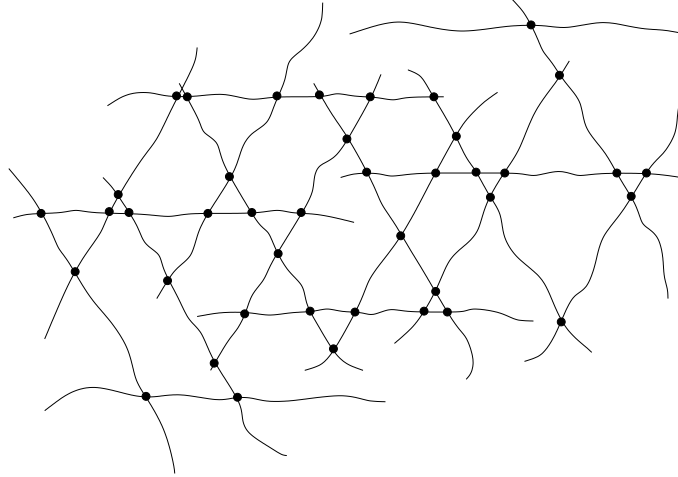


Figure 4.3: Sketch of the triangular phase ($M=3$) for sensitive cross-links or the hexatic phase ($M=6$) for unsensitive cross-links.

4.2 Discussion of the sol phase

Having discussed the physical expectations in the preceding section, we turn now to the mathematical analysis of our theory. First of all, we consider the trivial solution of the saddle-point equations (3.24) and (3.25) and their stability:

$$\tilde{\Omega}^\alpha(\mathbf{k}, \tilde{m}) = 0 \quad \text{and} \quad \Omega(\hat{\mathbf{k}}, \tilde{m}) = \delta_{\hat{\mathbf{k}}, \hat{\mathbf{0}}} \delta_{\tilde{m}, \tilde{0}} \quad . \quad (4.1)$$

This corresponds to a fluid state that is translationally and rotationally invariant as can be readily seen by the following argument. In a fluid phase every monomer (i, s) is free to explore the whole volume of the system and take any orientation. This leads then to an expectation value

$$\left\langle e^{i\hat{\mathbf{k}}\hat{\mathbf{r}}_i(s)} e^{i\tilde{m}\tilde{\psi}_i(s)} \right\rangle = \delta_{\hat{\mathbf{k}}, \hat{\mathbf{0}}} \delta_{\tilde{m}, \tilde{0}} \quad (4.2)$$

because the complex phases for non-vanishing $\hat{\mathbf{k}}$ and \tilde{m} cancel each other out. Inserting the above result into equations (3.35) and (3.36) it carries over to the fields and we find that the fluid phase is characterized by equation (4.1).

The next step is to clarify if this stationary point of \mathcal{F} is stable or not, i.e. if it corresponds to a minimum of the replica free energy or not. In order to

do so, we expand the replica free energy (3.22) in second order around zero:

$$\begin{aligned}
 \mathcal{F}(\{\tilde{\Omega}^\alpha\}, \Omega) &= \sum_{\alpha=0}^n \sum_{\tilde{\mathbf{k}}} \sum_{\tilde{m}} |\tilde{\Omega}^\alpha(\mathbf{k}, \tilde{m})|^2 + \frac{\mu^2}{2V^n} \overline{\sum}'_{\hat{\mathbf{k}}, \tilde{m}} |\Omega(\hat{\mathbf{k}}, \tilde{m})|^2 \quad (4.3) \\
 &+ 2 \sum_{\alpha=0}^n \sum_{\tilde{\mathbf{k}}_1, \tilde{\mathbf{k}}_2} \sum_{\tilde{m}_1, \tilde{m}_2} \tilde{\Omega}^\alpha(\mathbf{k}_1, \tilde{m}_1) \tilde{\Omega}^\alpha(\mathbf{k}_2, \tilde{m}_2) \sqrt{\tilde{\Delta}_{\tilde{m}_1}} \sqrt{\tilde{\Delta}_{\tilde{m}_2}} \times \\
 &\quad \times \int_{s_1, s_2} \left\langle e^{i(\mathbf{k}_1^\alpha \mathbf{r}^\alpha(s_1) + \mathbf{k}_2^\alpha \mathbf{r}^\alpha(s_2))} e^{i(\tilde{m}_1 \check{\psi}(s_1) + \tilde{m}_2 \check{\psi}(s_2))} \right\rangle \\
 &- \frac{\mu^4}{2V^{2n}} \overline{\sum}'_{\hat{\mathbf{k}}_1, \tilde{m}_1} \overline{\sum}'_{\hat{\mathbf{k}}_2, \tilde{m}_2} \Omega(\hat{\mathbf{k}}_1, \tilde{m}_1) \Omega(\hat{\mathbf{k}}_2, \tilde{m}_2) \sqrt{\Delta_{\tilde{m}_1}} \sqrt{\Delta_{\tilde{m}_2}} \times \\
 &\quad \times \int_{s_1, s_2} \left\langle e^{i(\hat{\mathbf{k}}_1 \hat{\mathbf{r}}(s_1) + \hat{\mathbf{k}}_2 \hat{\mathbf{r}}(s_2))} e^{i(\tilde{m}_1 \check{\psi}(s_1) + \tilde{m}_2 \check{\psi}(s_2))} \right\rangle + \mathcal{O}(\Omega^3)
 \end{aligned}$$

The symbol $\overline{\sum}'$ denotes the sum over $\hat{\mathbf{k}}$ taken from the 0RS and the HRS and all values of \tilde{m} leaving out $(\hat{\mathbf{0}}, \check{0})$ because the corresponding field corresponds to the normalization and thus equals 1.

In principle, there are also mixed terms of 1RS- and 0RS/HRS-fields in the second order contribution, but the corresponding coefficients vanish. In order to decide about the stability of the fluid phase, we need to analyze the eigenvalues of the kernel of the quadratic expression (4.3). The phase is stable as long as all the eigenvalues are positive. The gaussian contributions are already diagonal with positive eigenvalues 1, but for the log-trace contributions the situation is more involved. Here, the quadratic form is not diagonal and in order to obtain the eigenvalues we need to evaluate the correlation functions first. In the following two sections, we are going to discuss the stability for the combination of 0RS and HRS and the 1RS.

4.2.1 Stability of the 0RS and HRS

In order to study the stability of the 0RS and HRS we only need to consider the kernel of the second order log-trace contribution, that we will denote by \mathcal{K} , because the Gaussian contribution is already diagonal. The kernel reads

$$\begin{aligned}
 \mathcal{K}(\hat{\mathbf{k}}_1, \hat{\mathbf{k}}_2, \tilde{m}_1, \tilde{m}_2) &:= \sqrt{\Delta_{\tilde{m}_1}} \sqrt{\Delta_{\tilde{m}_2}} \int_{s_1, s_2} \left\langle e^{i(\hat{\mathbf{k}}_1 \hat{\mathbf{r}}(s_1) + \hat{\mathbf{k}}_2 \hat{\mathbf{r}}(s_2))} e^{i(\tilde{m}_1 \check{\psi}(s_1) + \tilde{m}_2 \check{\psi}(s_2))} \right\rangle \\
 &=: \sqrt{\Delta_{\tilde{m}_1}} \sqrt{\Delta_{\tilde{m}_2}} C_{\hat{\mathbf{k}}_1, \hat{\mathbf{k}}_2, \tilde{m}_1, \tilde{m}_2} \\
 &= \left(\sqrt{\Delta} C \sqrt{\Delta} \right) (\hat{\mathbf{k}}_1, \hat{\mathbf{k}}_2, \tilde{m}_1, \tilde{m}_2) \quad . \quad (4.4)
 \end{aligned}$$

The second line of (4.4) can be interpreted as a matrix multiplication of the correlation matrix C with two diagonal matrices $\sqrt{\Delta}$ having eigenvalues $\sqrt{\Delta_{\tilde{m}}}$. So far, we have not succeeded in calculating the exact eigenvalues of \mathcal{K} , but it

is possible to derive an upper boundary for their absolute values. With this result it will be possible to derive a boundary in the cross-link density μ^2 up to which the trivial solution is stable.

First of all, it is possible to diagonalize the correlation function C in the special case of stiff rods. Switching to angular variables instead of \tilde{m} , it becomes diagonal (see Appendix A.3 for details):

$$\begin{aligned} C(\hat{\mathbf{k}}_1, \hat{\mathbf{k}}_2, \check{\varphi}_1, \check{\varphi}_2) &= \int_{s_1, s_2} \left\langle e^{i(\hat{\mathbf{k}}_1 \hat{\mathbf{r}}(s_1) + \hat{\mathbf{k}}_2 \hat{\mathbf{r}}(s_2))} \delta(\check{\varphi}_1 - \check{\psi}(s_1)) \delta(\check{\varphi}_2 - \check{\psi}(s_2)) \right\rangle \quad (4.5) \\ &= \delta_{\hat{\mathbf{k}}_1, -\hat{\mathbf{k}}_2} \delta(\check{\varphi}_1 - \check{\varphi}_2) \int \frac{d\psi^{(0)}}{2\pi} \frac{2 - 2 \cos \left(\mathbf{k}^{(0)} \mathbf{t}_{\psi}^{(0)} + \check{\mathbf{k}} \check{\mathbf{t}}_{\varphi_1} \right)}{\left(\mathbf{k}^{(0)} \mathbf{t}_{\psi}^{(0)} + \check{\mathbf{k}} \check{\mathbf{t}}_{\varphi_1} \right)^2}. \end{aligned}$$

Having a closer look at the fraction inside the ψ -integration, it turns out that its values lie within the interval $[0, 1]$, i.e. the maximal eigenvalue is $c_{max} = 1$. This holds then for the eigenvalues of C too, because the integral over $\psi^{(0)}$ is normalized. With the knowledge of this boundary for the eigenvalues of C and having the eigenvalues of the matrices $\sqrt{\Delta}$, too, we can derive an upper boundary for the absolute value of the eigenvalues of \mathcal{K} by means of the inequality

$$|AB \mathbf{v}| \leq |a_{max}| |b_{max}| |\mathbf{v}| \quad (4.6)$$

for matrices A and B with maximal eigenvalues a_{max} and b_{max} and eigenvector \mathbf{v} . In our case, it follows from $|\sqrt{\Delta_{\tilde{m}}}| \leq 1$ and $c_{max} = 1$ that the absolute value of the eigenvalues of \mathcal{K} lies within the interval $[0, 1]$.

What does this imply for the stability of the solution $\Omega(\hat{\mathbf{k}}, \tilde{m}) = 0$? Assuming we had diagonalized \mathcal{K} , the HRS-contribution would have the form

$$\mathcal{F}_{HRS}(\Omega) = \frac{\mu^2}{2V^n} \sum_{\hat{\mathbf{k}}} \sum_{\tilde{m}} |\Omega(\hat{\mathbf{k}}, \tilde{m})|^2 \left(1 - \frac{\mu^2}{V^n} \mathcal{K}(\hat{\mathbf{k}}, \tilde{m}) \right). \quad (4.7)$$

In the limit $n \rightarrow 0$, the factors of V^{-n} can be omitted. Therefore, it follows from $|\mathcal{K}(\hat{\mathbf{k}}, \tilde{m})| \leq 1$ that the HRS part of the solution is stable up to at least $\mu^2 = 1$.

In the following, we show that the sol phase indeed becomes unstable for $\mu^2 > 1$. To this end, it is sufficient to find one direction in which variations lead to a decrease of the free energy. Consider for example the vector $\vec{\Omega}$ where only the entry $\Omega^*(\hat{\mathbf{k}}_0, \vec{0})$ with $\hat{\mathbf{k}}_0 := \{0, \mathbf{k}_0, -\mathbf{k}_0, 0, \dots\}$ is non-zero. For this special vector, that is in accordance with the MTI of the expected amorphous

solid phase, the correlation function C reads

$$\begin{aligned} C(-\hat{\mathbf{k}}_0, \hat{\mathbf{k}}_0, \check{0}, \check{0}) &= \int_{s_1, s_2} \left\langle e^{-i(\mathbf{k}_0 \mathbf{r}^{(1)}(s_1) - \mathbf{k}_0 \mathbf{r}^{(2)}(s_1))} e^{i(\mathbf{k}_0 \mathbf{r}^{(1)}(s_2) - \mathbf{k}_0 \mathbf{r}^{(2)}(s_2))} \right\rangle \\ &= \int_{s_1, s_2} J_0^2(k_0(s_1 - s_2)) \xrightarrow{k_0 \rightarrow 0} 1 \quad . \end{aligned} \quad (4.8)$$

The corresponding calculation was referred to Appendix A.3. Consequently, for the quadratic form in the limit of small k_0 we have

$$\begin{aligned} & \left| \Omega^*(\hat{\mathbf{k}}_0, \check{0}) \right|^2 \frac{\mu^2}{2V^n} \left(1 - \frac{\mu^2}{V^n} \int_{s_1, s_2} J_0^2(k_0(s_1 - s_2)) \right) \\ \xrightarrow{k_0 \rightarrow 0} & \left| \Omega^*(\hat{\mathbf{k}}_0, \check{0}) \right|^2 \frac{\mu^2}{2V^n} \left(1 - \frac{\mu^2}{V^n} \right) \\ & \leq 0 \quad \text{for } \mu^2 > 1 \end{aligned} \quad (4.9)$$

and it follows that it is precisely at $\mu^2 = 1$ that the first HRS modes of the order parameter become unstable.

4.2.2 Stability 1RS

The discussion of the stability of the 1RS part of (4.3) is very similar to that for the HRS in the preceding section. The correlation function of the log-trace part is a special case of the HRS correlation function and, hence, the eigenvalues of its correlation function lie within the range $[0, 1]$ too. What is different, however, are the matrices $\sqrt{\tilde{\Delta}^\alpha}$ because of the excluded volume interaction (2.11) that we introduced in order to provide stability for the 1RS:

$$\sqrt{\tilde{\Delta}_{\tilde{m}}^\alpha} = \sqrt{\frac{\lambda^2 N}{2V} \prod_{\beta \neq \alpha=1}^n \delta_{m^\beta, 0} - \frac{\mu^2}{2V^n} \Delta_{\tilde{m}}} \quad (4.10)$$

Without excluded volume interaction, i.e. $\lambda^2 = 0$, we have $\sqrt{\tilde{\Delta}_{\tilde{m}}^\alpha} = i \sqrt{\frac{\mu^2}{2V^n} \Delta_{\tilde{m}}}$ and the second expansion of the 1RS in (4.3) has the same coefficients as for the HRS. Consequently, we find in this case again, that the sol phase is stable up to the cross-link density of $\mu^2 = 1$, above which the first long wavelength modes become unstable.

However, as we are going to show in the following, the solution $\tilde{\Omega}^\alpha = 0$ of the 1RS saddle-point equation is linearly stable for arbitrary values of μ^2 , if we choose the excluded volume interaction to be strong enough. To that purpose we subdivide the fields of the 1RS, $\tilde{\Omega}^\alpha(\mathbf{k}, \tilde{m})$, into the fields with index \tilde{m} such that only the entry m^α is non-vanishing, and those fields corresponding to the other possible values of \tilde{m} . In the former case, the fields that we will denote

by $\Omega^\alpha(\mathbf{k}, m)$ describe M -fold orientationally symmetric density fluctuations with wave vector \mathbf{k} in replica α and thus have a clear physical meaning. The other fields, on the other hand, break replica symmetry insofar that they describe density fluctuations in replica α accompanied by purely orientational fluctuations in other replicas. Therefore, these fields are unphysical and need to equal zero.

In order to study the stability of the 1RS with respect to fluctuations of the physical fields $\Omega^\alpha(\mathbf{k}, m)$, it is sufficient to study stability for one replica only. The expansion of the corresponding free energy up to second order reads

$$\begin{aligned} \mathcal{F}_{1RS} = & \sum_{\tilde{\mathbf{k}}} \sum_{\mathbf{k}} |\tilde{\Omega}(\mathbf{k}, m)|^2 \\ & + 2 \sum_{\tilde{\mathbf{k}}_1, \tilde{\mathbf{k}}_2} \sum_{m_1, m_2} \tilde{\Omega}(\mathbf{k}_1, m_1) \tilde{\Omega}(\mathbf{k}_2, m_2) \\ & \sqrt{\tilde{\Delta}_{m_1}} \sqrt{\tilde{\Delta}_{m_2}} \underbrace{\int_{s_1, s_2} \langle e^{i(\mathbf{k}_1 \mathbf{r}_1 + \mathbf{k}_2 \mathbf{r}_2)} e^{i(m_1 \psi_1 + m_2 \psi_2)} \rangle}_{\mathcal{C}(\mathbf{k}_1, \mathbf{k}_2; m_1, m_2)}. \end{aligned} \quad (4.11)$$

If we choose $\lambda^2 > \mu^2$ the kernel $\tilde{\Delta}_m = \frac{\lambda^2}{2} - \frac{\mu^2}{2} \cos(m\theta)$ is positive. It is thus possible to redefine the fields by introducing $\bar{\Omega}(\mathbf{k}, m) := \sqrt{\tilde{\Delta}_m} \tilde{\Omega}(\mathbf{k}, m)$ without affecting the stability. The corresponding free energy is given by

$$\begin{aligned} \bar{\mathcal{F}}_{1RS} = & \sum_{\tilde{\mathbf{k}}} \sum_{\mathbf{k}} \frac{2}{\lambda^2 - \mu^2 \cos(m\theta)} |\bar{\Omega}(\mathbf{k}, m)|^2 \\ & + 2 \sum_{\tilde{\mathbf{k}}_1, \tilde{\mathbf{k}}_2} \sum_{m_1, m_2} \bar{\Omega}(\mathbf{k}_1, m_1) \bar{\Omega}(\mathbf{k}_2, m_2) \mathcal{C}(\mathbf{k}_1, \mathbf{k}_2; m_1, m_2) \end{aligned} \quad (4.12)$$

Let us now consider the two contributions to $\bar{\mathcal{F}}_{1RS}$ separately. It is evident that the first term is a positive quadratic form provided that λ^2 is large enough. The correlation function in the second contribution on the other hand is a special case of (4.5), and the second quadratic form in (4.12) is positive semi-definite.

Altogether, we have shown stability of the 1RS with respect to fluctuations around $\tilde{\Omega}^\alpha(\mathbf{k}, m) = 0$ provided that we have chosen the excluded volume interaction to be strong enough. Our argument applies for arbitrary values of the cross-link density μ^2 , but we had to restrict our analysis to the special case of stiff rods. Nevertheless, we believe that this result will hold for wormlike chains with finite bending rigidity as well.

4.3 Discussion of the gel phase

We found in the preceding section that the fluid phase is stable up to $\mu^2 = 1$. Above this threshold it becomes unstable, and to find a new stable minimum

we would need to find a new solution of the saddle-point equations (3.24) and (3.25). Unfortunately, the saddle-point equations are very complicated and so far, it has not been possible to solve them analytically.

As an alternative for obtaining information about the physics beyond the fluid phase, we are going to pursue a **variational approach**. The starting point is equation (3.35) which relates the field Ω_{SP} to the physical quantity Q , thus attributing a clear physical interpretation to Ω_{SP} . With that knowledge it is possible to construct Ansätze for Ω_{SP} based on physical assumptions and symmetry considerations in order to probe the appearance of different physical phases. The physical values of the variational parameters are then determined by inserting the Ansätze into the replica free energy \mathcal{F} , extracting the physical free energy $[F]$ as the coefficient linear in the replica index n , and minimizing $[F]$ with respect to the variational parameters.

4.3.1 Ansatz for the amorphous solid state

In this section we are going to derive variational Ansätze for the different physical states that we believe to be relevant in our system. In the first part, we present how we describe spatial and orientational localization of the polymers and the simplifications used. In the second part, we obtain the different Ansätze by including the corresponding symmetries.

The starting point of our considerations is equation (3.35):

$$\Omega_{SP}(\hat{\mathbf{k}}, \check{\varphi}) \sim \left[\frac{1}{N} \sum_{i=1}^N \int_s \left\langle e^{i\hat{\mathbf{k}}\hat{\mathbf{r}}_i(s)} \delta(\check{\varphi} - \check{\psi}_i(s)) \right\rangle_{n+1} \right] .$$

Here, a few simplifications are possible. Performing the disorder average before the average over the polymers $\frac{1}{N} \sum_i \int_s$ we can use the fact that the polymers are now equivalent and omit the sum over i . The individual monomers of a polymer may on the other hand display a behavior that depends on their position on the polymers contour: it makes a difference if a monomer is situated in the middle of the polymer or if it is situated close to an end. The reason is that at the ends of a polymer the probability that a cross-links is in the vicinity of a monomer is smaller and the monomers will be less localized. However, we *assume* all the polymer's monomers to be equivalent in order to simplify the expression further. It reads then

$$\Omega_{SP}(\hat{\mathbf{k}}, \check{\varphi}) \sim \left[\left\langle e^{i\hat{\mathbf{k}}\hat{\mathbf{r}}_i(s)} \delta(\check{\varphi} - \psi_i(s)) \right\rangle_{n+1} \right] \quad (4.13)$$

where (i, s) denotes some arbitrary monomer.

Within the macroscopic cluster we expect both positional and orientational localization of the polymers. In order to express localization mathematically

we decompose position vector and angle of orientation in a mean position and preferential orientation respectively and fluctuations around these values:

$$\begin{aligned}\mathbf{r}_i^\alpha(s) &= \mathbf{r}_{i,0}^\alpha + \Delta\mathbf{r}_i^\alpha(s) \quad ; \\ \psi_i^\alpha(s) &= \psi_{i,0}^\alpha + \Delta\psi_i^\alpha(s) \quad .\end{aligned}\tag{4.14}$$

We express now the disorder average [...] in terms of the distribution $\mathcal{P}(\hat{\mathbf{r}}_0, \check{\psi}_0)$ of mean positions and orientations of the monomers and obtain

$$\Omega_{SP}(\hat{\mathbf{k}}, \check{\varphi}) \sim \int d\hat{\mathbf{r}}_0 d\check{\psi}_0 \mathcal{P}(\hat{\mathbf{r}}_0, \check{\psi}_0) e^{i\hat{\mathbf{k}}\hat{\mathbf{r}}_0} \left\langle e^{i\hat{\mathbf{k}}\Delta\mathbf{r}_0} \delta(\check{\varphi} - (\check{\psi}_0 + \Delta\check{\psi}_0)) \right\rangle .\tag{4.15}$$

At this point we make the following simplifying assumptions:

- we assume that the joint distribution of mean position and orientations \mathcal{P} factorizes

$$\mathcal{P}(\hat{\mathbf{r}}_0, \check{\psi}_0) = \mathcal{P}_s(\hat{\mathbf{r}}_0) \times \mathcal{P}_o(\check{\psi}_0)\tag{4.16}$$

and introduce the separate distributions \mathcal{P}_s and \mathcal{P}_o of mean positions and orientations;

- we assume that positional and orientational fluctuations, $\Delta\mathbf{r}_i^\alpha(s)$ and $\Delta\psi_i^\alpha(s)$, are uncorrelated, i.e.

$$\left\langle e^{i\hat{\mathbf{k}}\Delta\mathbf{r}_0} \delta(\check{\varphi} - (\check{\psi}_0 + \Delta\check{\psi}_0)) \right\rangle = \left\langle e^{i\hat{\mathbf{k}}\Delta\mathbf{r}_0} \right\rangle \left\langle \delta(\check{\varphi} - (\check{\psi}_0 + \Delta\check{\psi}_0)) \right\rangle .\tag{4.17}$$

With these simplifications Ω_{SP} splits up into a spatial and an orientational part and reads

$$\begin{aligned}\Omega_{SP}(\hat{\mathbf{k}}, \check{\varphi}) &\sim \int d\hat{\mathbf{r}}_0 \mathcal{P}_s(\hat{\mathbf{r}}_0) e^{i\hat{\mathbf{k}}\hat{\mathbf{r}}_0} \left\langle e^{i\hat{\mathbf{k}}\Delta\mathbf{r}_0} \right\rangle \times \\ &\times \int d\check{\psi}_0 \mathcal{P}_o(\check{\psi}_0) \left\langle \delta(\check{\varphi} - (\check{\psi}_0 + \Delta\check{\psi}_0)) \right\rangle .\end{aligned}\tag{4.18}$$

Note that by this approach we incorporate rotational symmetries only into the orientational part of the Ansatz. This is, actually, not quite correct, because a rotation affects both position and tangential vectors

$$(\mathbf{r}, \varphi) \rightarrow (R_{\varphi_o} \mathbf{r}, \varphi + \varphi_o) \quad ,\tag{4.19}$$

where the matrix R_{φ_o} is supposed to express an arbitrary rotation with respect to some point by an angle φ_o .

We first consider the **spatial contribution**. In order to describe the spatial fluctuations we use a simple gaussian Ansatz. For a single replica it reads in Fourier space

$$\langle \delta(\mathbf{x} - \Delta\mathbf{r}_i(s)) \rangle = \frac{1}{2\pi\xi^2} e^{-\frac{1}{2\xi^2}\mathbf{x}^2} \quad \text{and} \quad \langle e^{i\mathbf{k}\Delta\mathbf{r}_i(s)} \rangle = e^{-\frac{\xi^2}{2}\mathbf{k}^2} .\tag{4.20}$$

The parameter ξ is the localization length.

As discussed in section 4.1, MTI is a generic ingredient to all amorphous solid phases considered here. It basically means that the mean position of each monomer $\mathbf{r}_{0,i}(s)$ is situated everywhere in the system with constant probability. Furthermore, we assume that for a given disorder configuration every monomer (i, s) is located at the *same* position in all $(n+1)$ replicas.² This assumption is equivalent to postulating **replica symmetry** and is mathematically expressed by

$$\mathcal{P}_s(\hat{\mathbf{r}}) = \int d\mathbf{r}_0 \prod_{\alpha=0}^n \delta(\mathbf{r}^\alpha - \mathbf{r}_0) \tilde{\mathcal{P}}_s(\mathbf{r}_0) \quad . \quad (4.21)$$

MTI implies furthermore that $\tilde{\mathcal{P}}_s(\mathbf{r}_0) = \frac{1}{V}$ and for the distribution of mean positions we obtain

$$\mathcal{P}_s(\hat{\mathbf{r}}) = \int \frac{d\mathbf{r}_0}{V} \prod_{\alpha=0}^n \delta(\mathbf{r}^\alpha - \mathbf{r}_0) \quad \text{and} \quad \mathcal{P}_s(\hat{\mathbf{k}}) = \delta_{\sum_{\alpha=0}^n \mathbf{k}^\alpha, \mathbf{0}} \quad (4.22)$$

in Fourier space. Altogether, the spatial contribution to Ω_{SP} is given by

$$\int_{\check{\varphi}} \Omega_{SP}(\hat{\mathbf{k}}, \check{\varphi}) = \delta_{\sum_{\alpha=0}^n \mathbf{k}^\alpha, \mathbf{0}} e^{-\frac{\xi^2}{2} \hat{\mathbf{k}}^2} \quad (4.23)$$

We now turn to the **orientational contribution**. We want to parametrize the orientational fluctuations by a 2π -periodic function and choose

$$\langle \delta(\varphi - \Delta\psi_i(s)) \rangle = \frac{1}{I_0(\eta)} e^{\eta \cos \varphi} \quad . \quad (4.24)$$

Here, the variational parameter η controls the variance of the orientational fluctuations around the preferred direction. I_0 denotes a modified Bessel function of the first kind.

We consider first the case of the **SIAS** that features MRI. Including isotropy and demanding that the mean orientation of one monomer must be the same in all replicas, i.e. $\psi_0^\alpha = \psi_0 \forall \alpha = 1, \dots, n$, we arrive at the following distributions of mean orientations:

$$\mathcal{P}_o(\check{\psi}) = \int \frac{d\psi_0}{2\pi} \prod_{\alpha=1}^n \delta(\psi^\alpha - \psi_0) \quad . \quad (4.25)$$

²Actually, the $(n+1)$ -fold replica symmetry is broken by our modified DE distribution. However, the positions in the cross-linking replica and the positions in the thermal replicas are definitely correlated; for simplicity we continue assuming full symmetry.

Altogether, for the orientational part of (4.18) we find

$$\begin{aligned}\Omega_{SP}(\hat{\mathbf{k}} = \hat{\mathbf{0}}, \check{\varphi}) &= \frac{1}{I_0^n(\eta)} \int_{\psi_0} e^{\eta \sum_{\alpha=1}^n \cos(\varphi^\alpha - \psi_0)} \\ &= \frac{1}{I_0^n(\eta)} I_0\left(\eta \left| \sum_{\alpha=1}^n \mathbf{t}^\alpha \right|\right).\end{aligned}\quad (4.26)$$

where $\check{\mathbf{t}}$ is defined by $\mathbf{t}^\alpha := (\sin \varphi^\alpha, \cos \varphi^\alpha)$.

What happens if there is long-range order with a discrete M -fold rotational symmetry? In this case, we consider two different Ansätze:

The simpler of the two possibilities is to require M equidistant preferential axes, but to leave aside the postulate that a monomer needs to have the same preferential direction in all the replicas. In this case the Ansatz for the distribution of preferred orientations \mathcal{P}_o is given by

$$\mathcal{P}_o(\check{\psi}_0) = \prod_{\alpha=1}^n \left(\frac{1}{M} \sum_{l=1}^M \delta\left(\psi_0^\alpha - \frac{2\pi}{M}l\right) \right) \quad (4.27)$$

and the corresponding orientational Ansatz reads

$$\Omega_{SP}(\hat{\mathbf{k}} = \hat{\mathbf{0}}, \check{\varphi}) = \prod_{\alpha=1}^n \left(\frac{1}{M} \sum_{l=1}^M \frac{1}{I_0(\eta)} e^{\eta \cos(\varphi^\alpha - \frac{2\pi}{M}l)} \right) . \quad (4.28)$$

In fact, there is a more compact way to write down an Ansatz incorporating the same symmetry

$$\Omega_{SP}(\hat{\mathbf{k}} = \hat{\mathbf{0}}, \check{\varphi}) = \frac{1}{I_0^n(\eta)} e^{\eta \sum_{\alpha=1}^n \cos(M\varphi^\alpha)} , \quad (4.29)$$

and we use this variant for our analysis.

The second Ansatz requires analogously to the SIAS that, if a polymer is orientationally localized to some direction in one replica, it is bound to point in the same direction within the other replicas, too. The corresponding distribution of preferential orientations then reads

$$\mathcal{P}_o(\check{\psi}) = \frac{1}{M} \sum_{l=1}^M \prod_{\alpha=1}^n \delta\left(\psi^\alpha - \frac{2\pi}{M}l\right) \quad (4.30)$$

and resulting orientational Ansatz is given by

$$\Omega_{SP}(\hat{\mathbf{k}} = \hat{\mathbf{0}}, \check{\varphi}) = \frac{1}{M} \sum_{l=1}^M \frac{1}{I_0^n(\eta)} e^{\eta \sum_{\alpha=1}^n \cos(\varphi^\alpha - \frac{2\pi}{M}l)} . \quad (4.31)$$

It is interesting to note that the distribution of mean orientations $\mathcal{P}_0(\check{m})$ expressed in Fourier space can be seen as the *signature* of the different symmetries that we incorporated into SIAS and the two M -fold symmetric Ansätze. In Fourier space we obtain

$$\mathcal{P}_o(\check{m}) = \delta_{\sum_{\alpha=1}^n m^{\alpha}, 0} \quad \text{for the SIAS,} \quad (4.32)$$

$$\mathcal{P}_{o,M1}(\check{m}) = \prod_{\alpha=1}^n \delta_{m^{\alpha}, \mathbb{Z}M} \quad \text{for the first } M\text{-fold Ansatz,} \quad (4.33)$$

$$\text{and} \quad \mathcal{P}_{o,M2}(\check{m}) = \delta_{\sum_{\alpha=1}^n m^{\alpha}, \mathbb{Z}M} \quad (4.34)$$

for the second M -fold Ansatz. The Kronecker deltas $\delta_{x, \mathbb{Z}M}$ are supposed to express that they are only non-zero if x is an integer multiple of M . The constraint on the modes \check{m} corresponding to the SIAS is much more restrictive than the constraint of the second M -fold Ansatz. This reflects the fact that the SIAS is more symmetric than the second M -fold Ansatz. Analogously, the symmetry operations of the first M -fold Ansatz comprise also those of the second M -fold Ansatz and consequently, the number of allowed modes \check{m} is smaller.

4.3.2 The Sol-Gel transition

As we have seen in the preceding sections, a gelation transition from a fluid to a gel phase will take place for a sufficient number of cross-links. In the gel phase a finite fraction of the particles belongs to the macroscopic cluster whereas the rest of the particles is still in a fluid state. Denoting the fraction of polymers belonging to the macroscopic cluster by Q , a general Ansatz for this gelation transition can be written as

$$\Omega(\hat{\mathbf{k}}, \check{m}) = (1 - Q) \delta_{\hat{\mathbf{k}}, \hat{\mathbf{0}}} \delta_{\check{m}, \hat{\mathbf{0}}} + Q \delta_{\sum_{\alpha} \mathbf{k}^{\alpha}, \mathbf{0}} \omega(\hat{\mathbf{k}}, \check{m}) \quad . \quad (4.35)$$

Here, $\omega(\hat{\mathbf{k}}, \check{m})$ describes the properties of the amorphous solid part and Q denotes the gel fraction, i.e. the fraction of particles that are localized. The Kronecker delta $\delta_{\sum_{\alpha} \mathbf{k}^{\alpha}, \mathbf{0}}$ imposes MTI that is present in all of our Ansätze. Inserting the generic Ansatz into the free energy (3.34) we obtain

$$\begin{aligned} & \mathcal{F}_{sp} \quad (4.36) \\ = & \frac{\mu^2}{2V^n} \left\{ 1 - Q^2 + Q^2 \overline{\sum_{\hat{\mathbf{k}}} \int_{\check{\varphi}\check{\varphi}'} \omega(\hat{\mathbf{k}}^2, \check{\varphi}) \Delta(\check{\varphi} - \check{\varphi}', \theta) \omega(\hat{\mathbf{k}}^2, \check{\varphi}') \delta_{\mathbf{0}, \sum_{\alpha=0}^n \mathbf{k}^{\alpha}} \right\} \\ & - \frac{\mu^2}{V^n} (1 - Q) - \ln \left\langle \exp \left\{ \frac{\mu^2 Q}{V^n} \overline{\sum_{\hat{\mathbf{k}}} \int_{\check{\varphi}\check{\varphi}'} \delta_{\mathbf{0}, \sum_{\alpha=0}^n \mathbf{k}^{\alpha}} \times \right. \right. \\ & \quad \left. \left. \times \Delta(\check{\varphi} - \check{\varphi}', \theta) \omega(\hat{\mathbf{k}}^2, \check{\varphi}) \int_s e^{i\hat{\mathbf{k}}\hat{\mathbf{r}}(s)} \delta(\check{\varphi}' - \check{\varphi}(s)) \right\} \right\rangle_{n+1}^{\mathcal{H}_{WLC}}, \end{aligned}$$

where the first line contains the gaussian contributions and second and third lines contain the log-trace contributions.

In order to derive the equation for the gel fraction Q we proceed analogously to [21]. Castillo *et al.* argue that the gel fraction can be obtained by considering only the non-intensive part of the free energy that consists of terms that are proportional to $\ln V$ in the limit $n \rightarrow 0$. The existence of these contributions is due to the omission of Gibbs symmetry factors in the configurational integral which would render the calculation impossible. In our case, we need to keep contributions up to Q^3 in order to obtain a non-trivial result. The expansion of the log-trace part up to that order reads schematically

$$-\ln \langle \exp(x) \rangle = -\langle x \rangle - \frac{1}{2} \{ \langle x^2 \rangle - \langle x \rangle^2 \} - \frac{1}{6} \langle x^3 \rangle - \frac{1}{3} \langle x \rangle^3 + \frac{1}{2} \langle x \rangle \langle x^2 \rangle \quad . \quad (4.37)$$

as the $\ln V$ -terms are related to the spatial part of the free energy only, the calculation of the gel fraction is the same for all Ansätze that we are going to consider. Collecting the relevant terms from (4.36) and Appendix B we obtain

$$F_{\text{gel-frac}} = \ln V \left\{ \frac{\mu^2 Q^2}{2} (1 - \mu^2) + \frac{\mu^6 Q^3}{6} + \mathcal{O}(Q^4) \right\} \quad . \quad (4.38)$$

Taking the derivative with respect to Q we obtain the result

$$Q = \begin{cases} 0 & \text{for } \mu^2 < 1 \\ \frac{2}{\mu^4} (\mu^2 - 1) & \text{for } \mu^2 \geq 1 \end{cases} \quad . \quad (4.39)$$

This equation has already been derived for a great number of systems that share the cross-linking mechanism described by the Deam-Edwards distribution [23, 21, 55, 56]. This result is in agreement with our stability analysis of the sol phase and in addition shows that the gel fraction increases linearly in μ^2 .

Chapter 5

Hard cross-links

5.1 M-fold long-range order

In this section we are going to investigate the requirements for the appearance of long-range orientational order. As we already discussed in 4.1 we believe that long-range M -fold symmetric order might be present, if the crossing angle θ is suitable, i.e. if $\theta = k\frac{2\pi}{M}$. Moreover, we expect that the emergence of long-range orientational order will depend crucially on the polymer's bending stiffness κ .

In 4.3.1 we derived a simple Ansatz for M -fold orientational symmetry that favors M orientational axes separated equidistantly by angles of $\frac{2\pi}{M}$. The full replica order parameter reads then

$$\omega(\hat{\mathbf{k}}, \varphi) = e^{-\frac{\xi^2}{2}\hat{\mathbf{k}}^2} \frac{e^{\eta \sum_{\alpha=1}^n \cos(M\varphi^\alpha)}}{I_0^n(\eta)} \quad . \quad (5.1)$$

Setting $\hat{\mathbf{k}} = \hat{\mathbf{0}}$, the order parameter equals the orientational probability distribution. In experiment, on the other hand, one has access to low order moments only. The simplest physical order parameter that is sensitive to the degree of long-range M -fold orientational order is given by

$$\mathcal{S}_M := \frac{1}{N} \sum_{i=1}^N \int_s \left\langle \cos(M\psi_i(s)) \right\rangle \quad (5.2)$$

and the question is how \mathcal{S}_M is related to the variational parameter η . As it

turns out, the physical order parameter goes in lowest order linearly with η :

$$\begin{aligned}
 \mathcal{S}_M &:= \frac{1}{N} \sum_{i=1}^N \int_s \langle \cos(M\psi_i(s)) \rangle & (5.3) \\
 &\sim \left[\langle \cos(M\psi_i(s)) \rangle \right] \\
 &= \int_{\varphi} \cos(M\varphi) \left[\langle \delta(\varphi - \psi_i(s)) \rangle \right] \\
 &\sim \int_{\varphi} \cos(M\varphi) \frac{1}{I_0(\eta)} e^{\eta \cos(M\varphi)} \\
 &= \frac{\eta}{2} + \mathcal{O}(\eta^2)
 \end{aligned}$$

In order to establish this connection, we used the self-averaging property and replaced the average over the polymers of the system by the disorder average. After that, it is possible to express the resulting expectation value in the third line in terms of the order parameter ω that depends on η .

We insert the Ansatz (5.1) in (4.36) and perform the $\hat{\mathbf{k}}$ summations and $\check{\varphi}$ integrations. If we have chosen M according to the symmetry considerations of section 4.1 the constraint Δ acts like a normal delta function on the fields ω and just eliminates one of the φ -integrations. We are left with the free energy as a function of three variational parameters: the gel fraction Q , the spatial localization length ξ and the degree of orientational order as measured by η . Their physical values are determined by the minimum of the free energy that we expand in lowest non-trivial order.

The behavior of the gel fraction Q has already been discussed in section 4.3.2. We need to include terms up to order Q^3 in order to get a non-trivial equation for the gel fraction. As for spatial localization, i.e. the behavior of ξ , it will turn out that $\frac{1}{\xi^2} \propto Q$. As the second order term of the log-trace part is already contributing a factor of Q^2 we include only terms up to linear order in $\frac{1}{\xi^2}$ in our expansion. On the other hand, this is sufficient to obtain non-trivial results. As for the variational parameter η , we will find that it actually jumps from zero to a finite value, i.e. that there is a first order orientational transition. Hence, it is not possible to do a systematic expansion in η . We expand the free energy all the same in η hoping to obtain at least a qualitatively correct picture. Details on the calculations are given in Appendix B.

Leaving out terms which do not depend on ξ or η and hence do not influence the position of the minimum of \mathcal{F} we obtain the following variational free

energy:

$$\begin{aligned}
 \frac{\mathcal{F}}{n} = \frac{\mu^2 Q^2}{2} & \left\{ -\frac{\mu^4 Q}{6} \ln \frac{L^2}{\xi^2} + \frac{\mu^2 L^2}{4\xi^2} g\left(\frac{L}{L_p}\right) \right. \\
 & + \delta_{M,1} \frac{\mu^2 L^2}{4\xi^2} \left\{ \eta^2 l\left(\frac{L}{L_p}\right) - \frac{\eta^4}{16} \tilde{l}\left(\frac{L}{L_p}\right) + \frac{\eta^6}{16} \tilde{\tilde{l}}\left(\frac{L}{L_p}\right) \right\} \\
 & + \frac{\eta^2}{2} \left(1 - \mu^2 h\left(\frac{M^2 L}{L_p}\right) \right) - \frac{7}{32} \eta^4 \left(1 - \mu^2 \tilde{h}\left(\frac{M^2 L}{L_p}\right) \right) \\
 & \left. + \frac{31}{288} \eta^6 \left(1 - \mu^2 \tilde{\tilde{h}}\left(\frac{M^2 L}{L_p}\right) \right) \right\}
 \end{aligned} \tag{5.4}$$

Note that for $M > 1$ this expansion of \mathcal{F} does not contain any terms that lead to a coupling of spatial and orientational behavior. Such terms will appear in higher order, but are not considered here because we restrict ourselves to the vicinity of the gel point.

The bending stiffness κ and the localization length ξ^2 are rescaled by the contour length L of the polymers. The functions g , h , \tilde{h} , $\tilde{\tilde{h}}$ and l , \tilde{l} , $\tilde{\tilde{l}}$ go to zero for large argument and are for small argument approximately given by

$$\begin{aligned}
 g(x) & \sim \frac{1}{6} - \frac{1}{30}x & (5.5) \\
 h(x) & \sim 1 - \frac{1}{3}x \quad , \quad \tilde{h}(x) \sim 1 - \frac{8}{21}x \quad , \quad \tilde{\tilde{h}}(x) \sim 1 - \frac{48}{93}x \\
 l(x) & \sim \frac{1}{6} - \frac{1}{10}x \quad , \quad \tilde{l}(x) \sim \frac{1}{3} - \frac{1}{5}x \quad , \quad \tilde{\tilde{l}}(x) \sim \frac{125}{72} - \frac{61}{30}x
 \end{aligned}$$

For the definitions of these functions see Appendix B.3.

The case $M \geq 2$

Demanding stationarity of \mathcal{F} (in the case $M \geq 2$) with respect to ξ^2 yields for the localization length the value

$$\frac{1}{\xi^2} = \frac{2}{3L^2} \frac{\mu^2 Q}{g\left(\frac{L}{L_p}\right)} = \frac{\mu^2 Q}{3R_g^2} \tag{5.6}$$

that corresponds to a minimum as can be seen easily from the form of the free energy (5.4). Hence the filaments are localized as soon as a percolating cluster of cross-linked chains has formed and the gel fraction is finite. The localization length is independent of M and its scale is set by the radius of gyration R_g^2 of the filament which is $\propto L^2$ for stiff chains and $\propto LL_p$ for random coils (see chapter 2.1 for details).

In Fig. 5.1 the generic transition scenario is depicted: for finite stiffness $\frac{L}{L_p}$ the incipient gel has no long-range orientational order. Increasing the number of cross-links beyond $\mu^2 = 1$ we find a first-order transition that corresponds to a minimum of the free energy at nonzero η , which is first metastable and eventually becomes the global minimum. The critical values of μ^2 for the first appearance of a metastable ordered state (μ_1^2), the first order phase transition (μ_2^2) and the disappearance of the metastable disordered state (μ_3^2) are shown in Fig. 5.2. In the limit $L_p \rightarrow \infty$ the phase transition coincides with the sol-gel transition, whereas for more flexible filaments higher cross-link densities are required. In the limit of stiff polymers we find that the transition takes place at

$$\mu_2^2 \sim 1 + 0.3303 M^2 L/L_p + \mathcal{O}\left(\left(M^2 L/L_p\right)^2\right) . \quad (5.7)$$

This equation is easily obtained from (5.4) by looking for the value of μ^2 where a non-trivial, positive zero of the purely orientational free energy as a function of η^2 appears. In addition, Fig. 5.2 shows the dependence of η_c , which is the non-zero value of the variational parameter η right at the phase transition, on the polymer flexibility. There is a tendency to a lower degree of orientational localization for higher values of the polymer stiffness which is surprising at first sight. On the other hand, the appearance of long-range order depends not only on the polymer stiffness but also on the cross-link density in the system. The critical density of cross-links μ_2^2 of the transition *decreases* for increasing polymer stiffness and there are thus two competing effects: stiffer polymers should lead to a stronger orientational localization of the polymers whereas the smaller number of cross-links should have the opposite effect. It seems that in our case the lower number of cross-links plays the dominant role in the dependence of $\eta_c(L/L_p)$.

We point out that the cross-linking angle $\theta = 2\pi/M$ enters the free energy as a rescaling of the polymer flexibility L/L_p through the parameter M^2 . This implies that the higher the value of M (the smaller the angle), the higher the polymer stiffness required for the transition at a given cross-link density. The reason for this scaling is that within our mean-field description we are dealing with one single chain in an effective medium. M -fold order has to be propagated along the chain from one cross-link to the next and the quadratic M^2 scaling reflects the properties of the WLC in the calculation of the corresponding correlator (see in Appendix B.3 equations (B.18) and following).

For a first-order transition the expansion in η^2 is not really justified and can only give qualitative results. Even worse, the expansion of \mathcal{F} in η^2 exhibits an oscillating behavior: the expansions up to order 2, 6, 10, ... provide a stable orientational free energy in a region around $\mu^2 = 1$ and $\frac{L}{L_p} = 0$, but the orders 4, 8, 12, ... are always unstable in the above region because they diverge asymptotically to minus infinity. However, considering the purely orientational

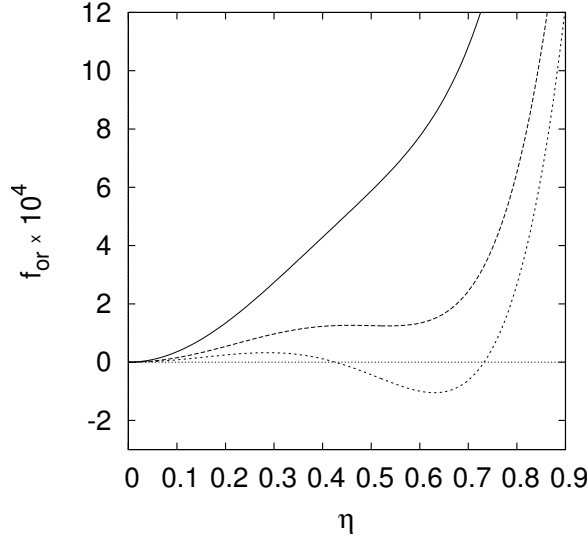


Figure 5.1: Plot of the orientational free energy of the 3-fold symmetric case for $L/L_p = 0.05$ and $\mu^2 = 1.1470, 1.1518, 1.1535$.

free energy

$$f_{or,hard} := \frac{\mu^2 Q^2}{2} \left\{ \ln \left(1 + 2 \sum_{q=1}^{\infty} \frac{I_q^2(\eta)}{I_0^2(\eta)} \right) - \mu^2 \int_{s_1, s_2} \ln \left(1 + 2 \sum_{q=1}^{\infty} \frac{I_q^2(\eta)}{I_0^2(\eta)} e^{-\frac{q^2 M^2}{2\kappa} |s_1 - s_2|} \right) \right\} \quad (5.8)$$

that we derive in Appendix (B.3) it is obvious that fixing the polymer stiffness κ to some finite value the gaussian part is larger than the log-trace contribution as long as the cross-link density μ^2 does not become too large. So, as long as we restrict ourselves to a region close enough to the sol-gel transition asymptotic stability is guaranteed and an at least qualitative picture can be obtained by truncating the expansion at order 6, 10 or even higher.

Polar ordering: $M = 1$

For the polar case, i.e. $M = 1$, there are additional terms in the free energy (5.4) which couple spatial and orientational part. At first sight it is tempting to argue that they can be neglected close to the transition because they are proportional to $\frac{1}{\xi^2} \sim Q$. On the other hand, the orientational transition is first order, i.e. η jumps to a finite value, and occurs for a given value of κ at a finite distance from the sol-gel transition, so that the fraction $\frac{\eta^2}{\xi^2}$ has become finite. Although the coupling term gives only a small contribution in the case

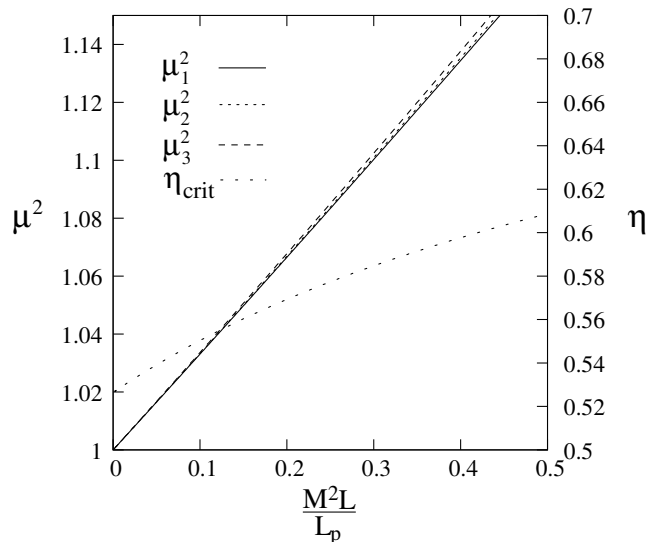


Figure 5.2: Variational parameter of the incipient ordered state η_c and cross-link densities μ_1^2 , μ_2^2 and μ_3^2 where a metastable ordered minimum appears, where it becomes the global minimum (phase transition) and where the minimum at zero corresponding to the disordered state becomes unstable respectively. Note that always $\mu_1^2 < \mu_2^2 < \mu_3^2$ for finite stiffness.

of rather stiff polymers it turns out not to be negligible: the orientational transition for a given polymer stiffness is shifted to significantly higher values of μ^2 . But still, the qualitative picture of the transition is valid.

In order to analyze the orientational transition we first calculate the stationarity equation with respect to $1/\xi^2$

$$\frac{L^2}{\xi^2} = \frac{2}{3} \frac{\mu^2 Q}{g(\frac{L}{L_p}) + \eta^2 l(\frac{L}{L_p}) - \frac{\eta^4}{16} \tilde{l}(\frac{L}{L_p}) + \frac{\eta^6}{16} \tilde{\tilde{l}}(\frac{L}{L_p})} \quad (5.9)$$

and insert the result again into the free energy (5.4). As it turns out, it is only the $\ln \frac{1}{\xi^2}$ -term that gives rise to new orientational contributions. Keeping terms up to order η^6 we obtain again a power series in η^2 . Numerical studies of this orientational free energy show that the transition scenario that we found for $M \geq 2$ is still valid, but the transition takes place at values of μ_2^2 that are larger with respect to what we would have obtained without coupling terms, i.e. compared to the μ_2^2 obtained from equation (5.7) by setting $M = 1$. In the limit of very stiff polymers we find approximately

$$\mu_2^2 \sim 1 + 0.9384 L/L_p + \mathcal{O}\left(\left(L/L_p\right)^2\right) \quad . \quad (5.10)$$

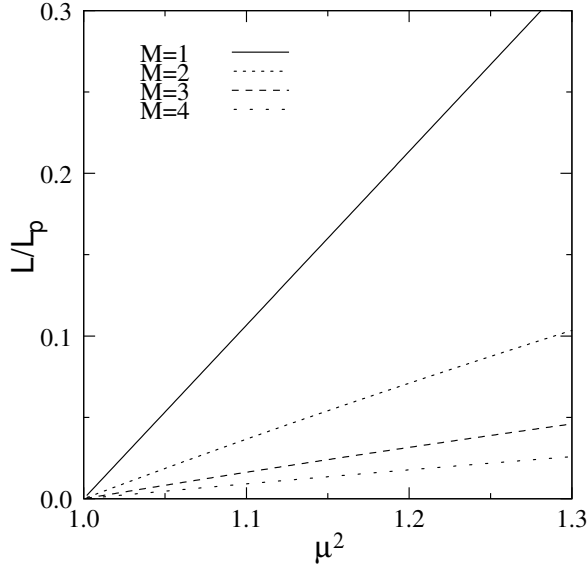


Figure 5.3: Phase boundaries for $M = 1, 2, 3, 4$: the higher the symmetry, the later the transition takes place.

The limit of stiff rods

The expectation for stiff rods is that the emergent macroscopic cluster is completely rigid, even right at the transition point where it is tree-like structure. Perfect positional and orientational localization correspond to $\frac{1}{\xi^2} = \eta = \infty$. Trying to describe such a transition by a Taylor expansion is thus a lost cause from the beginning. Not surprisingly, neither the behavior of ξ nor the behavior of η obtained from the approximated free energy (5.4) indicate a divergence of the degree of localization. However, considering the full orientational free energy (5.8) for infinite values of the bending stiffness κ , it can be written as

$$f_{or,hard} = \frac{\mu^2 Q^2}{2} (1 - \mu^2) \ln \left(1 + 2 \sum_{q=1}^{\infty} \frac{I_q^2(\eta)}{I_0^2(\eta)} \right). \quad (5.11)$$

The expression inside the logarithm being a monotonic increasing function in η , we find that it correctly predicts a phase transition right at $\mu^2 = 1$ from $\eta = 0$ to $\eta = \infty$, i.e. from the isotropy in the fluid phase to a perfectly rigid network in the gel phase.

Mismatch of θ and the M -fold Ansatz

So far, we were looking for long-range order in the case that the relation $\theta = k \frac{2\pi}{M}$ holds as suggested by the symmetry considerations of section 4.1. But what happens if cross-linking angle and M -fold Ansatz do not match?

As we show in Appendix B the gaussian contribution to the orientational free energy in its version for general θ can be written as

$$f_{or} = \frac{\mu^2 Q^2}{2} \left\{ \ln \left(\frac{I_0(2\eta \cos(M\theta/2))}{I_0^2(\eta)} \right) - \mu^2 \int_{s_1, s_2} \ln \left(1 + 2 \sum_{q=1}^{\infty} \frac{I_q^2(\eta)}{I_0^2(\eta)} e^{-\frac{q^2 M^2}{2\kappa} |s_1 - s_2|} \right) \right\}. \quad (5.12)$$

In Appendix B.1 we show that the gaussian contribution in the first line is asymptotically stable only as long as the before-mentioned relation between θ and M holds. An instability of the Gaussian leads to an instability of the complete orientational free energy, too, because the log-trace contribution itself is always asymptotically unstable. So, we see that if angle and Ansatz do not match, the orientational free energy is no longer well behaved.

One could interpret this result as an indication that long-range M -fold orientational order was only possible for crossing angles θ that perfectly match the symmetry. But in fact, this would be a quite artificial and somewhat unphysical result. We would rather expect long-range order to be possible as long as θ lies within a tolerance interval that may be very small, but finite. Moreover, how can we claim that there is no long-range orientational order possible for θ being an irrational multiple of 2π if each irrational number can be approximated arbitrarily well by rational numbers?

We believe that this behavior is an artifact of our model, possibly due to the hard orientational cross-link constraints. In chapter 6, we will explore the physics of the alternative model featuring soft cross-links that allow to a certain degree thermal fluctuations around the mean crossing angle.

5.2 Statistically isotropic amorphous solid

We found in the preceding section that (given a suitable cross-linking angle θ) there is a phase boundary $\mu^2(\frac{L}{L_p})$ above which long-range orientational order becomes possible. For lower cross-link densities, long-range orientational order vanishes. But the positional localization of the polymer segments that takes place in the macroscopic cluster is always accompanied by orientational localization. The corresponding alternative to long-range orientational order is a glassy state, where the average orientations of the polymer segments are frozen in random directions, so that isotropy is restored on a macroscopic level. We call this state a “statistically isotropic amorphous solid” (SIAS). We expect the SIAS for WLCs with a small persistence length, such that the order induced by a cross-link cannot be sustained along the contour length L of the chain.

Frozen orientations for polar filaments are described by the distribution (4.24) for a single site. However the direction of localization fluctuates from chain to chain, so that averaging over the whole sample implies an average over the locally preferred orientation φ_0 assuming all directions to be equally likely. For convenience we introduce the unit vectors $\mathbf{u}^\alpha = (\cos \varphi^\alpha, \sin \varphi^\alpha)$ and denoting the local preferential axes by \mathbf{e} we get

$$\int \frac{d\mathbf{e}}{2\pi} \exp\left(\eta \mathbf{e} \cdot \left(\sum_{\alpha=1}^n \mathbf{u}^\alpha\right)\right) = I_0\left(\eta \left|\sum_{\alpha=1}^n \mathbf{u}^\alpha\right|\right). \quad (5.13)$$

Altogether the order parameter for polar filaments in the glassy state then reads

$$\omega(\hat{\mathbf{k}}, \varphi) = e^{-\frac{\xi^2}{2} \hat{\mathbf{k}}^2} \frac{1}{I_0^n(\eta)} I_0\left(\eta \left|\sum_{\alpha=1}^n \mathbf{u}^\alpha\right|\right). \quad (5.14)$$

What is the physical order parameter and how does it scale with the parameter η ? Locally, we have for each localized polymer segment a finite polar moment $\langle \mathbf{t}_i(s) \rangle$. But macroscopically, i.e. summing the local polarization $\langle \mathbf{t}_i(s) \rangle$ over the whole sample, the polar moment is going to vanish because the polymers are pointing into isotropically distributed random directions. In order to detect this random orientational localization we need thus an Edwards-Anderson like order parameter that sums up the squares and choose

$$q_{EA} := \frac{1}{N} \sum_{i=1}^N \int_s \langle \mathbf{t}_i(s) \rangle \cdot \langle \mathbf{t}_i(s) \rangle. \quad (5.15)$$

With the same reasoning as for the M -fold order parameter in the preceding section (see equation (5.3)), we relate the variational parameter η to q_{EA} and find that

$$q_{EA} = \frac{\eta^2}{4} + \mathcal{O}(\eta^4) \quad (5.16)$$

for small η .

When calculating the SIAS free energy, we find for the gel fraction Q the same result as for the M -fold. On the other hand, we find in contrast to the M -fold that the localization length $\frac{1}{\xi^2}$ and the orientational order parameter η^2 scale linearly in the gel fraction Q and so, a Taylor expansion is justified as long as we stay close to the sol-gel transition point. As it turns out, we obtain the simplest non-trivial orientational free energy by including terms up to second order in η^2 and up to linear order in $\frac{1}{\xi^2}$. It reads

$$\begin{aligned} \frac{\mathcal{F}}{n} = & \frac{\mu^2 Q^2}{2} \left\{ -\frac{\mu^4 Q}{6} \ln \frac{L^2}{\xi^2} + \mu^2 \frac{L^2}{4\xi^2} g\left(\frac{L}{L_p}\right) \right. \\ & \left. -\frac{\eta^4}{16} \left(1 - \mu^2 h\left(\frac{2L}{L_p}\right)\right) + \frac{\eta^2 L^2}{8\xi^2} \mu^2 l\left(\frac{L}{L_p}\right) \right\}. \end{aligned} \quad (5.17)$$

The functions g, h, l are given approximately by (5.5) in the M -fold section. Minimizing the above free energy with respect to ξ^2 , yields in this order the same result as for the long-range ordered state, namely

$$\frac{L^2}{\xi^2} = \frac{2}{3} \frac{\mu^2 Q}{g(\frac{L}{L_p})}. \quad (5.18)$$

For the orientational part on the other hand, we find a different behavior. The stationarity equation with respect to η^2 gives rise to

$$\eta^2 = \frac{L^2}{\xi^2} \frac{\mu^2 l(\frac{L}{L_p})}{1 - \mu^2 h(\frac{2L}{L_p})} \quad (5.19)$$

The coupling term in (5.17) implies a non-zero value η^2 , i.e. orientational localization, as soon as positional localization sets in. Hence glassy orientational order is enslaved to positional localization and the orientational order parameter grows continuously at the gelation transition.

Increasing the density of cross-linkers μ^2 for a given finite polymer stiffness where the function $h(\frac{2L}{L_p})$ is smaller than 1, the denominator on the right hand side of (5.19) approaches zero, thus giving rise to a diverging η^2 . This behavior has no physical significance but marks the breakdown of our second order approximation of the orientational part when the η^4 -coefficient in (5.17) becomes unstable.

Note that, in contrast to the M -fold ordered case, the limit $n \rightarrow 0$ leads in the SIAS free energy to an extra minus sign for all the orientational contributions because of the coupling of the replicas in the corresponding order parameter (5.14). As a consequence, we have to maximize the free energy with respect to η instead of minimizing it as it is well known from spin glasses [17, 42].

5.3 Phase diagram

The results of the previous sections can be summarized in a phase diagram presented in Fig. 5.4¹. The control parameters are the cross-link density measured by μ^2 and the polymer flexibility measured by L/L_p . Irrespective of the stiffness of the filaments there is a continuous gelation transition accompanied by random local orientational ordering (SIAS phase) at the critical cross-link density $\mu_c^2 = 1$. This glassy ordering has been encountered previously for randomly linked molecules with many legs (p -Beine) [23, 54] and in the previous

¹When reading the phase diagram, one should keep in mind that the parameters μ^2 and L/L_p are *not* thermodynamic ones like a temperature or a chemical potential because changing either of them changes the disorder ensemble, too. This means that two points in the phase diagram correspond effectively to two *different* systems.

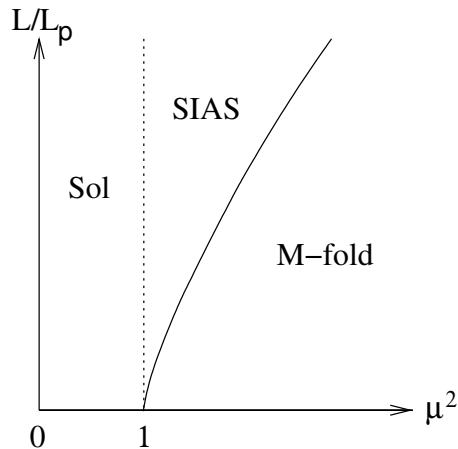


Figure 5.4: The generic phase diagram.

work of Benetatos and Zippelius on bundled semiflexible polymers [9]. The free energy of the SIAS is above the free energy of the sol, which however is unstable beyond $\mu^2 = 1$ (see section 4.2 for details) and hence, is not available in this region of the phase diagram.

What is new, is the appearance of a state with long-range orientational order, if the crossing angle $\theta = \frac{k}{M} 2\pi$ where $k, M \in \mathbb{Z}$. This phase is characterized by a spontaneous breaking of the rotational symmetry. For sensitive cross-links the symmetry of the orientational order is M -fold, for unsensitive cross-links and odd M the resulting phase has $2M$ -fold symmetry. The M -fold symmetric phase requires additional cross-linking well beyond the density where the gelation transition occurs and the SIAS becomes possible. The free energy of the long ranged ordered state is below the free energy of the isotropic sol as well as below the free energy of the SIAS. Hence, we expect it to win as soon as it appears, even though we cannot do a complete stability analysis beyond the variational Ansatz.

We find that the appearance of long-range order is pushed to higher values of μ^2 as the flexibility of the polymers is increased because it becomes more difficult to sustain the orientation of the polymers along the chain. Furthermore, it turns out that the larger the value of M the more cross-links are needed in order to reach the phase transition.

Although our variational Ansatz for long-range range M -fold order works only in the case of $\frac{2\pi}{\theta}$ being a rational number, we believe that the above phase diagram holds quite generically. A distinction between rational and irrational numbers seems in the context of physics quite artificial. In section 6 we are going to investigate, if this strange behavior may be cured by considering “soft cross-links” (defined in equation (2.9)) that allow to some degree for thermal fluctuations around the preferential direction instead of the hard cross-links

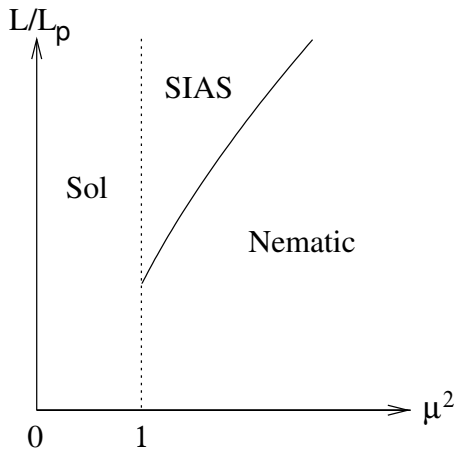


Figure 5.5: The qualitative phase diagram obtained by Benetatos and Zippelius for a 3d system of semiflexible polymers grouped into a random network by parallel or antiparallel aligning cross-linkers.

that impose the orientational constraints strictly.

It is interesting to relate Fig. 5.4 to the phase diagram Fig. 5.5 obtained in a previous work by Benetatos and Zippelius [9]. They consider a very similar three-dimensional system of cross-linked semiflexible polymers that corresponds in our terminology to the case of $\theta = 0$ and unsensitive cross-links. In contrast to our phase diagram where the transition line separating SIAS and 2-fold phase originates in the limit of stiff rods at $\mu^2 = 1$, they find that the transition line starts at $\mu^2 = 1$ but at a finite polymer stiffness. This means that for systems where the polymer's stiffness exceeds a certain threshold there is a direct transition from the isotropic sol to the nematic phase whereas in our case the M -fold state is always preceded by the SIAS.

This qualitative difference may be due to the dimensionalities of the two systems, but it is also possible that it originates in the different variational Ansatz that Benetatos and Zippelius apply in order to investigate the appearance of a nematic state. Unlike to our Ansatz, the polymers are treated as *unpolar* objects that have neither head nor tail. However, we believe that it is more likely that the different dimensionalities are the reason for this strong discrepancy between the phase diagrams. Moreover, it is well known that fluctuations have a stronger influence in a two-dimensional system than in higher dimensions. This would mean that long-range orientational order which is present in three dimensions for sufficiently stiff polymers in the emergent gel phase whereas is destroyed by the strong fluctuations in two dimensions.

5.4 M-fold order: alternative Ansatz

5.4.1 About the order parameter

In section 4.3.1 we discussed two different Ansätze describing M -fold symmetric long-range orientational order. The first and in a sense simpler Ansatz incorporates M -fold rotational symmetry for each replica separately thus allowing a polymer to point on average in different replicas into different directions (among the M possible axes). This Ansatz was studied in section 5.1 and gave rise to reasonable results. In this section, we consider the second Ansatz which incorporates in addition the feature that the polymers have to point on average in the same direction in all replicas.

The alternative variational Ansatz for M -fold orientational order is given by

$$\omega(\hat{\mathbf{k}}, \check{\varphi}) = e^{-\frac{\xi^2}{2}\hat{\mathbf{k}}^2} \frac{1}{I_0^n(\eta)} \frac{1}{M} \sum_{l=1}^M e^{\eta \sum_{\alpha=1}^n \cos(\varphi^\alpha - l\frac{2\pi}{M})} . \quad (5.20)$$

The structure of (5.20) is very much like that of the Ansatz for the SIAS (5.14), the only difference being that the average over all directions in the SIAS case is replaced by an average over M equidistant preferential axes. Note that we will in the following exclude the case $M = 1$ because in this case the two M -fold order Ansätze coincide. The corresponding analysis has already been done in section 5.1.

Interestingly, (5.20) shares properties of both an orientational glass and a long-range orientationally ordered state. The presence of M -fold orientational order can be measured by the physical order parameter \mathcal{S}_M . We obtain (proceeding similarly to (5.3))

$$\mathcal{S}_M = \frac{\eta^M}{2^M M!} + \mathcal{O}(\eta^{M+2}) , \quad (5.21)$$

which tells us that there is M -fold order present when the variational parameter η becomes finite. As for the glassy properties, the polarization vanishes,

$$\mathbf{p} := \frac{1}{N} \sum_{i=1}^N \int_s \langle \mathbf{t}_i(s) \rangle = \mathbf{0} , \quad (5.22)$$

whereas the Edwards-Anderson like order parameter q_{EA} has a finite value for finite η :

$$q_{EA} = \frac{1}{N} \sum_{i=1}^N \int_s \langle \mathbf{t}_i(s) \rangle \langle \mathbf{t}_i(s) \rangle = \frac{\eta^2}{4} + \mathcal{O}(\eta^4) \quad (5.23)$$

because the mean directions of the polymers are assumed to be frozen in (5.20).

5.4.2 Discussion of the free energy

We want to examine the free energy corresponding to (5.20) and insert the Ansatz into (4.36). Assuming that $\theta = k\frac{2\pi}{M}$ as suggested by symmetry the orientational part of the Ansatz $\omega(\hat{\mathbf{k}}, \check{\varphi})$ is invariant with respect to the action of the orientational kernel Δ . Anticipating the result that $\frac{1}{\xi^2}, \eta^2 \propto Q$ we keep contributions only to order Q^4 . The resulting free energy is given by

$$\begin{aligned} \frac{\mathcal{F}}{n} = & \frac{\mu^2 Q^2}{2} \left\{ -\frac{\mu^4 Q}{6} \ln \frac{1}{\xi^2} + \mu^2 \frac{1}{4\xi^2} g\left(\frac{L}{L_p}\right) \left(1 + \frac{\mu^2 Q}{9}\right) \right. \\ & - \mu^2 \frac{1}{16\xi^4} r\left(\frac{L}{L_p}\right) + \mu^2 \frac{\eta^2}{8\xi^2} l\left(\frac{L}{L_p}\right) \\ & \left. - \frac{1}{16} \eta^4 \left(1 + \frac{1}{2} \delta_{M,2} - \mu^2 \left\{ h\left(\frac{2L}{L_p}\right) + \delta_{M,2} \left(h\left(\frac{2L}{L_p}\right) - \frac{1}{2} h\left(\frac{4L}{L_p}\right) \right) \right\} \right) \right\}. \end{aligned} \quad (5.24)$$

The corresponding calculations were referred to Appendix D. The functions g , l and h are defined in Appendix B and their approximate expressions for rather stiff polymers are given in equation (5.5). The function $r(x)$, on the other hand, is defined in equation (D.7) and its lowest order expansion reads

$$r(x) = \frac{1}{6} - \frac{1}{10}x \quad . \quad (5.25)$$

The free energy (5.24) contains generic terms that are present for every value of M as well as terms that are only present for a specific M . Up to this order there are only M -specific terms for the case $M = 2$ in the expansion, and hence, we will find in this approximation for every M apart from this special case the same physical behavior. Terms exclusively present for values of $M \geq 3$ that give rise to differences between other M -fold free energies appear only in higher order. This can be seen readily by expanding the (unnormalized)

orientational part of our Ansatz:

$$\begin{aligned}
 & \frac{1}{M} \sum_{l=1}^M e^{\eta \sum_{\alpha=1}^n \cos(\psi^\alpha - \frac{2\pi}{M}l)} \tag{5.26} \\
 = & 1 + \eta \sum_{\alpha} \delta_{M,1} \cos \psi^\alpha \\
 + & \frac{\eta^2}{2} \sum_{\alpha,\beta} \frac{1}{2} (\delta_{M,1/2} \cos(\psi^\alpha + \psi^\beta) + \cos(\psi^\alpha - \psi^\beta)) \\
 + & \frac{\eta^3}{6} \sum_{\alpha,\beta,\gamma} \frac{1}{4} \left\{ \left(\cos(\psi^\alpha + \psi^\beta - \psi^\gamma) + \text{Perm.} \right) \delta_{M,1} \right. \\
 & \quad \left. + \cos(\psi^\alpha + \psi^\beta + \psi^\gamma) \delta_{M,1/3} \right\} \\
 + & \frac{\eta^4}{24} \sum_{\alpha,\beta,\gamma,\delta} \frac{1}{8} \left\{ \left(\cos(\psi^\alpha - \psi^\beta + \psi^\gamma - \psi^\delta) + \text{Perm.} \right) \right. \\
 & \quad \left. + \left(\cos(\psi^\alpha + \psi^\beta + \psi^\gamma - \psi^\delta) + \text{Perm.} \right) \delta_{M,1/2} \right. \\
 & \quad \left. + \cos(\psi^\alpha + \psi^\beta + \psi^\gamma + \psi^\delta) \delta_{M,1/2/4} \right\} \\
 + & \mathcal{O}(\eta^5)
 \end{aligned}$$

The abbreviation $\delta_{M,i/\dots/j}$ denotes a Kronecker delta that is non-zero only, if M equals one of the numbers i, \dots, j . Hence, the first terms that are specific for M -fold order appear only in order η^M .

The generic terms that are present irrespective of M are those where the angles $\frac{2\pi}{M}l$ have dropped out when expanding the exponential function in the first line of (5.26) and combining the resulting product of cosines into a sum of single cosines by means of trigonometric identities. Consequently, the average over l has no effect on these contributions and they appear for arbitrary M . On the other hand, the orientational distribution of the SIAS Ansatz (5.14) can be written as

$$\omega(\hat{\mathbf{k}} = \hat{\mathbf{0}}, \check{\psi}) = \frac{1}{I_0^n(\eta)} \int \frac{d\varphi_0}{2\pi} e^{\eta \sum_{\alpha=1}^n \cos(\psi^\alpha - \varphi_0)} \quad . \tag{5.27}$$

It is of the same structure as the orientational distribution (5.20) the only difference being that the average over the preferential direction φ_0 is continuous over all directions for the SIAS, whereas it includes only the finite set of M equidistant directions in the case of the M -fold distribution. Clearly, the terms in the expansion (5.26) that survive the average over l for arbitrary M

will also survive the average over full isotropy in the case of the SIAS. Hence, the generic terms in (5.26) actually correspond to the expansion of the orientational part of the SIAS order parameter Ansatz.

Turning back to the free energy (5.24) we see that the expansion contains the same powers of η^2 and $\frac{1}{\xi^2}$ irrespective of M . It is only the magnitude of the coefficients that differ and therefore, the SIAS transition scenario that we discussed in section 5.2 applies here in general. Consequently, the variational parameter η^2 is proportional to $\mu^2 - 1$ and hence, the cross-linker density grows continuously to finite values when increasing the cross-link density beyond $\mu^2 = 1$. This is in contrast to the first M -fold Ansatz that was discussed in section 5.1: we found a *first order* isotropic to M -fold order transition taking place for cross-link densities at a *finite distance* from the sol-gel transition at $\mu^2 = 1$.

On the other hand, in order to obtain the actual phase transition line that can be related to this previous result we need to compare the free energies of the SIAS and the M -fold ordered state. As there is in the approximation (5.24) only a free energy difference between the SIAS and the case $M = 2$, we will as a first step consider the transition between the SIAS and the 2-fold orientationally ordered phase. Afterwards, we are going consider higher order expansions of the free energies and discuss the transitions between SIAS and higher symmetry M -fold Ansätze.

5.4.3 Transition SIAS - 2-fold

As discussed in the preceding section the free energies of SIAS and 2-fold state are up to order Q^4 both of the form

$$\begin{aligned} \frac{\mathcal{F}}{n} = \frac{\mu^2 Q^2}{2} \left\{ -\frac{\mu^4 Q}{6} \ln \frac{1}{\xi^2} + \mu^2 \frac{1}{4\xi^2} g\left(\frac{L}{L_p}\right) \left(1 + \frac{\mu^2 Q}{9}\right) - \mu^2 \frac{1}{16\xi^4} r\left(\frac{L}{L_p}\right) \right. \\ \left. - \frac{\eta^4}{16} c(\mu^2, L_p) + \frac{\eta^2}{8\xi^2} \mu^2 l\left(\frac{L}{L_p}\right) \right\} + \mathcal{O}(Q^5) \quad . \quad (5.28) \end{aligned}$$

It is only the function $c(\mu^2, L/L_p)$ which differs in the two cases. It is defined by

$$c\left(\mu^2, \frac{L}{L_p}\right) := \begin{cases} 1 - \mu^2 h\left(\frac{2L}{L_p}\right) & \text{for the SIAS and by} \\ \frac{3}{2} - \mu^2 \left(2h\left(\frac{2L}{L_p}\right) - \frac{1}{2}h\left(\frac{4L}{L_p}\right)\right) & \text{for the 2-fold state.} \end{cases} \quad (5.29)$$

Both coefficients are positive for finite $\frac{L}{L_p}$ and μ^2 not too large and provide a stable² orientational free energy. As the coupling term is identical, we find that a continuous orientational phase transition takes place at $\mu^2 = 1$ in both cases. In the following we are going to compare the corresponding free energies in order to decide which one of the two phases is actually present depending on the parameters of the model.

The stationarity conditions with respect to the variational parameters $\frac{1}{\xi^2}$ and η^2 give rise to the equations

$$\frac{1}{\xi^2} = \frac{2}{3} \frac{\mu^2 Q}{g\left(\frac{L}{L_p}\right)} \left(1 - \frac{\mu^2 Q}{9} - \frac{\mu^4 Q}{3c} \frac{l^2\left(\frac{L}{L_p}\right)}{g^2\left(\frac{L}{L_p}\right)} + \frac{\mu^2 Q}{3} \frac{r\left(\frac{L}{L_p}\right)}{g^2\left(\frac{L}{L_p}\right)} \right) + \mathcal{O}(Q^3) \quad (5.30)$$

and

$$\eta^2 = \frac{2}{3c} \mu^4 Q \frac{l\left(\frac{L}{L_p}\right)}{g\left(\frac{L}{L_p}\right)} + \mathcal{O}(Q^2) \quad (5.31)$$

where we already replaced $\frac{1}{\xi^2}$ and η^2 on the right hand side of both equations by their corresponding stationary values. $c(\mu^2, L/L_p)$ appears in both equations and so, when inserting the stationary values into the free energy (5.28), we will create additional c -dependent terms that we need to take into account.

Are there new c -dependent contributions created by inserting the stationary value of $\frac{1}{\xi^2}$ into \mathcal{F} ? The relevant contribution in the stationarity equation (5.30) is proportional to Q^2 . This means that we can only obtain c dependent contributions from the terms $\propto \ln \frac{1}{\xi^2}$ and $\propto \frac{1}{\xi^2}$ because we are considering an expansion of the free energy up to order Q^4 . But as it turns out the first order corrections in (5.30) from these two terms just cancel. Inserting the stationarity equation for η (5.31) into the free energy we obtain c dependent contributions from both contributions. Putting them together and keeping only the relevant, i.e. c -dependent, part of the free energy that we denote by F_c , it reads

$$F_c = \frac{\mu^8 Q^2}{36c} \frac{l^2\left(\frac{L}{L_p}\right)}{g^2\left(\frac{L}{L_p}\right)} \propto \frac{1}{c}. \quad (5.32)$$

Hence, the phase with the higher value of c is the physical one. In order to get a first idea about the behavior of the functions $c(\mu^2, L/L_p)$ in the case of the SIAS and the 2-fold symmetric phase we expand them around the limit of stiff rods, i.e. around the point $L/L_p = 0$. The results are

$$c_{SIAS} \sim -(\mu^2 - 1) + \mu^2 \frac{2L}{3L_p} + \mathcal{O}\left(\frac{L^2}{L_p^2}\right) \quad (5.33)$$

²Remember that for the SIAS there is a sign reversal due to the replica limit. The same applies for the 2-fold as it will be discussed in the following.

and

$$c_{2-fold} \sim -\frac{3}{2}(\mu^2 - 1) + \mu^2 \frac{2L}{L_p} + \mathcal{O}\left(\frac{L^2}{L_p^2}\right) . \quad (5.34)$$

For large but finite stiffness we find that starting at the gelation transition, i.e. $\mu^2 = 1$, the 2-fold has lower free energy. But because of the large negative slope of the 2-fold, the 2-fold will eventually become metastable for larger cross-link densities μ^2 and the SIAS takes its place. This behavior is somewhat curious because we would expect the phases to appear the other way around. Plotting the free energies by means of Maple (see Fig. 5.6) this result is confirmed.

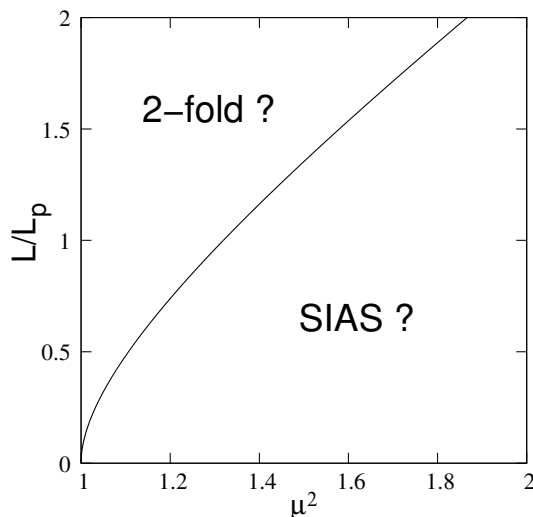


Figure 5.6: Plot of the phase boundary of SIAS and 2-fold state. Curiously, to the left of the boundary line, the 2-fold symmetric state has lower free energy, whereas on the right it is the SIAS.

Was has gone wrong? In fact, the transition line itself looks perfectly reasonable insofar as it indicates that more flexible polymers require more cross-links in order to reach the phase transition. The curious thing is that the *order* of the phases has interchanged. On the other hand, it is known from the theory of spin glasses [17, 42] that when using the replica method, the limit $n \rightarrow 0$ sometimes give rise to a reversal of sign of the free energy. Hence, it happens that it is not the minimum of the free energy that is contributing on saddle-point level but the maximum. We believe that the same artifact might be present here.

As it turns out, the replica structure of the two contributing terms, η^4 and $\frac{\eta^2}{\xi^2}$, indeed suggests that it is not the minimum of the two free energies but the maximum that is physically relevant. For the coupling term $\propto \frac{\eta^2}{\xi^2}$ we find

that it has a replica prefactor of $n(n-1) \sim -n$ that obviously gives rise to a change of sign in the limit $n \rightarrow 0$. For the term $\propto \eta^4$ the situation is slightly more complicated. Considering this term with its full replica structure, i.e. before dropping all powers in n but the linear which is the physically relevant, we find

$$\begin{aligned} \frac{\eta^4}{16} & \left(\underbrace{n(n-1)}_{\sim -n} + \delta_{M,2} \left(\underbrace{n(n-1) + \frac{n}{2}}_{\sim -n/2} \right) \right. \\ & \left. - \mu^2 \left\{ \underbrace{n(n-1)}_{-n} h\left(\frac{2L}{L_p}\right) + \delta_{M,2} \left(\underbrace{n(n-1)h\left(\frac{2L}{L_p}\right) + \frac{n}{2}h\left(\frac{L}{L_p}\right)}_{\sim -n(\dots)} \right) \right\} \right). \end{aligned} \quad (5.35)$$

In the case of the first three contributions it is clear that the replica method gives rise to additional minus signs. As for the last contribution, we know that $h(\frac{2L}{L_p}) > h(\frac{L}{L_p})$ the functions h defined in Appendix B.3 being monotonic decreasing functions and hence, there is an extra minus too.

We thus see that the replica limit induces a sign reversal for all the terms relevant for the comparison of SIAS and 2-fold free energies. Although all this is not a proof, it is at least an indication that when comparing the free energies of SIAS and 2-fold state it *might* be the maximum and not the minimum of the corresponding free energy that is physically relevant. If we assume this to be true we find upon increasing the number of cross-links a phase transition from the SIAS to the long-range ordered 2-fold symmetric state.

5.4.4 Transition SIAS-M-fold, $M \geq 3$

In this section we want to examine the possibility of a phase transition from the SIAS to an M -fold symmetric phase in the case of $M \geq 3$ provided that $\theta = 2\pi/M$. To this end, we consider the difference in free energy $\Delta F := F_{M\text{-fold}} - F_{SIAS}$ as a function of the model parameters μ^2 and L/L_p in order to decide if SIAS or M -fold phase is physically favored. In section 5.4.2, we argued that the expansions of the orientational distributions $\omega(\hat{\mathbf{k}} = \hat{\mathbf{0}}, \tilde{\varphi})$ corresponding to M -fold and SIAS differ only in terms of order η^M and higher. As a consequence, the first contribution to ΔF that will decide about the preferred physical state in a region close to the sol-gel transition will be of higher order too. In the following we are going to derive an expression for this contribution for arbitrary M .

From the stationarity equations (see equations (5.30) and (5.31) in lowest order) we know that $\eta^2 \propto \frac{1}{\xi^2} \propto Q$ and hence, we can do a systematic expansion in powers of the gel fraction. Consequently, we are looking for the contribution to ΔF that is of lowest order in Q . As we show in Appendix D.3 the

lowest order contribution to ΔF (D.14) is proportional to η^{2M} . Denoting by $c(\mu^2, L/L_p)$ the coefficient of this contribution we obtain a M -fold free energy of the following form:

$$\begin{aligned}
 F_{M\text{-fold}} = \frac{\mu^2 Q^2}{2} \left\{ -\frac{\mu^4 Q}{6} \ln \frac{1}{\xi^2} + \mu^2 \frac{1}{4\xi^2} g\left(\frac{L}{L_p}\right) + \dots \right. \\
 \left. + \mu^2 \frac{\eta^2}{8\xi^2} l\left(\frac{L}{L_p}\right) + \dots \right. \\
 \left. - \frac{1}{16} \eta^4 \left(1 - \mu^2 h\left(\frac{2L}{L_p}\right)\right) + \dots + \eta^{2M} c\left(\mu^2, \frac{L}{L_p}\right) + \dots \right\} \\
 + \frac{\mu^6 Q^3}{6} \left\{ \dots \right\} + \mathcal{O}(Q^4) \quad .
 \end{aligned} \tag{5.36}$$

In this expression, we left out all the contributions that are not relevant for the calculation of ΔF in lowest order. Besides the M -specific term $\propto \eta^{2M}$ we kept only the lowest order spatial and orientational contributions. All the other contributions present both for the M -fold and the SIAS and consequently dropping out of ΔF were omitted.

The stationarity equations obtained from (5.36) contain c -dependent higher order corrections that may create additional M -specific terms within the free energy. We consider first the stationarity equation with respect to η^2 :

$$\eta^2 = \mu^2 \frac{l\left(\frac{L}{L_p}\right)}{1 - \mu^2 h\left(\frac{2L}{L_p}\right)} \frac{1}{\xi^2} + \dots + M c \eta^{2(M-1)} + \dots \tag{5.37}$$

Note that the c -dependent contribution is proportional to Q^{M-1} . Keeping contributions up to order Q^{2+M} we may insert this correction into the coupling term $\propto \frac{\eta^2}{\xi^2}$ and in one of the factors of $\eta^4 = \eta^2 \times \eta^2$ of (5.36). The two possibilities to insert the c -dependent term into η^4 give rise to an additional factor of 2. Taking this into account it turns out that the contributions from the terms $\propto \frac{\eta^2}{\xi^2}$ and $\propto \eta^4$ cancel.

The stationarity equation with respect to $\frac{1}{\xi^2}$ reads

$$\begin{aligned}
 \frac{1}{\xi^2} &= \frac{2}{3} \frac{\mu^2 Q}{g\left(\frac{L}{L_p}\right)} \left(1 + \frac{\eta^2 l\left(\frac{L}{L_p}\right)}{2 g\left(\frac{L}{L_p}\right)} + \dots\right)^{-1} \\
 &\sim \frac{2}{3} \frac{\mu^2 Q}{g\left(\frac{L}{L_p}\right)} \left(1 - \frac{\eta^2 l\left(\frac{L}{L_p}\right)}{2 g\left(\frac{L}{L_p}\right)} + \dots\right) \quad .
 \end{aligned} \tag{5.38}$$

Replacing η^2 by its stationary value (5.37), we see that there may arise additional c -dependent terms also from here:

$$\frac{1}{\xi^2} = \frac{2}{3} \frac{\mu^2 Q}{g\left(\frac{L}{L_p}\right)} \left(1 + \dots - \frac{Mc}{2} \frac{l\left(\frac{L}{L_p}\right)}{g\left(\frac{L}{L_p}\right)} \eta^{2(M-1)} + \dots \right) . \quad (5.39)$$

In this equation the c -dependent contribution appears one order higher and is proportional to Q^M . Inserting (5.39) into the terms proportional to $\ln \xi^2$ and $\frac{1}{\xi^2}$ and extracting from the logarithm the lowest order c -dependent contribution it turns out that, again, the two corrections cancel.

Finally, the only contribution to ΔF up to order Q^{2+M} is the term $\propto \eta^{2M}$ itself. In order to study the physical consequences, we calculated its coefficient $c(\mu^2, L/L_p)$ for $M = 3, 4$. Replacing η^{2M} by the lowest order of its stationary value (5.37) we obtain

$$\begin{aligned} \Delta F_{3-fold} = & \left(\frac{2}{3} \frac{\mu^4 Q}{1 - \mu^2 h\left(\frac{2L}{L_p}\right)} \frac{l\left(\frac{L}{L_p}\right)}{g\left(\frac{L}{L_p}\right)} \right)^3 \times \\ & \times \left(\frac{1}{9} - \mu^2 \left\{ \frac{1}{3} h\left(\frac{3}{2\kappa}\right) - \frac{1}{4} h\left(\frac{5}{2\kappa}\right) + \frac{1}{36} h\left(\frac{9}{2\kappa}\right) \right\} \right) \end{aligned} \quad (5.40)$$

for $M = 3$ and

$$\begin{aligned} \Delta F_{4-fold} = & \left(\frac{2}{3} \frac{\mu^4 Q}{1 - \mu^2 h\left(\frac{2L}{L_p}\right)} \frac{l\left(\frac{L}{L_p}\right)}{g\left(\frac{L}{L_p}\right)} \right)^4 \times \\ & \times \left(-\frac{11}{24576} + \mu^2 \left\{ +\frac{1}{512} h\left(\frac{4}{2\kappa}\right) - \frac{1}{512} h\left(\frac{6}{2\kappa}\right) \right. \right. \\ & \left. \left. + \frac{1}{4096} h\left(\frac{8}{2\kappa}\right) + \frac{1}{4608} h\left(\frac{10}{2\kappa}\right) - \frac{1}{73728} h\left(\frac{16}{2\kappa}\right) \right\} \right) \end{aligned} \quad (5.41)$$

for $M = 4$. The functions ΔF_{3-fold} and ΔF_{4-fold} are monotonic in μ^2 and upon increasing the cross-link density from $\mu^2 = 1$ to higher values they eventually run into a change of sign. For $M = 3$ from positive to negative values, i.e. from the SIAS to the 3-fold phase, for $M = 4$ the other way around. Hence, we encounter in the latter case the problem that the position of SIAS and long-range orientationally ordered state in the phase diagram are interchanged, similarly to what we found for $M = 2$ in the previous section.

On the other hand, if we identify the solution $\kappa = \kappa(\mu^2)$ of the equation $c(\mu^2, \kappa) = 0$ with the phase boundary and plot the transition lines for $M =$

2, 3, 4 we obtain a reasonable picture (see Fig. 5.7): the phase boundaries have a similar shape and for higher values of M there is a tendency of the phase transition to take place at higher cross-link densities. This is in agreement with the behavior found in section 5.1 for the first M -fold Ansatz.

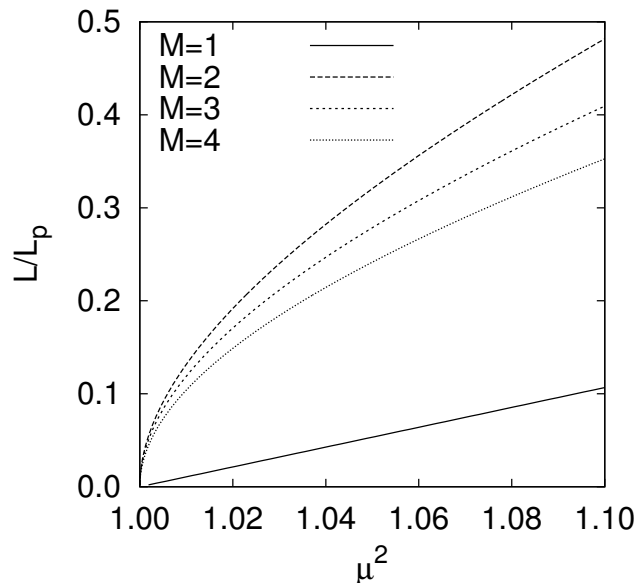


Figure 5.7: Phase boundaries of the transitions SIAS to M -fold where $M = 1, 2, 3, 4$.

Moreover, as we show in Appendix D.3, the sign of ΔF_{4-fold} is reversed when taking the replica limit $n \rightarrow 0$ whereas for $M = 3$ it is not. Because of that one might conjecture similarly to $M = 2$ in the previous section, that for $M = 4$ it might be not the lower free energy that is physically favored but the higher.

5.4.5 Discussion

The alternative M -fold Ansatz discussed in this chapter gives rise to results similar to those of the original M -fold Ansatz, but suffers from a number of complications. On the positive side, taking into account only the results for $M = 2, 3, 4$ and assuming that the sign-issue of ΔF in the cases of $M = 2$ and $M = 4$ can be explained as an artifact due to the replica method, the Ansatz gives rise to reasonable results. Analogous to the first M -fold Ansatz, we find that a phase transition to a long-range ordered state with higher M -fold symmetry requires a higher cross-link density. Moreover, the phase transition

takes place at considerably lower cross-link densities as for the previous M -fold Ansatz. This *could* be interpreted as an indication the alternative M -fold Ansatz describes the M -fold state better. However, if we compare the transition line corresponding to $M = 1$ in Fig. 5.7 to those of $M = 2, 3, 4$ we see that the polar transition that is discussed in section 5.1 is predicted to take place at considerably higher cross-link densities. In this sense the case $M = 1$ does not fit into the pattern of $M = 2, 3, 4$. This finding seems rather curious, because we don't see any reason why the polar case should be set apart.

All in all, there is no reason to prefer this Ansatz with its accompanying complications over the simpler M -fold Ansatz that provides in concert with the SIAS Ansatz a consistent and reasonable picture of the phase behavior of the amorphous solid.

Chapter 6

Soft cross-links

In section 5.1 we discovered that for our model M -fold long-range orientational order was only possible provided that the crossing-angle is a rational multiple of 2π , i.e. $\theta = k\frac{2\pi}{M}$, $k \in \mathbb{Z}$. This means in particular that the theory distinguishes between the cases of the crossing angle θ being an irrational and a rational multiple of 2π . This result seems quite artificial because every irrational number can be approximated arbitrarily well by rational numbers. We believe that this behavior might be due to the use of the “hard cross-links” (2.8) that impose the orientational constraints strictly by means of delta functions. Consequently, we investigate in the following the impact of the “soft cross-links” (2.9) on the behavior of the system. In contrast to the δ -function orientational constraints they allow for thermal fluctuations around the preferred cross-linking angle. Besides the question if the soft cross-links do cure the aforementioned problem or not, we will also investigate the influence of the additional orientational fluctuations at the cross-links on the physical behavior: it is very likely that the emergence of the M -fold state is delayed to higher cross-link densities because the soft cross-links introduce additional floppiness into the network that needs to be stabilized. But in principle, it is also possible that the long-range ordered phase disappears. For the SIAS, on the other hand, we do not expect qualitative changes because in section 5.2 the SIAS already turned out to be quite insensitive with respect to the polymer’s stiffness. Therefore, it seems rather unlikely that orientational localization could be lost due to the additional thermal fluctuations at the cross-links.

6.1 Long-range ordered case

In this section we consider the impact of the soft cross-links on the M -fold ordered phase. To begin with, we restrict ourselves to the case of $M \geq 2$ where there is in lowest order no contribution coupling $\frac{1}{\xi^2}$ and η to each other (see Appendices B.2 and B.3 for the related calculations). This allows us to

analyze the orientational part separately. It reads

$$f_{or,soft} = \frac{\mu^2 Q^2}{2} \left\{ \begin{aligned} & \ln \left(1 + 2 \sum_{q=1}^{\infty} \frac{I_q^2(\eta)}{I_0^2(\eta)} \frac{I_{Mq}(\gamma)}{I_0(\gamma)} \cos(qM\theta) \right) \\ & - \mu^2 \int_{s_1, s_2} \ln \left(1 + 2 \sum_{q=1}^{\infty} \frac{I_q^2(\eta)}{I_0^2(\eta)} \frac{I_{Mq}^2(\gamma)}{I_0^2(\gamma)} e^{-\frac{q^2 M^2}{2\kappa} |s_1 - s_2|} \right) \end{aligned} \right\}. \quad (6.1)$$

The soft cross-links give rise to additional factors of $\frac{I_{Mq}(\gamma)}{I_0(\gamma)}$ that equal 1 in the limit of hard cross-links. Hence, considering $\gamma \rightarrow \infty$ the orientational free energy corresponding to hard cross-links (5.8) is recovered (where θ was chosen such that the cosine equals one).

θ matching the symmetry: delayed phase transition

First of all, we want to investigate the impact of the soft cross-links in the simpler case that $M\theta$ equals an integer multiple of 2π so that the cosine in the first line of (6.1) equals 1. The factors of $\frac{I_{Mq}(\gamma)}{I_0(\gamma)}$ appear linearly in the gaussian and quadratically in the log-trace contribution. Their range lying between 0 and 1 it is clear that the log-trace contribution is weakened with respect to the Gaussian. On the other hand, the function $I_q^2(\eta)/I_0^2(\eta)$ is strictly monotonic increasing and consequently, it is the log-trace part that is responsible for the appearance of a non-trivial global minimum. So, the log-trace part being weakened with respect to the Gaussian the phase transition should indeed be delayed.

This hypothesis is confirmed by a numerical analysis of the orientational free energy (6.1) expanded up to sixth order. As depicted in Fig. 6.1 we find that for finite values of γ the orientational phase transition takes place at a finite distance from the sol-gel transition at $\mu^2 = 1$. Even for stiff rods, we need additional cross-linkers to reach the orientationally long-range ordered phase. Generally speaking, it turns out that the softer the cross-links are, the later the orientational transition takes place. On the other hand, Fig. 6.1 shows nicely that for increasing values of γ the transition curves $\mu_\gamma^2(L/L_p)$ are approaching the bottom curve that corresponds to hard cross-links.

Similarly to the case of hard cross-links, we find that the higher the rotational symmetry of the phase under consideration is, i.e. the higher the value of M , the later the corresponding isotropic to M -fold order transition takes place. The reason is that, as before, the polymer stiffness κ in the purely orientational free energy is rescaled by a factor of M^{-2} as can be seen from the second line of (6.1). On the other hand, we find analogously to the hard cross-links model that the transition occurs later for more flexible polymers and therefore, the reduced effective polymer stiffness κ/M^2 gives rise to a de-

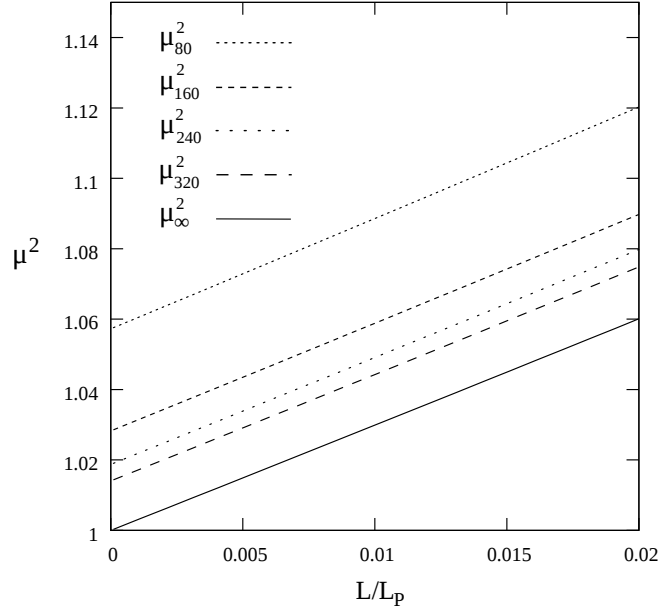


Figure 6.1: Plot of the critical $\mu^2(L/L_p)$ where the phase transition takes place for $M = 3$ and softness parameters $\gamma = 80, 160, 240, 320$ and hard cross-links.

layered phase transition.

The polar case for $M = 1$ involves again additional coupling terms between the spatial and orientational variational parameters. These terms are calculated in Appendix B.3 and are found to be proportional to $\frac{\eta^2}{\xi^2}$, $\frac{\eta^4}{\xi^2}$ and $\frac{\eta^6}{\xi^2}$. Therefore, the structure of the resulting orientational free energy is the same as for the hard cross-links (5.8). The coupling terms give rise to η -dependencies in the stationarity equation with respect to $\frac{1}{\xi^2}$. They need to be inserted again into the free energy in order to obtain all orientational contributions up to order η^6 . Like for the hard cross-links, a numerical analysis of the orientational free energy shows finally that the coupling terms do not lead to a qualitatively different behavior.

Mismatch of θ and the M-fold Ansatz

We turn now to the question what happens if the applied M -fold Ansatz does *not* match the symmetry suggested by the crossing-angle θ , i.e. if we apply the Ansatz for M -fold rotational symmetry to a system where the crossing-angle θ does not equal one of the values $\theta = k\frac{2\pi}{M}$; $k \in \mathbb{Z}$. This case comprises the situation that θ is an irrational multiple of 2π as well as the situation that we try for a “regular” θ the wrong Ansatz, e.g. that we use for $\theta = \frac{2\pi}{6}$ a 7-fold Ansatz.

In section 5.1 we considered hard cross-links and found that for a mismatch of crossing-angle and M -fold Ansatz the orientational free energy was asymptotically unstable. We interpreted this unphysical behavior as an indication that our simple M -fold variational Ansatz no longer applied to this situation. In this section, we are going to investigate if the soft and hence more realistic cross-links will extend the range of applicability of the M -fold Ansatz or not.

As a first step we consider the gaussian contribution and study the effect of an increasing deviation ϵ from the optimal angle $\frac{2\pi}{M}$. Note that the orientational free energy (6.1) is symmetric with respect to positive or negative deviations, i.e. the sign of ϵ does not matter. To understand this consider the cosine within the gaussian contribution that depends on the cross-linking angle θ :

$$\cos(qM\theta) = \cos(qM(2\pi/M + \epsilon)) = \cos(qM\epsilon) \quad (6.2)$$

Hence, the free energy is invariant with respect to a sign reversal of ϵ .

Because of the soft cross-links it is possible to approximate the infinite sums over the modes q in (6.1) by finite sums that include only terms up to the cutoff-index q_c : as depicted in Fig. 6.2 the factors of $\frac{I_{Mq}(\gamma)}{I_0(\gamma)}$ in Gaussian and log-trace contribution are for a given value of γ approaching zero when increasing the index q . Moreover, it is easy to derive the useful upper boundary

$$\left| \frac{I_{Mq}(\gamma)}{I_0(\gamma)} \right| \leq \frac{c(\gamma)}{M^2 q^2} \quad \forall q \in \mathbb{N} \quad (6.3)$$

with $c(\gamma)$ being some positive constant: starting from the integral representation of the Bessel function I_q and performing two successive partial integrations we obtain

$$\begin{aligned} I_q(\gamma) &= \int_{\varphi} e^{\gamma \cos \varphi} e^{-iq\varphi} \quad (6.4) \\ &= \frac{1}{2\pi(-iq)} e^{\gamma \cos \varphi} e^{-iq\varphi} \Big|_0^{2\pi} + \frac{1}{iq} \int_{\varphi} e^{\gamma \cos \varphi} \gamma(-\sin \varphi) e^{-iq\varphi} \\ &= -\frac{\gamma}{q^2} e^{\gamma \cos \varphi} \sin \varphi e^{-iq\varphi} \Big|_0^{2\pi} + \frac{\gamma}{q^2} \int_{\varphi} e^{\gamma \cos \varphi} e^{-iq\varphi} \{-\gamma \sin^2 \varphi + \cos \varphi\} . \end{aligned}$$

Therefore, the Bessel function is bounded from above by

$$|I_q(\gamma)| \leq \frac{\gamma}{q^2} \int_{\varphi} e^{\gamma \cos \varphi} \{-\gamma \sin^2 \varphi + \cos \varphi\} . \quad (6.5)$$

This means that $\frac{I_{Mq}(\gamma)}{I_0(\gamma)}$ is bounded by a converging series that provides an estimate for the error due to the neglected terms. Choosing q_c large so that the error is negligible and remembering furthermore that the function $\frac{I_q^2(\eta)}{I_0^2(\eta)}$ is

monotonic increasing with values between 0 and 1, we see that the gaussian part is asymptotically stable provided that

$$\cos(qM\theta) = \cos(qM\epsilon) > 0 \quad \text{for } q = 1, \dots, q_c \quad . \quad (6.6)$$

Consequently, we need to choose ϵ small enough, so that the cosine remains positive up to q_c . Considering again Fig. 6.2, we see that the cutoff q_c can be chosen the smaller, the smaller γ is, i.e. the smaller softer the cross-links are. Hence the tolerance with respect to deviations ϵ is increased by making the cross-links softer.

This result already is very promising, but of course, the stability of the full orientational free energy is determined not only by the gaussian contribution, but by the interplay of the positive gaussian and the negative log-trace contribution. So, in principle, we need to show that there is a parameter region in the coordinate system of κ , μ^2 , γ and ϵ where the *complete* orientational free energy is stable and in which the phase transition takes place. Unfortunately, we were so far not able to come up with a meaningful analytical argument. Nonetheless, one should keep in mind that the behavior of the Gaussian suggests that the soft cross-links could be a remedy to cure the somewhat artificial restrictions of the applicability of the M -fold variational Ansatz (5.1) even though we still lack a complete theoretical argument.

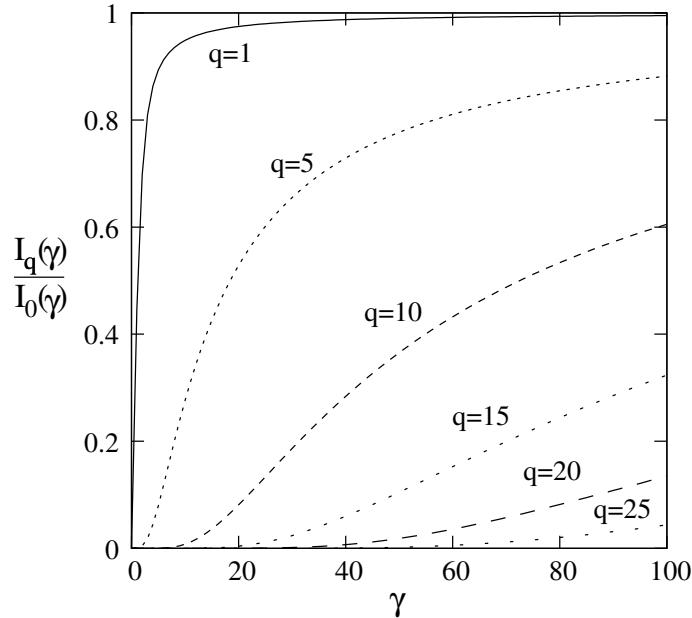


Figure 6.2: Plot of the cutoff function $\frac{I_q(\gamma)}{I_0(\gamma)}$ for different values of q .

We do now a numerical analysis of the orientational free energy (6.1) expanded up to the 10th order. Fixing the cross-link density to a value right beyond the transition, i.e. $\mu^2 > \mu_c^2$, and varying the crossing angle θ around the value $\frac{2\pi}{M}$ we checked that the M -fold phase is robust and does not vanish for small deviations. In Fig. 6.3, we show as an example the effect of deviations for the case of $M = 3$ where the non-trivial minimum turns out to be robust up to deviations of about $\epsilon = \pm 0.18$. On the other hand, it is somewhat

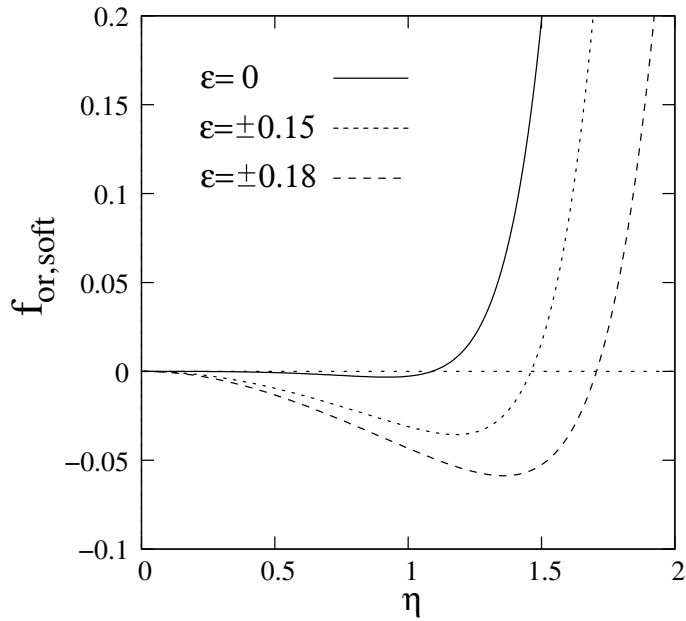


Figure 6.3: Plot of the orientational free energy for $M = 3$ and crossing angles $\theta = \frac{2\pi}{3} \pm \epsilon$; $\gamma = 20, \kappa = 50$; the $\pm\epsilon$ -curves lie on top of each other.

curious that the minimum of the free energy actually deepens when increasing the deviation from $\theta = \frac{2\pi}{M}$. In fact, $\theta = \frac{2\pi}{M}$ is the crossing angle that suits best the M -fold orientational symmetry of the phase and one would rather expect that this angle provides the lowest free energy. But of course, we should not compare free energies that correspond to different crossing angles, i.e. that belong to different models. A meaningful comparison of free energies can only be done by applying different M -fold Ansätze to a *single* model with a fixed crossing angle θ .

Before we proceed to this examination, there is a second point to be noted: if we compare the critical cross-link densities μ_c^2 where the phase transition takes place for deviations $\epsilon = 0, 0.15, 0.18$ we find that the larger ϵ is, the earlier the transition to 3-fold order takes place. More precisely, we find for the cross-link densities approximately the values $\mu_c = 1.13, 1.08, 1.03$ respectively (with the parameters $\gamma = 20$ and $\kappa = 50$). Again, one would rather expect

that for $\epsilon = 0$, i.e. for the crossing angle that corresponds to the symmetry of the Ansatz, the transitions should be triggered most easily.

We compare now for a system with a fixed crossing angle $\theta = \frac{2\pi}{M}$ the free energies corresponding to $(M-1)$ -, M - and $(M+1)$ -fold symmetric Ansätze in order to see which one is physically favored. As an example we consider $M = 8$ because in this case the corresponding crossing angles $\theta = \frac{2\pi}{7}$, $\frac{2\pi}{8}$ and $\frac{2\pi}{9}$ are rather close to each other. Considering the critical cross-link density μ_c^2 we find that the transition from the isotropic phase (corresponding to $\eta = 0$) to 7-fold order takes place first, followed then by 9-fold and last by 8-fold order. In Fig. 6.4 we show the corresponding curves for a cross-link density of $\mu = 1.1$ where 7-fold order just became favorable with respect to the isotropic state. The free energy functions belonging to $M = 8$ and $M = 9$ have not yet developed a non-trivial global minimum. The curve for $M = 9$ lies well below that corresponding to $M = 8$ and is much closer to providing a phase transition.

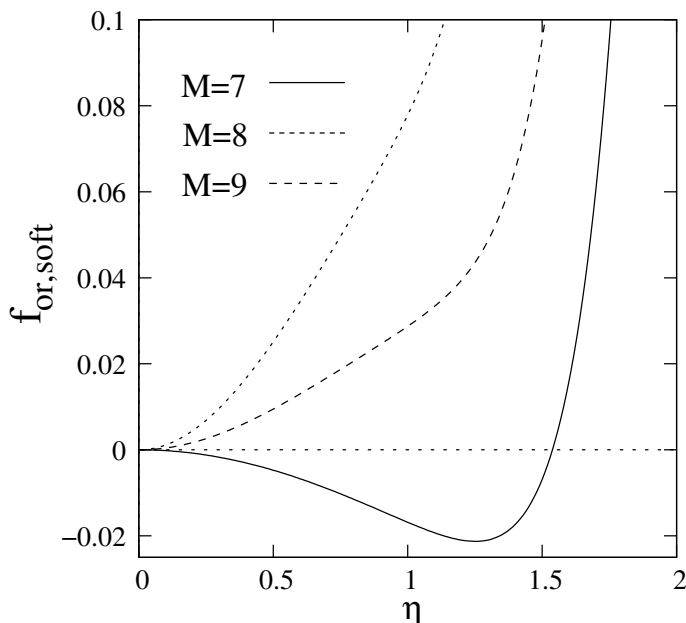


Figure 6.4: Plot of the free energies for $\theta = \frac{2\pi}{8}$ and $M = 7, 8, 9$ and for the parameters $\mu = 1.1$, $\gamma = 80$ and $\kappa = 50$.

These observations cast serious doubts on the correctness of the results and in particular on the applicability of the M -fold Ansatz in situations where $M\theta$ is not an integer multiple of 2π . Both 7-fold and 9-fold symmetric Ansätze are predicted to be preferable to 8-fold order in the sense that the corresponding phase transitions occur already at lower cross-link densities. Considering a

parameter region where all the three of them have developed a non-trivial minimum it is not $M = 8$ that has lowest free energy but $M = 7$. These results utterly contradict the physical expectations.

Up to now, the origin of these curious results is not understood. On the one hand, it is possible that the soft cross-links do not resolve the instability issues encountered in the hard cross-link case and, therefore, that our findings are just a reflection of this fact in the behavior of the lowest order terms. But, on the other hand, we have not excluded yet the possibility that it is just a problem generated by the truncation of the power series in η corresponding to the orientational free energy. Anyhow, it is clear that further investigations are needed in order to clarify the root of the observed behavior.

6.2 Statistically isotropic amorphous solid

For the SIAS, the introduction of soft cross-link does not lead to qualitative changes of the behavior. Applying the same approximation as in section 5.2 for the hard cross-links we obtain the free energy

$$\frac{\mathcal{F}}{n} = \frac{\mu^2 Q^2}{2} \left\{ -\frac{\mu^4 Q}{6} \ln \frac{L^2}{\xi^2} + \mu^2 \frac{L^2}{4\xi^2} g\left(\frac{L}{L_p}\right) - \frac{\eta^4}{16} \Lambda(\gamma) \left(1 - \mu^2 \Lambda(\gamma) h\left(\frac{2L}{L_p}\right) \right) + \frac{\eta^2 L^2}{8\xi^2} \mu^2 \Lambda(\gamma) l\left(\frac{L}{L_p}\right) \right\} . \quad (6.7)$$

Here, we have introduced the shorthand notation $\Lambda(\gamma) := \frac{I_1^2(\gamma)}{I_0^2(\gamma)}$ for the additional factors that stem from the soft cross-links. The range of $\Lambda(\gamma)$ lies between 0 and 1, low values corresponding to soft cross-links and high values to stiff cross-links. Again, the functions g, h, l are given by (5.6) in the M -fold section. The stationarity equations with respect to ξ^2 gives rise to

$$\frac{L^2}{\xi^2} \sim \frac{2}{3} \frac{\mu^2 Q}{g\left(\frac{L}{L_p}\right)} \quad (6.8)$$

and for the orientational parameter we find

$$\eta^2 \sim \frac{L^2}{\xi^2} \frac{\mu^2 l\left(\frac{L}{L_p}\right)}{1 - \mu^2 \Lambda(\gamma) h\left(\frac{2L}{L_p}\right)} . \quad (6.9)$$

Varying γ we see that the softer the cross-links are, the smaller is also the variational parameter η , i.e. the degree of orientational order. This is perfectly reasonable because we expect that floppiness of the cross-links as well as floppiness of the polymers should lead to a decrease of orientational localization. The spatial localization, on the other hand, is in lowest order not influenced by the soft cross-links, but it will be in higher order as a result of the coupling of spatial and orientational localization.

6.3 Phase diagram

Because of the additional model parameter γ controlling the amount of thermal fluctuations about the preferential intersection angle at the cross-links, the phase diagram has become richer in comparison to that corresponding to hard cross-links Fig. 5.4. As can be seen from Fig. 6.5 the transition line from the

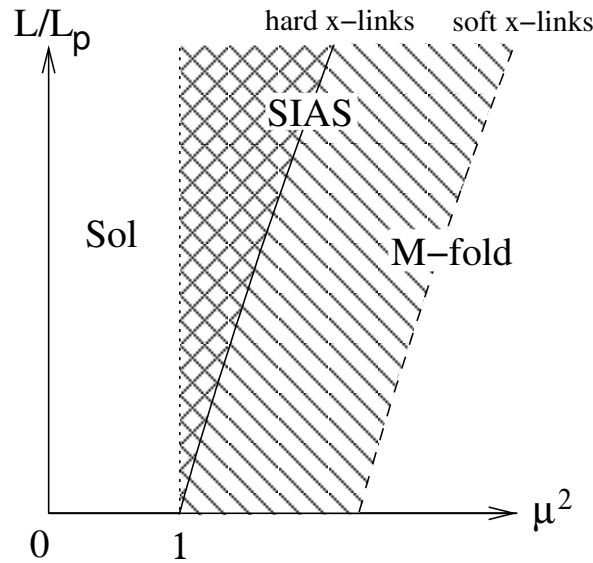


Figure 6.5: The phase diagram for soft cross-links: to the right of the vertical dotted line, SIAS order becomes stable. M -fold order appears to the right of the continuous tilted line for hard cross-links and to the right of the dashed tilted line for soft x-links.

SIAS to the long-range ordered phase that originated for the hard cross-links at $\mu^2 = 1$ is shifted to the right for finite values of γ . Even in the limit of stiff rods, additional cross-links are necessary for the appearance of long-range order because the soft cross-links act as an additional source of floppiness in the network that needs to be stabilized.

Besides, other features of the phase behavior of the hard cross-links carry over directly. As before, more flexible polymers require a higher critical cross-linker density for the appearance of long-range order. Furthermore, it is still true that the higher the M -fold symmetry of the phase under consideration, the later the transition takes place.

Chapter 7

Summary, discussion and outlook

We have studied the orientational phases of a model describing random networks of cross-linked semiflexible (bio-)polymers in two dimensions. Generalizing the work of Benetatos and Zippelius [9], the polymers are interconnected by “orientational cross-links” that impose a *finite* intersection angle. Within a variational approach, we were able to show that, besides a statistically isotropic amorphous solid (SIAS) that has been encountered previously in a variety of systems [54, 23, 9], there are also more exotic gels. These are characterized by random positional order coexisting with long ranged orientational order and their symmetry is governed by the crossing angle.

A short summary of our results is as follows: upon increasing the number of cross-linkers up to about one per polymer we find a gelation transition from a liquid to a gel phase which features both positional and orientational localization. The physical behavior, and in particular the presence of different orientational structures within the gel phase, was examined by means of different variational Ansätze. In chapter 5 we explored the behavior of networks created using “hard cross-links” where the participating polymers must intersect each other *precisely* with the corresponding crossing angle. In section 5.1 we were able to show by means of a simple variational Ansatz that long-range M -fold rotationally symmetric order is possible, provided that the crossing angle θ is of the form $\theta = k\frac{2\pi}{M}$; $k \in \mathbb{Z}$, i.e. if the crossing angle is a rational multiple of 2π . We believe that this condition for the appearance of long-range order, which seems in a physical context quite artificial, might be due to the restrictions of our simple variational Ansatz. The other requirements for this phase are quite intuitive: if the polymer’s resistance to bending is lower, more cross-links are needed to establish long-range orientational order. Moreover, a phase transition towards a higher M -fold symmetry also needs a larger number of cross-links. The gap between the gelation transition, at about one cross-link

per polymer, and the emergence of long-range orientational order is filled by the SIAS discussed in section 5.2. The SIAS is characterized by random orientational localization of the polymers and in this sense displays glassy features. It is always found to be available for cross-link densities beyond the gelation transition, irrespective of the crossing angle and the polymer stiffness. The physical information collected so far gives rise to a reasonable phase diagram that is presented in section 5.3. We compare this transition scenario to the results of Benetatos and Zippelius [9] which correspond to the special case of $M = 2$ in our model. It is pointed out that the differences between the phase diagrams of the two models are likely to stem from the different dimensionalities. In the last section of this chapter, 5.4, we consider a more elaborate variational Ansatz describing M -fold orientational order. In comparison to the M -fold Ansatz that was discussed in section 5.1, it predicts the phase transition from the SIAS to M -fold order to happen for considerably smaller cross-link densities. However, this Ansatz suffers from mathematical complications that have not yet been resolved. Moreover, within this alternative Ansatz the case $M = 1$, i.e. the case of polar order, plays a special role and it gives rise to results that do not fit into what we obtain for the general case of $M \geq 2$.

The restriction of long-range orientational order to crossing angles that are rational multiples of 2π is physically not satisfying. As we suspect that the strict orientational constraint of the hard cross-links might be the root of this strange behavior, we explore in chapter 6 the possibility of “soft cross-links”. These cross-links allow for thermal fluctuations of the interconnected polymers about the average crossing angle θ . However, the introduction of soft cross-links does not change the peculiar behavior encountered for hard cross-links. Nevertheless, it is very interesting to examine the effect on the phase behavior upon varying the width of the thermal fluctuations at the cross-linkers. We find that the larger these fluctuations are, the later the M -fold transition takes place. In particular, the usage of the more realistic soft cross-linkers leads to a qualitatively different phase diagram. Even in the limiting case of perfectly stiff polymers, the appearance of long-range order no longer coincides with the gelation transition as it did for hard cross-linkers, but is shifted to higher cross-link densities.

The main result of this thesis is the appearance of exotic gels with long-range orientational order for suitable crossing angles θ . This type of orientational order has already been theoretically described by Bruinsma *et al.* [13, 11]. They consider actin networks modeled by stiff rods that are attached to each other by reversible cross-links. In contrast to our minimalistic approach where the cross-links are the only driving force for an orientational transition, Bruinsma *et al.* incorporate the effects of linker proteins and elec-

trostatic interactions as well as steric repulsions between the rods into their model. However, as their approach is an extension of the Onsager theory [43] it is not able to account for structural features such as the gelation transition or the spatial heterogeneities in the resulting network. Our theory, in comparison, yields a far more detailed insight into the structure of the amorphous solid phase.

It is worth mentioning that long-range orientational order in combination with spatial disorder has been observed in a variety of physical systems with quite different constituents and underlying physical mechanisms. Tetratic ordering, which corresponds to $M = 4$ in our system, was found for example in liquid-crystalline systems by means of computer simulations [15, 59] as well as in experiments [61, 37]. In all these systems the transition is driven by the shape of the constituents. A hexatic phase with 6-fold orientational order has been proposed as an intermediate phase in the process of dislocation-mediated melting in two dimensions [26, 40]. A very nice illustration of the hexatic phase (although in a mechanical, non-equilibrium system) is found in [41].

Because of the peculiarities of two dimensions, we expect thermal fluctuations to affect positional localization [35, 22]. It is known in the context of the before-mentioned two-dimensional defect-mediated melting that at finite temperature positional order can only be quasi-long ranged whereas orientational order can be truly long ranged [39]. A study of the corresponding phenomena for our positionally amorphous and orientationally ordered system is a very interesting direction for further investigation.

Outlook

A possible extension of our work concerns more elaborate variational Ansätze probing the appearance of combined M -fold and glassy orientational order. Here, the chains in the gel fraction are assumed to be orientationally localized in preferential directions which vary from chain to chain but macroscopically average into an M -fold pattern. A corresponding Ansatz could for instance be [8]

$$\omega(\hat{\mathbf{k}}, \check{\varphi}) = e^{-\frac{\hat{\mathbf{k}}^2}{2\xi^2}} \int d\varphi_0 \Phi(\varphi_0) \frac{e^{\eta \sum_{\alpha=1}^n \cos(M(\varphi^\alpha - \varphi_0))}}{I_0^n(\eta)},$$

where $\int d\varphi_0 \Phi(\varphi_0) = 1$. In the above equation, a polymer segment in the percolating cluster is orientationally localized about the axis φ_0 modulo $2\pi/M$ (M -fold ordering). The direction of the localization axis varies in the sample and follows the quenched distribution $\Phi(\varphi_0)$ that we define as

$$\Phi(\varphi_0) = \exp(\nu \cos(\varphi_0)) / I_0(\nu) \quad .$$

For $\nu = 0$, the SIAS Ansatz is recovered whereas for $\nu \rightarrow \infty$ the M -fold Ansatz discussed in section 5.1 is obtained. For finite ν , isotropy (or more precisely MRI) is broken and the SIAS is replaced by a state featuring M -fold rotational symmetry as well as glassiness; the M preferential localization directions are specified with a variance controlled by the parameter ν . Note that glassiness is always expressed by a coupling of different replicas. A variational analysis of the free energy which corresponds to these more elaborate Ansätze could elucidate the relation between the SIAS and the M -fold orders.

Exploring the physics of a three-dimensional generalization of our model is another possible pathway of further research. The higher dimensionality will surely give rise to new complex network structures that need to be analyzed by means of suitable variational Ansätze. Technically, such an extension has to deal with the fact that a finite cross-linking angle between two wormlike chains prescribes a cone and not a plane.

Note that the finite bending rigidity is an essential ingredient of our model. It allows the effective decoupling of positional and orientational degrees of freedom close to the gelation transition. In the case of infinitely stiff polymers on the other hand, a rigid cross-link would automatically fix both position and orientation. The nature of the emerging network is an interesting problem necessitating a different theoretical approach.

Finally, it would be very interesting to study the mechanical properties of orientationally ordered networks. In fact, mechanical properties of random networks have been examined for isotropic systems within the same theoretical framework [54, 55]. Besides, there are more recent works which already dealt with problems related to our model with its anisotropic structure; namely how to describe local fluctuations of the elastic moduli [33, 34], and how to obtain the elastic moduli for a system that possesses spontaneous nematic ordering [60].

Appendix A

Evaluating expectation values

A.1 The WLC propagator

The WLC propagator $G(\varphi, s_1; \varphi', s_2)$ quantifies the probability that the tangential vector of monomer s_1 points into the direction φ provided that the tangential vector of monomer s_2 points into the direction φ' :

$$\begin{aligned} G(\varphi, s_1; \varphi', s_2) &:= \left\langle \delta(\varphi - \psi(s_1)) \delta(\varphi' - \psi(s_2)) \right\rangle^{\mathcal{H}_{WLC}} \quad (\text{A.1}) \\ &= \frac{1}{\mathcal{N}} \int_{s_1}^{s_2} \mathcal{D}\{\mathbf{t}\} e^{-\frac{\kappa}{2} \int_{s_1}^{s_2} d\tau \left(\frac{d\mathbf{t}}{d\tau}\right)^2} . \end{aligned}$$

Here, \mathcal{N} denotes the normalization of the path integral and $\psi(s)$ is the angle corresponding to the tangential vector $\mathbf{t}(s) = (\cos \psi(s), \sin \psi(s))$ of length one which indicates the orientation of monomer s . In principle, the path integral includes all the monomers $s \in [0, L]$, but only monomers between s_1 and s_2 are relevant and the other degrees of freedom can be integrated out. In order to perform the remaining path integral we write down a discretized version of the above expression. We approximate the continuous degrees of freedom by a finite number l of them such that \mathbf{t}_1 corresponds to $\mathbf{t}(s_1)$ and that \mathbf{t}_l corresponds to $\mathbf{t}(s_2)$. The distance ϵ between neighbors is determined by $l\epsilon = |s_2 - s_1|$. Expressing the integral and the derivatives of the WLC Hamiltonian by their discretized versions and calling the normalization constant for the discretized path integral \mathcal{N}_ϵ we arrive at [30]:

$$\begin{aligned} G_\epsilon &= \frac{1}{\mathcal{N}_\epsilon} \prod_{i=2}^{l-1} \left(\int \frac{d\varphi_i}{2\pi} \right) \exp \left(-\frac{\kappa}{2} \epsilon \sum_{i=1}^{l-1} \left(\frac{\mathbf{t}_i - \mathbf{t}_{i+1}}{\epsilon} \right)^2 \right) \\ &= \frac{1}{\mathcal{N}_\epsilon} \prod_{i=2}^{l-1} \left(\int \frac{d\varphi_i}{2\pi} \right) \exp \left(-\frac{\kappa}{\epsilon} \sum_{i=1}^{l-1} (1 - \cos(\varphi_i - \varphi_{i+1})) \right) . \end{aligned}$$

In order to perform the integrations over the φ_i it is convenient to decouple φ_i and φ_{i+1} by means of the relation

$$e^{a \cos \varphi} = \sum_{q=-\infty}^{\infty} I_q(a) e^{iq\varphi} \quad ,$$

where the $I_q(a)$ denote modified Bessel functions. Performing the integrations we obtain

$$G_\epsilon = \frac{1}{\mathcal{N}_\epsilon} \sum_{q=-\infty}^{\infty} \left(e^{-\frac{\kappa}{\epsilon}} I_q(\kappa/\epsilon) \right)^{l-1} e^{iq(\varphi_1 - \varphi_l)} \quad ,$$

and integrating over $\frac{\varphi_1}{2\pi}$ and $\frac{\varphi_l}{2\pi}$ it turns out that the normalization is given by

$$\mathcal{N}_\epsilon = \left(\exp(-\kappa/\epsilon) I_0(\kappa/\epsilon) \right)^{l-1} \quad . \quad (\text{A.2})$$

The final step is to take the limit $\epsilon \rightarrow 0$ keeping $l\epsilon = |s_1 - s_2|$ constant. It is thus possible to express the modified Bessel functions by the asymptotic expansion

$$I_q(a) \sim \frac{\exp(a)}{\sqrt{2\pi a}} \left(1 - \frac{4q^2 - 1}{8a} + \dots \right) \quad , \quad (\text{A.3})$$

and the propagator converges to

$$G(\varphi, s_1; \varphi', s_2) = \sum_{q=-\infty}^{\infty} e^{-\frac{1}{2\kappa} q^2 |s_1 - s_2|} e^{iq(\varphi - \varphi')} \quad . \quad (\text{A.4})$$

In the special case that $|s_1 - s_2|/2\kappa = |s_1 - s_2|/L_p$ is very small, i.e. if we consider correlations on a length-scale significantly shorter than the persistence length of the polymer, we are allowed to replace the sum over q by an integral. Performing the integration, the result is

$$G(\varphi, s_1; \varphi', s_2) = \sqrt{\pi L_p / |s_1 - s_2|} e^{-\frac{L_p}{4|s_1 - s_2|} (\varphi - \varphi')^2} \quad . \quad (\text{A.5})$$

Therefore, the fluctuations of φ' around φ are gaussian provided that their distance $|s_1 - s_2|$ is considerably smaller than the persistence length.

A.2 Rules for expectation values

For a general 2-point correlation function of the real valued observables \mathcal{O}_1 and \mathcal{O}_2 measured at positions s_1 and s_2 respectively we find by means of the

WLC propagator (A.4):

$$\begin{aligned} & \left\langle \mathcal{O}_1(\psi(s_1)) \mathcal{O}_2(\psi(s_2)) \right\rangle^{\mathcal{H}_{WLC}} \\ &= \sum_{q=-\infty}^{\infty} e^{-\frac{1}{2\kappa} q^2 |s_1 - s_2|} \hat{\mathcal{O}}_1(q) \hat{\mathcal{O}}_2^*(q) \quad . \end{aligned} \quad (\text{A.6})$$

$\hat{\mathcal{O}}_1$ and $\hat{\mathcal{O}}_2$ denote the Fourier transforms of the observables. Hence, it is only the Fourier components with the same q which are coupled by the WLC propagator, and the rate of the exponential decay of correlations along the filament scales with q^2 .

In the limit of stiff rods, i.e. $\kappa \rightarrow \infty$, the expectation value can be expressed by

$$\begin{aligned} & \lim_{\kappa \rightarrow \infty} \sum_{q=-\infty}^{\infty} e^{-\frac{1}{2\kappa} q^2 |s_1 - s_2|} \hat{\mathcal{O}}_1(q) \hat{\mathcal{O}}_2^*(q) \\ &= \sum_{q=-\infty}^{\infty} \hat{\mathcal{O}}_1(q) \hat{\mathcal{O}}_2^*(q) \\ &= \int_{\varphi} \mathcal{O}_1(\varphi) \mathcal{O}_2(\varphi) \quad , \end{aligned} \quad (\text{A.7})$$

where we applied Parseval's theorem in order to obtain the last line and where we used the fact that we consider real valued observables. In particular, this equation implies that

$$\begin{aligned} & \left\langle \omega(\hat{\mathbf{0}}, \check{\psi}(s_1)) \omega(\hat{\mathbf{0}}, \check{\psi}(s_2)) \right\rangle \\ &= \int_{\check{\varphi}} \omega^2(\hat{\mathbf{0}}, \check{\varphi}) \quad . \end{aligned} \quad (\text{A.8})$$

This relation will help in subsequent Appendices to calculate the second order orientational contributions to the free energy because it states that the gaussian contribution is obtained from the second order log-trace part by simply considering the limit of infinite stiffness. Moreover, all the relations that we are going to derive in the following for expectation values, i.e. that apply to the log-trace part, carry over to corresponding calculations in the context of the gaussian part.

There is an important rule that allows in some cases to conclude without explicit calculations that an expectation value vanishes:

$$\left\langle \cos \left(\sum_{l=1}^m \sigma_l \psi(s_l) \right) \right\rangle \propto \delta_{\sum_l \sigma_l, 0} \quad . \quad (\text{A.9})$$

Here, the monomers s_l involved are arbitrary and the σ_l can equal either $+1$ or -1 . A non-vanishing expectation value is only possible if the σ_l add up to zero, i.e. if the number of positive signs equals the number of negative signs.

In particular, it follows from (A.9) that an expectation value of the above form vanishes if there is an odd number of variables $\psi(s)$ involved. Applying some basic trigonometric identities, one can derive the following useful special case:

$$\left\langle \cos \psi(s_1) \dots \cos \psi(s_l) \right\rangle = 0 \quad ; \quad \forall l \text{ being odd.} \quad (\text{A.10})$$

In order to prove (A.9) it is sufficient to show that the same relation holds for the expectation value $\left\langle e^{i \sum_{l=1}^m \sigma_l \psi(s_l)} \right\rangle$. By means of the WLC propagator (A.4) we obtain the following expression:

$$\begin{aligned} & \left\langle e^{i \sum_{l=1}^m \sigma_l \psi(s_l)} \right\rangle \quad (\text{A.11}) \\ &= \sum_{q_1, \dots, q_{m-1} \in \mathbb{Z}} \exp \left(-\frac{1}{2\kappa} \sum_{l=1}^{m-1} q_l^2 |s_l - s_{l-1}| \right) \left(\frac{1}{2\pi} \right)^m \int d\psi_1 \dots d\psi_m \times \\ & \quad \times e^{i\sigma_1 \psi_1} e^{iq_1 \psi_1} \times \prod_{l=2}^{m-1} e^{i\sigma_l \psi_l} e^{i(q_l - q_{l-1}) \psi_l} \times e^{i\sigma_m \psi_m} e^{-iq_{m-1} \psi_m} \\ &= \sum_{q_1, \dots, q_{m-1} \in \mathbb{Z}} \exp \left(-\frac{1}{2\kappa} \sum_{l=1}^{m-1} q_l^2 |s_l - s_{l-1}| \right) \times \\ & \quad \times \delta_{q_1, -\sigma_1} \times \prod_{l=2}^{m-1} \delta_{q_l - q_{l-1}, -\sigma_l} \times \delta_{q_{m-1}, \sigma_m} \quad . \end{aligned}$$

Therefore, the q_l are coupled and we see that the expectation value is only non-zero if the σ_l fulfill the following condition:

$$-\sigma_1 + \sum_{l=2}^{m-1} (-\sigma_l) = \sigma_m \quad . \quad (\text{A.12})$$

This is equivalent to the condition that the sum over the σ_l vanishes and equation (A.9) is shown to hold.

A.3 Correlators

In this section, we present the calculations of the correlators needed in section 4.2.1 in order to analyze the stability of the sol phase in the ORS and HRS. The correlation functions are computed in the special case of stiff rods and

consequently, the polymers have only two degrees of freedom, their positions and their orientations. The position in space of monomer s is expressed as

$$\mathbf{r}(s) = \mathbf{r}_o + s \mathbf{t} \quad \forall s \in [0, L] \quad , \quad (\text{A.13})$$

where \mathbf{r}_o denotes the spatial position of one of the polymer's ends and where \mathbf{t} denotes its orientation. A general thermal average of several observables \mathcal{O}_i where $i = 1, \dots, l$ is then calculated by

$$\langle \mathcal{O}_1 \times \dots \times \mathcal{O}_l \rangle = \int_V \frac{d\mathbf{r}_o}{V} \int_0^{2\pi} \frac{d\psi}{2\pi} \mathcal{O}_1 \times \dots \times \mathcal{O}_l \quad . \quad (\text{A.14})$$

By means of these relations, the first correlation function is easily calculated:

$$\begin{aligned} & C(\hat{\mathbf{k}}_1, \hat{\mathbf{k}}_2, \check{\varphi}_1, \check{\varphi}_2) \quad (\text{A.15}) \\ &= \int_{s_1, s_2} \left\langle e^{i(\hat{\mathbf{k}}_1 \hat{\mathbf{r}}(s_1) + \hat{\mathbf{k}}_2 \hat{\mathbf{r}}(s_2))} \delta(\check{\varphi}_1 - \check{\psi}(s_1)) \delta(\check{\varphi}_2 - \check{\psi}(s_2)) \right\rangle \\ &= \int_{s_1, s_2} \int \frac{d\hat{\mathbf{r}}_o}{V^{n+1}} \int_{\check{\psi}} e^{i(\hat{\mathbf{k}}_1(\hat{\mathbf{r}}_o + s_1 \hat{\mathbf{t}}_\psi) + \hat{\mathbf{k}}_2(\hat{\mathbf{r}}_o + s_2 \hat{\mathbf{t}}_\psi))} \delta(\check{\varphi}_1 - \check{\psi}(s_1)) \delta(\check{\varphi}_2 - \check{\psi}(s_2)) \\ &= \delta_{\hat{\mathbf{k}}_1, -\hat{\mathbf{k}}_2} \delta(\check{\varphi}_1 - \check{\varphi}_2) \int_{\psi^{(0)}} \int_{s_1, s_2} e^{i(s_1 - s_2)(\mathbf{k}_1^{(0)} \mathbf{t}_\psi^{(0)} + \check{\mathbf{k}}_1 \check{\mathbf{t}}_1)} \\ &= \delta_{\hat{\mathbf{k}}_1, -\hat{\mathbf{k}}_2} \delta(\check{\varphi}_1 - \check{\varphi}_2) \int_{\psi^{(0)}} \frac{2 - 2 \cos(\mathbf{k}^{(0)} \mathbf{t}_\psi^{(0)} + \check{\mathbf{k}} \check{\mathbf{t}}_{\varphi_1})}{(\mathbf{k}^{(0)} \mathbf{t}_\psi^{(0)} + \check{\mathbf{k}} \check{\mathbf{t}}_{\varphi_1})^2} . \end{aligned}$$

We denote by $\psi^{(0)}$ the orientation of the polymer in the 0-replica and use this type of notation for the other quantities correspondingly. The tangential vector \mathbf{t}_ψ is defined by $\mathbf{t}_\psi := (\cos \psi, \sin \psi)$. The second correlation function gives rise to

$$\begin{aligned} C(-\hat{\mathbf{k}}_0, \hat{\mathbf{k}}_0, \check{0}, \check{0}) &= \int_{s_1, s_2} \left\langle e^{-i(\mathbf{k}_0 \mathbf{r}^{(1)}(s_1) - \mathbf{k}_0 \mathbf{r}^{(2)}(s_1))} e^{i(\mathbf{k}_0 \mathbf{r}^{(1)}(s_2) - \mathbf{k}_0 \mathbf{r}^{(2)}(s_2))} \right\rangle \\ &= \int_{s_1, s_2} \left| \left\langle e^{-i(\mathbf{k}_0 \mathbf{r}(s_1) - \mathbf{k}_0 \mathbf{r}(s_2))} \right\rangle \right|^2 \quad (\text{A.16}) \\ &= \int_{s_1, s_2} \left| \int_{\psi} e^{-i(s_1 - s_2) k_0 \cos \psi} \right|^2 \\ &= \int_{s_1, s_2} J_0^2(k_0(s_1 - s_2)) \quad , \end{aligned}$$

where the Bessel function $J_0(x)$ is defined by

$$J_0(x) = \int_{\psi} \exp(ix \cos \psi) \quad . \quad (\text{A.17})$$

Appendix B

Calculations M-fold I

B.1 Gaussian

In this Appendix, we present some details on the derivation of the variational free energy (5.4) that corresponds to the Ansatz (5.1) for the amorphous solid with M -fold discrete rotational symmetry.

Inserting (5.1) into the general replica free energy (4.36) the gaussian part reads

$$f_G = \frac{\mu^2 Q^2}{2V^n} \sum_{\hat{\mathbf{k}}} \delta_{\sum_{\alpha=0}^n \mathbf{k}^\alpha, 0} e^{-\xi^2 \hat{\mathbf{k}}^2} \int_{\check{\varphi}_1, \check{\varphi}_2} \Delta(\check{\varphi}_1, \check{\varphi}_2) \times \\ \times \frac{1}{I_0^{2n}(\eta)} e^{\eta \sum_{\alpha=1}^n (\cos(M\varphi_1^\alpha) + \cos(M\varphi_2^\alpha))}$$

The spatial part is readily computed by replacing the sum over the replicated Fourier variables $\hat{\mathbf{k}}$ by an integral and representing the delta function in Fourier space. Performing the resulting integrations we arrive at

$$f_G = \frac{1}{n+1} \left(\frac{1}{4\pi\xi^2} \right)^n f_o .$$

For the orientational contribution f_o we find in the case of sensitive cross-links:

$$f_o = \int_{\check{\varphi}_1, \check{\varphi}_2} \Delta(\check{\varphi}_1 - \check{\varphi}_2, \theta) \frac{e^{\eta \sum_{\alpha=1}^n (\cos(M\varphi_1^\alpha) + \cos(M\varphi_2^\alpha))}}{I_0^{2n}(\eta)} \\ \sim 1 + n \ln \left(\int_{\varphi_1, \varphi_2} \Delta(\varphi_1 - \varphi_2, \theta) \frac{e^{\eta (\cos(M\varphi_1) + \cos(M\varphi_2))}}{I_0^2(\eta)} \right) \\ = 1 + n \ln \left(1 + 2 \sum_{q=1}^{\infty} \frac{I_q^2(\eta)}{I_0^2(\eta)} \frac{I_{Mq}(\gamma)}{I_0(\gamma)} \cos(Mq\theta) \right) .$$

In order to obtain the last line we replaced the three functions depending on the φ 's by their Fourier representations. Performing the integrations lead to

Kronecker Deltas that cancel two of the three sums over Fourier modes. For **unsensitive** cross-linkers, on the other hand, the corresponding expression reads

$$f_o = 1 + n \ln \left(1 + 2 \sum_{q=1}^{\infty} \delta_{Mq, 2\mathbb{Z}} \frac{I_q^2(\eta)}{I_0^2(\eta)} \frac{I_{Mq}(\gamma)}{I_0(\gamma)} \cos(Mq\theta) \right) . \quad (\text{B.1})$$

The Kronecker delta $\delta_{q, 2\mathbb{Z}}$ is non-zero only if q is an even integer. Therefore, for M being an odd number the contributions corresponding to odd q are projected out. For even M we obtain the same result as for the sensitive cross-links.

Note that in the case of hard cross-links ($\gamma = \infty$) there is an alternative expression for the f_o given by

$$\begin{aligned} f_o &\sim 1 + n \ln \left(\int_{\varphi_1, \varphi_2} \Delta(\varphi_1 - \varphi_2, \theta) \frac{e^{\eta(\cos(M\varphi_1) + \cos(M\varphi_2))}}{I_0^2(\eta)} \right) \\ &\sim 1 + n \ln \left(\frac{1}{I_0^2(\eta)} \int_{\varphi} e^{\eta(\cos(M(\varphi+\theta)) + \cos(M\varphi))} \right) \\ &\sim 1 + n \ln \left(\frac{1}{I_0^2(\eta)} \int_{\varphi} e^{2\eta(\cos(M\varphi + \frac{M\theta}{2})) \cos(\frac{M\theta}{2})} \right) \\ &\sim 1 + n \ln \left(\frac{I_0(2\eta \cos(\frac{M\theta}{2}))}{I_0^2(\eta)} \right) \end{aligned}$$

for sensitive cross-links and

$$f_o \sim 1 + n \ln \left(\frac{1}{I_0^2(\eta)} \frac{1}{2} \left\{ I_0(2\eta \cos(\frac{M\theta}{2})) + I_0(2\eta \cos(\frac{M(\theta + \pi)}{2})) \right\} \right) \quad (\text{B.2})$$

in the unsensitive case. These two expressions are well-suited for examining the asymptotic stability of the gaussian contribution. By means of the asymptotic expansion of the Bessel functions (A.3) in lowest order, it is easy to show that for sensitive cross-linkers, it is only for crossing-angles $\theta = \frac{k2\pi}{M}$ $k \in \mathbb{Z}$ that an M -fold Ansatz gives rise to a stable Gaussian. Similarly, for unsensitive cross-links a stable Gaussian can be obtained only for crossing-angles of the form $\theta = \frac{k2\pi}{M}$, but in addition it is required that for M odd the variational Ansatz has $2M$ -fold order.

Altogether we find for the Gaussian contribution in linear order in the replica index n

$$f_G = \frac{\mu^2 Q^2}{2} \left\{ -1 - \ln(4\pi\xi^2) + \ln \left(1 + 2 \sum_{q=1}^{\infty} \frac{I_q^2(\eta)}{I_0^2(\eta)} \frac{I_{Mq}(\gamma)}{I_0(\gamma)} \right) \right\}.$$

B.2 Log-trace part

We expand the log-trace contribution up to third order in the gel fraction Q :

$$f_{lt} = \mu^2 Q f_{lt,1} + \frac{\mu^4 Q^2}{2} (f_{lt,2} - f_{lt,1}^2) + \frac{\mu^6 Q^3}{6} (f_{lt,3} + 2f_{lt,1}^3 - 3f_{lt,1}f_{lt,2}) + \mathcal{O}(Q^4).$$

The first-order term gives a trivial contribution because of

$$\begin{aligned} f_{lt,1} &= \left\langle \frac{1}{V^n} \overline{\sum_{\hat{\mathbf{k}}} \int_{\check{\varphi}, \check{\varphi}'} \delta_{\mathbf{0}, \sum_{\alpha=0}^n \mathbf{k}^\alpha} e^{-\xi^2 \hat{\mathbf{k}}^2} \frac{e^{\gamma \sum_{\alpha=1}^n \cos(\varphi^\alpha - \varphi'^\alpha - \theta)}}{I_0^n(\gamma)} \times \right. & (B.3) \\ &\quad \left. \times \frac{e^{\eta \sum_{\alpha} \cos(M\varphi'^\alpha)}}{I_0^n(\eta)} \int_s e^{i\hat{\mathbf{k}}\hat{\mathbf{r}}(s)} \delta(\check{\varphi}' - \check{\psi}(s)) \right\rangle \\ &= \frac{1}{V^n} \int_s \left\langle \int_{\check{\varphi}} \frac{e^{\gamma \sum_{\alpha=1}^n \cos(\varphi^\alpha - \psi(s)^\alpha - \theta)}}{I_0^n(\gamma)} \frac{e^{\eta \sum_{\alpha} \cos(M\varphi^\alpha)}}{I_0^n(\eta)} \right\rangle \\ &= \frac{1}{V^n}. \end{aligned}$$

In the second step we use $\hat{\mathbf{r}}(s) = \hat{\mathbf{r}}(0) + \int_0^s d\tau \hat{\mathbf{t}}(\tau)$ and transform the original path integral $\mathcal{D}\{\hat{\mathbf{r}}(s)\}$ into an integral $\frac{d\hat{\mathbf{r}}(0)}{V^{n+1}}$ and a path integral $\mathcal{D}\{\hat{\psi}(s)\}$ over angular variables. Performing the $\hat{\mathbf{r}}(0)$ integration we get a Kronecker delta setting $\hat{\mathbf{k}}$ to zero. The last line of (B.3) follows from the fact that the functions are normalized and that the two integrations with respect to $\check{\varphi}$ and $\check{\psi}(s)$ simply lead to 1.

The second-order contribution reads

$$\begin{aligned} & f_{lt,2} & (B.4) \\ &= \frac{1}{V^{2n}} \int_{s_1, s_2} \left\langle \overline{\sum_{\hat{\mathbf{k}}_1} \overline{\sum_{\hat{\mathbf{k}}_2} \delta_{\mathbf{0}, \sum_{\alpha=0}^n \mathbf{k}_1^\alpha} \delta_{\mathbf{0}, \sum_{\alpha=0}^n \mathbf{k}_2^\alpha} e^{-\xi^2 (\hat{\mathbf{k}}_1^2 + \hat{\mathbf{k}}_2^2)/2} e^{i(\hat{\mathbf{k}}_1 \hat{\mathbf{r}}(s_1) + \hat{\mathbf{k}}_2 \hat{\mathbf{r}}(s_2))}} \right. \\ &\quad \int_{\check{\varphi}_1, \check{\varphi}'_1} \int_{\check{\varphi}_2, \check{\varphi}'_2} \Delta(\check{\varphi}_1 - \check{\varphi}'_1, \theta) \Delta(\check{\varphi}_2 - \check{\varphi}'_2, \theta) \\ &\quad \left. \delta(\check{\varphi}'_1 - \check{\psi}(s_1)) \delta(\check{\varphi}'_2 - \check{\psi}(s_2)) \frac{e^{\eta \sum_{\alpha=1}^n \{\cos(M\varphi_1^\alpha) + \cos(M\varphi_2^\alpha)\}}}{I_0^{2n}(\eta)} \right\rangle. \end{aligned}$$

Before expanding the expression in the variational parameters, we need to perform the summations over $\hat{\mathbf{k}}_1$ and $\hat{\mathbf{k}}_2$. We integrate over $d\hat{\mathbf{r}}(0)$ as before and get a Kronecker Delta imposing $\hat{\mathbf{k}}_1 = -\hat{\mathbf{k}}_2$. Hence, there is only one summation

left. We replace this sum by an integral and represent the Kronecker delta in Fourier space. After two Gaussian integrations we find

$$\begin{aligned}
 f_{lt,2} = & \frac{1}{V^n} \left(\frac{1}{4\pi\xi^2} \right)^n \frac{1}{n+1} \int_{s_1, s_2} \left\langle e^{\frac{1}{4\xi^2} \left(\frac{1}{n+1} \sum_{\alpha\beta=0}^n \mathbf{f}^\alpha \mathbf{f}^\beta - \sum_{\alpha=0}^n (\mathbf{f}^\alpha)^2 \right)} \times \right. \\
 & \times \int_{\Delta\check{\varphi}_1, \Delta\check{\varphi}_2} \frac{e^{\gamma \sum_{\alpha=1}^n (\cos(\Delta\varphi_1^\alpha) + \cos(\Delta\varphi_2^\alpha))}}{I_0^{2n}(\gamma)} \times \\
 & \left. \times \frac{e^{\eta \sum_{\alpha=1}^n \{\cos(M(\psi_1^\alpha + \Delta\varphi_1^\alpha)) + \cos(M(\psi_2^\alpha + \Delta\varphi_2^\alpha))\}}}{I_0^{2n}(\eta)} \right\rangle
 \end{aligned} \quad (\text{B.5})$$

using the shorthand notations $\mathbf{f}^\alpha \equiv \int_{s_1}^{s_2} ds \mathbf{t}^\alpha(s)$ and $\psi_i^\alpha := \psi^\alpha(s_i)$. This expression is ready to be expanded in the variational parameters $\frac{1}{\xi^2}$ and η and the remaining task consists then in calculating the corresponding correlation functions. Details are given in Appendix B.3.

For the calculation of the third-order term, we proceed the same way as before and thus need to perform three sums over wave vectors. Using the abbreviation $\mathbf{f}_l^\alpha \equiv \int_{s_3}^{s_l} d\tau \mathbf{t}^\alpha(\tau)$ the result reads

$$\begin{aligned}
 f_{lt,3} = & \frac{1}{V^n} \left(\frac{1}{4\pi\xi^2} \right)^n \left(\frac{1}{3\pi\xi^2} \right)^n \left(\frac{1}{n+1} \right)^2 \int_{s_1, s_2, s_3} \\
 & \left\langle \exp \left\{ \frac{1}{3\xi^2} \left(\frac{1}{n+1} \sum_{\alpha, \beta=0}^n (\mathbf{f}_1^\alpha \mathbf{f}_1^\beta + \mathbf{f}_2^\alpha \mathbf{f}_2^\beta + \mathbf{f}_1^\alpha \mathbf{f}_2^\beta) \right. \right. \right. \\
 & \quad \left. \left. \left. - \sum_{\alpha=0}^n ((\mathbf{f}_1^\alpha)^2 + (\mathbf{f}_2^\alpha)^2 + \mathbf{f}_1^\alpha \mathbf{f}_2^\alpha) \right) \right\} \times \right. \\
 & \times \int_{\Delta\check{\varphi}_1, \Delta\check{\varphi}_2, \Delta\check{\varphi}_3} \frac{e^{\gamma \sum_{\alpha=1}^n (\cos(\Delta\varphi_1^\alpha) + \cos(\Delta\varphi_2^\alpha) + \cos(\Delta\varphi_3^\alpha))}}{I_0^{2n}(\gamma)} \times \\
 & \left. \times \frac{e^{\eta \sum_{\alpha=1}^n \{\cos(M(\psi_1^\alpha + \Delta\varphi_1^\alpha)) + \cos(M(\psi_2^\alpha + \Delta\varphi_2^\alpha)) + \cos(M(\psi_3^\alpha + \Delta\varphi_3^\alpha))\}}}{I_0^{3n}(\eta)} \right\rangle.
 \end{aligned} \quad (\text{B.6})$$

B.3 Evaluation of the expectation values

Expanding the M -fold free energy derived in the previous two sections we include terms from the second order log-trace contribution (B.5) up to first order in $\frac{1}{\xi^2}$ and up to sixth order in η . These contributions involve a number of correlation functions which are calculated in the following. Calculating the correlation function corresponding to the **spatial contribution** $\propto \frac{1}{\xi^2}$ we

obtain

$$\begin{aligned}
 & \int_{s_1, s_2} \left(\frac{1}{n+1} \sum_{\alpha, \beta=0}^n \langle \mathbf{f}^\alpha \mathbf{f}^\beta \rangle - \sum_{\alpha=0}^n \langle (\mathbf{f}^\alpha)^2 \rangle \right) \\
 = & -n \int_{s_1, s_2} \int_{s_1}^{s_2} d\tau \int_{s_1}^{s_2} d\tau' \langle \mathbf{t}(\tau) \mathbf{t}(\tau') \rangle \\
 = & -n \int_{s_1, s_2} \int_{s_1}^{s_2} d\tau \int_{s_1}^{s_2} d\tau' e^{-\frac{1}{2\kappa}|\tau-\tau'|} \\
 =: & -nL^2 g\left(\frac{L}{L_p}\right) \tag{B.7}
 \end{aligned}$$

The first expectation value in the first line contributes only for $\alpha = \beta$ and is combined with the second expectation value. Noticing that each replica gives rise to the same contribution we obtain the prefactor of $-n$. It is interesting to note that the function g is closely related to the radius of gyration R_g .

$$\begin{aligned}
 R_g^2 & := \frac{1}{2} \int_{s_1, s_2} \langle (\mathbf{r}(s_1) - \mathbf{r}(s_2))^2 \rangle \tag{B.8} \\
 & = \frac{1}{2} \int_{s_1, s_2} \int_{s_2}^{s_1} d\tau d\tau' \langle \mathbf{t}(\tau) \mathbf{t}(\tau') \rangle \\
 & = \frac{L^2}{2} g\left(\frac{L}{L_p}\right)
 \end{aligned}$$

In order to calculate the lowest order **coupling terms** we expand the spatial part of (B.5) in first order. For $\theta = \frac{k}{M}2\pi$ we find

$$\begin{aligned}
 f_{coupl} & := \frac{1}{4\xi^2} \left\langle \left\{ \frac{1}{n+1} \sum_{\alpha \neq \beta=0}^n \mathbf{f}^\alpha \mathbf{f}^\beta - \frac{n}{n+1} \sum_{\alpha=0}^n (\mathbf{f}^\alpha)^2 \right\} \times \right. \tag{B.9} \\
 & \quad \times \int_{\Delta\varphi_1, \Delta\varphi_2} \frac{e^{\gamma \sum_{\alpha=1}^n (\cos \Delta\varphi_1^\alpha + \cos \Delta\varphi_2^\alpha)}}{I_0^{2n}(\gamma)} \times \\
 & \quad \left. \times \frac{e^{\eta \sum_{\gamma=1}^n \{\cos(M(\psi_1^\gamma + \Delta\varphi_1^\gamma)) + \cos(M(\psi_2^\gamma + \Delta\varphi_2^\gamma))\}}}{I_0^{2n}(\eta)} \right\rangle.
 \end{aligned}$$

We can omit the second term in the first line of (B.9) because it is already proportional to n and will give rise to contributions proportional to n^2 . Keeping for the moment only terms that are directly involved in the calculation of

B.3. EVALUATION OF THE EXPECTATION VALUES

the thermal expectation value, we have to consider the following expression:

$$\begin{aligned}
f_{coupl} &\sim \sum_{\alpha \neq \beta=1}^n \left\langle \left\{ \cos \psi_\tau^\alpha \cos \psi_{\tau'}^\beta + \sin \psi_\tau^\alpha \sin \psi_{\tau'}^\beta \right\} \times \right. \\
&\quad \left. \times e^{\eta \sum_{\gamma=1}^n \left\{ \cos(M(\psi_1^\gamma + \Delta\varphi_1^\gamma)) + \cos(M(\psi_2^\gamma + \Delta\varphi_2^\gamma)) \right\}} \right\rangle \\
&= -n \delta_{M,1} \left\{ \underbrace{\left\langle \cos \psi_\tau^1 e^{\eta(c_1^1 + c_2^1)} \right\rangle \left\langle \cos \psi_\tau^2 e^{\eta(c_1^2 + c_2^2)} \right\rangle}_{(*)} \right. \\
&\quad \left. + \left\langle \sin \psi_\tau^1 e^{\eta(c_1^1 + c_2^1)} \right\rangle \left\langle \sin \psi_\tau^2 e^{\eta(c_1^2 + c_2^2)} \right\rangle \right\} \times \\
&\quad \times \underbrace{\prod_{\gamma=3}^n \left\langle e^{\eta(c_1^\gamma + c_2^\gamma)} \right\rangle}_{(**)} . \tag{B.10}
\end{aligned}$$

Here, we used the abbreviations $c_i^\alpha := \cos(\psi^\alpha(s_i) + \Delta\varphi_i^\alpha)$. This expectation value is only non-vanishing for $M = 1$ because of the relation (A.6): the Fourier transform of $\cos(\psi_\tau)$ has contributions for the modes $q = \pm 1$, but the Fourier transform of $\exp(\eta \cos(M\psi(s_1)))$ for the modes $q = \pm \mathbb{Z}M$. Therefore, it is only in the case of $M = 1$ that the Fourier transforms of the cosine and the exponential function have non-zero Fourier modes which couple and provide a non-vanishing result. The prefactor of $-n \sim n(n-1)$ stems from the number of ways to combine the indices α and β from the spatial contribution with the γ 's from the orientational contribution.

We need to compute three types of expectation values. Including again the terms due to the cross-link constraints they are given by

$$\begin{aligned}
&\frac{1}{I_0^2(\gamma)} \int_{\Delta\varphi_1, \Delta\varphi_2} e^{\gamma \cos \Delta\varphi_1} e^{\gamma \cos \Delta\varphi_2} \times \\
&\quad \times \left\langle \cos(\psi_\tau) e^{\eta \{ \cos(\psi_1 + \Delta\varphi_1) + \cos(\psi_2 + \Delta\varphi_2) \}} \right\rangle \\
&= \sum_{q \in \mathbb{N}_0} I_q(\eta) I_{q+1}(\eta) \frac{I_q(\gamma) I_{q+1}(\gamma)}{I_0^2(\gamma)} \times \\
&\quad \times \frac{1}{2} \left\{ e^{-\frac{1}{2\kappa}(q^2|s_1 - \tau| + (q+1)^2|s_2 - \tau|)} + e^{-\frac{1}{2\kappa}((q+1)^2|s_1 - \tau| + q^2|s_2 - \tau|)} \right\}
\end{aligned} \tag{B.11}$$

which stems from (*) in (B.10),

$$\begin{aligned} & \frac{1}{I_0^2(\gamma)} \int_{\Delta\varphi_1, \Delta\varphi_2} e^{\gamma \cos \Delta\varphi_1} e^{\gamma \cos \Delta\varphi_2} \times \\ & \times \left\langle \sin(\psi_\tau) e^{\eta \{\cos(\psi_1 + \Delta\varphi_1) + \cos(\psi_2 + \Delta\varphi_2)\}} \right\rangle = 0 \end{aligned} \quad (\text{B.12})$$

which stems from the vanishing term one line below, and lastly the correlation function corresponding to (**):

$$\begin{aligned} & \frac{1}{I_0^2(\gamma)} \int_{\Delta\varphi_1, \Delta\varphi_2} e^{\gamma \cos \Delta\varphi_1} e^{\gamma \cos \Delta\varphi_2} \times \\ & \times \left\langle e^{\eta \{\cos(\psi(s_1) + \Delta\varphi_1) + \cos(\psi(s_2) + \Delta\varphi_2)\}} \right\rangle \\ & = I_0^2(\eta) + 2 \sum_{q \in \mathbb{N}} I_q^2(\eta) \frac{I_q^2(\gamma)}{I_0^2(\gamma)} e^{-\frac{1}{2\kappa} q^2 |s_1 - s_2|} . \end{aligned} \quad (\text{B.13})$$

From (B.10) we obtain the coefficients of the coupling terms proportional to $\frac{\eta^2}{\xi^2}$, $\frac{\eta^4}{\xi^2}$ and $\frac{\eta^6}{\xi^2}$ by sampling all the ways to collect the corresponding powers in η from the different factors. For e.g. $\frac{\eta^2}{\xi^2}$ the only way to collect a factor of η^2 is to expand the two averages in (*) in first order and leave out (**). The result is

$$\begin{aligned} f_{\text{coupl}} \sim & -\mu^2 \frac{1}{4\xi^2} \left\{ \eta^2 \frac{I_q^2}{I_0^2} l(\alpha) \right. \\ & + \frac{\eta^4}{4} \left(-\frac{I_1^2}{I_0^2} l(\alpha) + \frac{I_1^2 I_2}{I_0^3} l_3(\alpha) - 4 \frac{I_1^4}{I_0^4} l_2(\alpha) \right) \\ & + \frac{\eta^6}{4} \left(\frac{155}{48} \frac{I_1^2}{I_0^2} l(\alpha) - \frac{5}{12} \frac{I_1^2 I_2}{I_0^3} l_3(\alpha) \right. \\ & \quad + \frac{1}{16} \frac{I_1^2 I_2^2}{I_0^4} l_5(\alpha) + \frac{1}{24} \frac{I_1 I_2 I_3}{I_0^3} l_4(\alpha) \\ & \quad \left. \left. - \frac{1}{4} \frac{I_1^2 I_2^2}{I_0^4} l_6(\alpha) - \frac{I_1^4 I_2}{I_0^5} l_7(\alpha) + 8 \frac{I_1^4}{I_0^4} l_2(\alpha) \right) \right\} \end{aligned} \quad (\text{B.14})$$

where the correlation functions are defined by

$$\begin{aligned}
 l(x) &:= \frac{7 - 8e^{-x} + e^{-2x} - 6x + 2x^2}{2x^4} , & (B.15) \\
 l_2(x) &:= \frac{-11 - 9e^{-2x} + 2e^{-3x} + 18e^{-x} + 6x}{9x^4} , \\
 l_3(x) &:= \frac{1}{600x^4} \left(-291 - 100e^{-2x} + 400e^{-x} + 16e^{-5x} - 25e^{-4x} + 180x \right) , \\
 l_4(x) &:= \frac{1}{81000x^4} \left(-653 - 1296e^{-5x} \right. \\
 &\quad \left. + 2025e^{-4x} + 324e^{-10x} - 400e^{-9x} + 1260x \right) , \\
 l_5(x) &:= \frac{1}{7200x^4} \left(-297 + 400e^{-2x} - 128e^{-5x} + 25e^{-8x} + 360x \right) , \\
 l_6(x) &:= \frac{1}{1800x^4} \left(-37 + 100e^{-6x} - 288e^{-5x} + 225e^{-4x} + 60x \right) , \\
 l_7(x) &:= \frac{1}{1350x^4} \left(-114 - 100e^{-3x} + 225e^{-2x} + 25e^{-6x} - 36e^{-5x} + 120x \right) .
 \end{aligned}$$

In the case of **hard cross-links** it is convenient to introduce the following functions:

$$\tilde{l}(x) := 16 \left(l(x) + 4l_2(x) - l_3(x) \right) \quad (B.16)$$

and

$$\begin{aligned}
 \tilde{\tilde{l}}(x) &:= \left(\frac{155}{3}l(x) + 128l_2(x) - \frac{20}{3}l_3(x) \right. \\
 &\quad \left. + \frac{2}{3}l_4(x) + l_5(x) - 4l_6(x) - 16l_7(x) \right) .
 \end{aligned} \quad (B.17)$$

Turning to the calculation of the purely **orientational part** of (B.5) we notice first that it is factorizing in the replica index α . It is thus possible to take the replica limit directly by means of the expansion $\langle \dots \rangle^n = 1 + n \ln \langle \dots \rangle + \mathcal{O}(n^2)$ and we obtain

$$\begin{aligned}
 f_{or} &= 1 + n \int_{s_1, s_2} \ln \left(\left\langle \int_{\Delta\varphi_1, \Delta\varphi_2} \frac{e^{\gamma(\cos \Delta\varphi_1 + \cos \Delta\varphi_2)}}{I_0^2(\gamma)} \times \right. \right. \\
 &\quad \left. \left. \times \frac{e^{\eta(\cos(M(\psi_1 + \Delta\varphi_1)) + \cos(M(\psi_2 + \Delta\varphi_2)))}}{I_0^2(\eta)} \right\rangle \right) .
 \end{aligned} \quad (B.18)$$

The thermal average can be performed using formula (A.6). Keeping only the

contributions linear in the replica index n we obtain

$$f_{or} = \int_{s_1, s_2} \ln \left(\left\langle \int_{\Delta\varphi_1, \Delta\varphi_2} \frac{e^{\gamma(\cos \Delta\varphi_1 + \cos \Delta\varphi_2)}}{I_0^2(\gamma)} \times \right. \right. \quad (\text{B.19})$$

$$\left. \left. \times \sum_{q \in \mathbb{Z}} e^{-\frac{q^2}{2\kappa}|s_1 - s_2|} \frac{I_q^2(\eta)}{I_0^2(\eta)} e^{iq(\Delta\varphi_1 - \Delta\varphi_2)} \right\rangle \right).$$

The $\Delta\varphi$ -integrations lead to a Fourier transformation of the soft cross-link contributions. Noticing that the resulting expression is symmetric in q , it can be written as

$$f_{or} = \int_{s_1, s_2} \ln \left(1 + 2 \sum_{q=1}^{\infty} \frac{I_q^2(\eta)}{I_0^2(\eta)} \frac{I_{Mq}^2(\gamma)}{I_0^2(\gamma)} e^{-\frac{q^2 M^2}{2\kappa}|s_1 - s_2|} \right). \quad (\text{B.20})$$

When expanding this expression in η and performing the s_1 - and s_2 -integrations it is convenient to introduce the Debye function $h(x)$:

$$h\left(\frac{L}{L_p}\right) := \int_{s_1, s_2} e^{-\frac{1}{2\kappa}|s_1 - s_2|}. \quad (\text{B.21})$$

In the case of hard cross-links we need furthermore the following two functions:

$$\tilde{h}(x) \equiv h(x) + h(2x) - \frac{1}{4}h(4x) \quad (\text{B.22})$$

which belongs to the term of the log-trace contribution $\propto \eta^4$ and

$$\begin{aligned} \tilde{\tilde{h}}(x) \equiv & \frac{11}{16}h(x) + 3h(2x) + h(3x) - \frac{1}{4}h(4x) \\ & - \frac{3}{8}h(5x) + \frac{1}{48}h(9x) \end{aligned} \quad (\text{B.23})$$

corresponding to the term $\propto \eta^6$.

Appendix C

Calculations SIAS

C.1 Gaussian part

The gaussian contribution to the SIAS variational free energies (5.17) for hard and (6.7) for soft cross-links is given by

$$f_g = \frac{\mu^2 Q^2}{2V^n} \sum_{\hat{\mathbf{k}}} \delta_{\mathbf{0}, \sum_{\alpha=0}^n \mathbf{k}^\alpha} e^{-\xi^2 \hat{\mathbf{k}}^2} \times \int_{\tilde{\varphi}, \tilde{\varphi}'} \Delta(\tilde{\varphi} - \tilde{\varphi}', \theta) \frac{I_0(\eta |\sum_{\alpha=1}^n \mathbf{u}^\alpha|) I_0(\eta |\sum_{\alpha=1}^n \mathbf{u}'^\alpha|)}{I_0^{2n}(\eta)} \quad (\text{C.1})$$

where $\mathbf{u}^\alpha = (\cos \varphi^\alpha, \sin \varphi^\alpha)$. The spatial part is treated in the same way as for the M -fold case, but the orientational contribution is slightly more complicated because it does not factorize in the replica index. By means of the integral representation of the Bessel function,

$$I_0(\eta) = \frac{1}{2\pi} \int_0^{2\pi} d\vartheta e^{\eta \cos \vartheta}, \quad (\text{C.2})$$

we get a factorizing expression and find in linear order in n for the orientational part of the free energy

$$f_o = 1 + n \int_{\vartheta_1, \vartheta_2} \ln \left(\int_{\varphi_1, \varphi_2} \Delta(\varphi_1 - \varphi_2, \theta) \times \frac{1}{I_0^2(\eta)} e^{\eta(\cos(\varphi_1 + \vartheta_1) + \cos(\varphi_2 + \vartheta_2))} \right) \quad (\text{C.3})$$

$$= 1 + n \int_{\vartheta} \ln \left(1 + 2 \sum_{q \in \mathbb{N}} \frac{I_q^2(\eta)}{I_0^2(\eta)} \frac{I_q(\gamma)}{I_0(\gamma)} \cos(\vartheta) \right).$$

In order to obtain the last line we simply switch from the angular variables to Fourier space. The expression is then easily expanded up to the desired order.

C.2 Log-trace part

The first-order contribution of the log-trace part gives the same (trivial) result as for the long-range ordered case. As for the second and third order terms we need first of all to perform the \mathbf{k} summations. This calculation is done exactly in the same way as before. The corresponding results can be obtained from those of the M -fold case by simply replacing the M -fold orientational distributions in (B.5) and (B.6) by the corresponding SIAS distributions.

The calculation of the expectation values in the second order contributions of the SIAS log-trace part can be done along the same lines as above using again the integral representation of the Bessel function (C.2). The calculation of the lowest order **spatial contributions** is the exactly same as for the M -fold case. For the **purely orientational** we obtain

$$f_{lt2,or} = \int_{s_1, s_2} \int_{\vartheta_1, \vartheta_2} \ln \left(1 + 2 \sum_{q=1}^{\infty} \frac{I_q^2(\eta) I_q^2(\gamma)}{I_0^2(\eta) I_0^2(\gamma)} \times \right. \\ \left. \times e^{-\frac{q^2}{2\kappa} |s_1 - s_2|} \cos(q(\vartheta_1 - \vartheta_2)) \right). \quad (C.4)$$

Expanding this expression in η and performing the s_1 - and s_2 -integrations, we need the function $h(s)$ which we introduced already in equation (B.21) in the previous section. The lowest order **coupling term** is given by

$$\frac{1}{4\xi^2} \left\langle \left(\frac{1}{n+1} \sum_{\alpha \neq \beta=0}^n \mathbf{f}^\alpha \mathbf{f}^\beta - \frac{n}{n+1} \sum_{\alpha=0}^n (\mathbf{f}^\alpha)^2 \right) \times \right. \\ \times \int_{\vartheta_1, \vartheta_2} \int_{\Delta\check{\varphi}_1, \Delta\check{\varphi}_2} \frac{e^{\gamma \sum_{\alpha=1}^n (\cos \Delta\varphi_1^\alpha + \cos \Delta\varphi_2^\alpha)}}{I_0^{2n}(\gamma)} \times \\ \times \frac{\eta^2}{2} \sum_{\gamma, \delta=1}^n \left(\cos(\psi_1^\gamma - \vartheta_1 + \Delta\varphi_1^\gamma) + \cos(\psi_2^\gamma - \vartheta_2 + \Delta\varphi_2^\gamma) \right) \\ \left. \times \left(\cos(\psi_1^\delta - \vartheta_1 + \Delta\varphi_1^\delta) + \cos(\psi_2^\delta - \vartheta_2 + \Delta\varphi_2^\delta) \right) \right\rangle \quad (C.5)$$

The second term in the first line having a prefactor of n it will give rise to contribution of order n^2 . Hence, it can be dropped because only terms linear in n contribute to the physical free energy. Integrating with respect to the ϑ -variables and then with respect to the φ -variables yields

$$-n \frac{\eta^2}{8\xi^2} \frac{I_1^2(\gamma)}{I_0^2(\gamma)} l(\alpha) \quad , \quad (C.6)$$

where the function $l(x)$ is defined in equation (B.15) of the preceding section.

Appendix D

Calculations M-fold II

D.1 Gaussian part

The gaussian contribution is given by

$$f_g = \frac{\mu^2 Q^2}{2V^n} \sum_{\hat{\mathbf{k}}} \delta_{\mathbf{0}, \sum_{\alpha=0}^n \mathbf{k}^\alpha} e^{-\xi^2 \hat{\mathbf{k}}^2} \times \quad (\text{D.1})$$

$$\times \int_{\check{\varphi}_1, \check{\varphi}_2} \Delta(\check{\varphi}_1 - \check{\varphi}_2, \theta) \frac{1}{M} \sum_{l_1=1}^M \frac{e^{\eta \sum_{\alpha} \cos(\varphi_1^\alpha - \theta_{l_1})}}{I_0^n(\eta)} \times \frac{1}{M} \sum_{l_2=1}^M \frac{e^{\eta \sum_{\alpha} \cos(\varphi_2^\alpha - \theta_{l_2})}}{I_0^n(\eta)}$$

where we introduced the notation $\theta_l := l \frac{2\pi}{M}$. The spatial part is the same as for the Ansätze discussed in the preceding sections and gives rise to the same result. The orientational part f_o , on the other hand, can be simplified considerably. Noticing that the second line of (D.1) factorizes in the replica index α , it is possible to take the replica limit $n \rightarrow 0$ by means of the relation $(\cdot)^n = 1 + n \ln(\cdot) + \mathcal{O}(n^2)$. We obtain

$$f_o \sim 1 + n \frac{1}{M^2} \sum_{l_1, l_2=1}^M \ln \left(\int_{\varphi} \frac{e^{\eta \{\cos(\varphi - \theta_{l_1} + \theta) + \cos(\varphi - \theta_{l_2})\}}}{I_0^2(\eta)} \right) . \quad (\text{D.2})$$

There are two different ways to represent this contribution. The first variant amounts to combining the two cosines inside the exponential function by means of $\cos x + \cos y = 2 \cos(\frac{x+y}{2}) \cos(\frac{x-y}{2})$ and performing the φ -integration. The result is

$$f_o \sim 1 + n \frac{1}{M} \sum_{l=1}^M \ln \left(\frac{I_0(2\eta \cos(\frac{\theta_l - \theta}{2}))}{I_0^2(\eta)} \right) . \quad (\text{D.3})$$

This expression is well-suited for addressing the question if the purely orientational part of the gaussian contribution is asymptotically stable. For large

values of η we find

$$\begin{aligned}
 & \lim_{\eta \rightarrow \infty} \frac{1}{M} \sum_{l=1}^M \ln \frac{I_0(2\eta \cos(l\pi/M - \theta/2))}{I_0^2(\eta)} \quad (\text{D.4}) \\
 &= \lim_{\eta \rightarrow \infty} -2 \ln I_0(\eta) + \frac{1}{M} \sum_{l=1}^M \ln I_0(2\eta \cos(l\pi/M - \theta/2)) \\
 &\leq \lim_{\eta \rightarrow \infty} -2 \ln I_0(\eta) + \frac{1}{M} \ln I_0(2\eta) + \frac{M-1}{M} \ln I_0(2\eta(1-\epsilon)) \\
 &\sim \lim_{\eta \rightarrow \infty} 2\eta(-\epsilon) \frac{M-1}{M} = -\infty \quad ,
 \end{aligned}$$

where ϵ has to be chosen sufficiently small. In the last line, we used the asymptotic expansion of the Bessel function $I_0(x)$ (A.3) in lowest order. Hence, the gaussian orientational contribution diverges for large values of η to $-\infty$.

We obtain the second variant of f_o by expressing the two exponentials in (D.2) in Fourier space and integrating over φ . This yields

$$f_o \sim 1 + n \frac{1}{M} \sum_{l=1}^M \ln \left(1 + 2 \sum_{q=1}^{\infty} \frac{I_q^2(\eta)}{I_0^2(\eta)} \cos(q(\theta_l - \theta)) \right) \quad , \quad (\text{D.5})$$

which is equivalent to (D.3). After expanding either (D.3) or (D.5) in η , one has to perform the sums over the M orientational axes. This gives rise to Kronecker deltas indicating for which value of M each contribution is present.

D.2 Log-trace part

After performing the $\hat{\mathbf{k}}$ summations and the $\check{\varphi}$ -integrations the second order contribution of the log-trace part reads

$$\begin{aligned}
 f_{lt2} &= -\frac{1}{2} \frac{\mu^4 Q^2}{V^n} \left(\frac{1}{4\pi\xi^2} \right)^n \frac{1}{n+1} \int_{s_1, s_2} \left\langle e^{\frac{1}{4\xi^2} \left(\frac{1}{n+1} \sum_{\alpha\beta=0}^n \check{f}^\alpha \check{f}^\beta - \sum_{\alpha=0}^n (\check{f}^\alpha)^2 \right)} \times (\text{D.6}) \right. \\
 &\quad \left. \times \frac{1}{M} \sum_{l_1=1}^M \frac{e^{\eta \sum_{\alpha} \cos(\psi_1^\alpha - \theta_{l_1} + \theta)}}{I_0^n(\eta)} \times \frac{1}{M} \sum_{l_2=1}^M \frac{e^{\eta \sum_{\alpha} \cos(\psi_2^\alpha - \theta_{l_2} + \theta)}}{I_0^n(\eta)} \right\rangle .
 \end{aligned}$$

Here, we use the abbreviations $\theta_l := l \frac{2\pi}{M}$ and $\psi_i := \psi(s_i)$. The crossing angle θ appearing two times in the orientational part is omitted because it can be shifted to the spatial part by means of a rotation $\psi(s) \rightarrow \psi(s) - \theta$, $\forall s$. The spatial part itself is rotationally invariant and therefore, θ drops out.

We now expand the free energy in $\frac{1}{\xi^2}$ and η . The lowest order term $\propto \frac{1}{\xi^2}$ of the **spatial part** has already been calculated in Appendix B.1. As for the

$\frac{1}{\xi^4}$ contribution, only the terms with $\alpha \neq \beta$ and $\gamma \neq \delta$ contribute and hence, there are $2(n+1)n$ equivalent contributions. The corresponding expectation value gives rise to

$$\begin{aligned}
 r\left(\frac{L}{L_p}\right) &:= \frac{1}{nL^2} \int_{s_1, s_2} \left(\frac{1}{n+1} \sum_{\alpha, \beta=0}^n \langle \vec{f}^\alpha \vec{f}^\beta \rangle - \sum_{\alpha=0}^n \langle (\vec{f}^\alpha)^2 \rangle \right) \times \\
 &\quad \times \left(\frac{1}{n+1} \sum_{\gamma, \delta=0}^n \langle \vec{f}^\gamma \vec{f}^\delta \rangle - \sum_{\gamma=0}^n \langle (\vec{f}^\gamma)^2 \rangle \right) \\
 &= 4 \int_{s_1, s_2} \int_{s_2}^{s_1} d\tau_1 d\tau'_1 d\tau_2 d\tau'_2 \langle \cos(\psi_{\tau_1}) \cos(\psi_{\tau_2}) \rangle \langle \cos(\psi_{\tau'_1}) \cos(\psi_{\tau'_2}) \rangle \\
 &= \int_{s_1, s_2} \int_{s_2}^{s_1} d\tau_1 d\tau'_1 d\tau_2 d\tau'_2 e^{-\frac{1}{2\kappa}(|\tau_1 - \tau_2| + |\tau'_1 - \tau'_2|)} .
 \end{aligned} \tag{D.7}$$

In the limit of small n the purely **orientational part** reads

$$f_{lt2,o} \propto 1+n \int_{s_1, s_2} \frac{1}{M^2} \sum_{l_1, l_2=1}^M \ln \left\langle \frac{\exp\left(\eta\{\cos(\psi_1 - \theta_{l_1}) + \cos(\psi_2 - \theta_{l_2})\}\right)}{I_0^2(\eta)} \right\rangle . \tag{D.8}$$

By means of equation (A.6) the expectation value is easily computed and we obtain the result

$$f_{lt2,o} \propto 1+n \int_{s_1, s_2} \frac{1}{M} \sum_{l=1}^M \ln \left(1 + 2 \sum_{q=1}^n e^{-\frac{q^2}{2\kappa}|s_1 - s_2|} \frac{I_q^2(\eta)}{I_0^2(\eta)} \cos(q\theta_l) \right) . \tag{D.9}$$

Lastly, we need to calculate the **coupling terms** proportional to $\frac{\eta}{\xi^2}$ and $\frac{\eta^2}{\xi^2}$. The term $\propto \frac{\eta}{\xi^2}$ does not contribute because it involves an odd number of angular variables. Therefore, the expectation value vanishes according to the rule (A.10). The term $\propto \frac{\eta^2}{\xi^2}$ reads

$$\begin{aligned}
 \frac{\eta^2}{8\xi^2} &\left\langle \left(\frac{1}{n+1} \sum_{\alpha \neq \beta=0}^n \vec{f}^\alpha \vec{f}^\beta - \frac{n}{n+1} \sum_{\alpha=0}^n (\vec{f}^\alpha)^2 \right) \times \right. \\
 &\quad \left. \times \sum_{\gamma, \delta=1}^n \left\{ \cos(\psi_1^\gamma - \theta_{l_1}) \cos(\psi_1^\delta - \theta_{l_1}) + \cos(\psi_2^\gamma - \theta_{l_2}) \cos(\psi_2^\delta - \theta_{l_2}) \right\} \right\rangle .
 \end{aligned} \tag{D.10}$$

The second term of the spatial part can be omitted because it gives rise to contributions proportional to n^2 . In order to make sure that the result is non-vanishing we have to pair the indices α, β with γ, δ . There are $2n(n-1)$ possibilities to do so. We thus need the pair correlators

$$\begin{aligned}
 \langle \cos(\psi_\tau) \cos(\psi_s - \theta_l) \rangle &= \frac{1}{2} e^{-\frac{1}{2\kappa}|\tau - s|} \cos(\theta_l) \quad , \\
 \text{and } \langle \sin(\psi_\tau) \cos(\psi_s - \theta_l) \rangle &= \frac{1}{2} e^{-\frac{1}{2\kappa}|\tau - s|} \sin(\theta_l) \quad .
 \end{aligned}$$

Putting all the contributions together and carrying out the sums and the four integrals we arrive at the result

$$n(n-1)\frac{\eta^2}{8\xi^2}l\left(\frac{L}{L_p}\right)\sim -n\frac{\eta^2}{8\xi^2}l\left(\frac{L}{L_p}\right)\quad , \quad (\text{D.11})$$

where the function $l(x)$ already has been defined in equation (B.15).

D.3 Lowest order contribution to ΔF

In section 5.4.1, we showed that the orientational distributions of the SIAS and the alternative M -fold Ansatz are quite similar. More precisely, expanding the corresponding orientational distributions it is only in order η^M that there is a term which exclusively is present for the M -fold but not for the SIAS Ansatz. This term will give rise to contributions to the quantity $\Delta F = F_{M\text{-fold}} - F_{SIAS}$ that we consider in sections 5.4.3 and 5.4.4 in order to decide if M -fold order or the SIAS is physically favored. In the following, we will look for the contribution to ΔF being of lowest order in the gel fraction Q . This term decides about the physical state just beyond the the sol-gel transition where $Q \ll 1$.

First of all, we consider the purely orientational contributions. The expansion of the orientational distribution of the M -fold Ansatz up to the first M -specific term reads

$$\begin{aligned} \omega_{M\text{-fold}}(\hat{\mathbf{O}}, \check{\psi}) = \frac{1}{I_0^n(\eta)} \left\{ 1 + \frac{\eta^2}{2} \sum_{\alpha_1, \alpha_2=1}^n \cos(\psi^{\alpha_1} - \psi^{\alpha_2}) \right. & (\text{D.12}) \\ + \frac{\eta^4}{8} \sum_{\alpha_1, \alpha_2, \alpha_3, \alpha_4=1}^n \cos(\psi^{\alpha_1} - \psi^{\alpha_2} + \psi^{\alpha_3} - \psi^{\alpha_4}) & \\ + \dots & \\ + \frac{\eta^M}{M!} \sum_{\alpha_1, \dots, \alpha_M} \cos\left(\sum_{i=1}^M \psi^{\alpha_i}\right) & \\ + \mathcal{O}(\eta^{M+1}) & \left. \right\}. \end{aligned}$$

Note that in the case of M being even, there is also a SIAS contribution of order η^M that we did not include explicitly in the above formula. The in

second order purely orientational contribution to ΔF can be written as

$$\begin{aligned} \Delta \mathcal{F}_{or} = & \frac{\mu^2 Q^2}{2} \int_{\check{\varphi}} \left\{ \omega_{M-fold}^2(\hat{\mathbf{0}}, \check{\varphi}) - \omega_{SIAS}^2(\hat{\mathbf{0}}, \check{\varphi}) \right\} \\ & - \frac{\mu^4 Q^2}{2} \int_{s_1, s_2} \left\{ \left\langle \omega_{M-fold}(\hat{\mathbf{0}}, \check{\psi}(s_1)) \omega_{M-fold}(\hat{\mathbf{0}}, \check{\psi}(s_2)) \right\rangle \right. \\ & \left. - \left\langle \omega_{SIAS}(\hat{\mathbf{0}}, \check{\psi}(s_1)) \omega_{SIAS}(\hat{\mathbf{0}}, \check{\psi}(s_2)) \right\rangle \right\} . \end{aligned} \quad (\text{D.13})$$

The first line corresponds to the gaussian contributions and the second and third lines to the second order log-trace contributions.

Considering (D.13) what is the lowest order contribution? Because of the rule (A.9) applying to the log-trace part as well as to the Gaussian (see equation (A.8)) it is clear that in the ω_{M-fold}^2 contribution there are no coupling terms between the M-specific and the other terms. Hence, all the terms of ω_{M-fold}^2 which are not M-specific cancel with those from the ω_{SIAS}^2 contribution. The lowest order contribution is then given by

$$\begin{aligned} \Delta \mathcal{F}_{or} \sim & \frac{\mu^2 Q^2}{2} \frac{\eta^{2M}}{(M!)^2} \sum_{\alpha_1, \dots, \alpha_M} \sum_{\beta_1, \dots, \beta_M} \int_{\check{\varphi}} \cos \left(\sum_{i=1}^M \varphi^{\alpha_i} \right) \cos \left(\sum_{i=1}^M \varphi^{\beta_i} \right) \\ & - \frac{\mu^4 Q^2}{2} \int_{s_1, s_2} \frac{\eta^{2M}}{(M!)^2} \sum_{\alpha_1, \dots, \alpha_M} \sum_{\beta_1, \dots, \beta_M} \\ & \left\langle \cos \left(\sum_{i=1}^M \psi^{\alpha_i}(s_1) \right) \cos \left(\sum_{i=1}^M \psi^{\beta_i}(s_2) \right) \right\rangle \end{aligned} \quad (\text{D.14})$$

Note that this contribution is $\propto Q^{2+M}$ with the gel fraction. In (D.14) we omitted the normalization factors $I_0^{-n}(\eta)$ appearing in front of (D.12) because they don't contribute in the limit $n \rightarrow 0$.

Are there other M-specific terms of lower or equal order in Q than (D.14)? To answer this question we consider the possibility of spatial-orientational coupling terms. Afterwards we will have a look at contributions to ΔF that stem from higher order terms of the expansion of the log-trace part.

We consider a general coupling term by expanding the spatial part of (D.6) in order R and taking from the orientational part the first M-specific contribution which appears in order η^M . Note that we can restrict our analysis to M being *even* because otherwise the expectation value involves an odd number of angular variables and hence vanishes according to (A.10). If all coupling terms up to order $R = M/2$ vanish it is clear that there is no coupling term of

lower order than the orientational contribution (D.14). The generic coupling terms reads:

$$\begin{aligned}
 & \left(\frac{1}{\xi^2}\right)^R \eta^M \left\langle \prod_{l=1}^R \left(\frac{1}{n+1} \sum_{\alpha^l \neq \beta^l=0}^n \vec{t}_{\tau_l}^{\alpha_l} \vec{t}_{\tau_l'}^{\beta_l} - \frac{n}{n+1} \sum_{\alpha_l=0}^n \vec{t}_{\tau_l}^{\alpha_l} \vec{t}_{\tau_l'}^{\alpha_l} \right) \times \right. \\
 & \qquad \qquad \qquad \left. \times \sum_{\gamma_1, \dots, \gamma_M=1}^n \cos \left(\sum_{l=1}^M \psi^{\gamma_l}(s) \right) \right\rangle \\
 & \propto \left\langle \prod_{l=1}^R \left(\frac{1}{n+1} \sum_{\alpha^l \neq \beta^l=0}^n \cos(\psi_{\tau_l}^{\alpha_l} - \psi_{\tau_l'}^{\beta_l}) \right) \sum_{\gamma_1, \dots, \gamma_M=1}^n \cos \left(\sum_{l=1}^M \psi^{\gamma_l}(s) \right) \right\rangle .
 \end{aligned} \tag{D.15}$$

In the first line, we omit the second spatial term because it gives rise to terms proportional to n^2 which we don't take into account. In the second line, we expressed the scalar product of unity vectors by a cosine of their corresponding angles. Putting all angles $\psi(s)$ into the argument of a single cosine by applying repeatedly the identity $\cos x \cos y = \frac{1}{2}(\cos(x-y) + \cos(x+y))$ it is clear that the expectation value vanishes because of the rule (A.9): the sum of the signs of the spatial part's angular variables is always zero whereas for the orientational part's angular variables it is not.

So far, we only considered the second order term of the log-trace contribution. As for the higher order terms, the X th order contribution comes already with a prefactor $\propto Q^X$. The corresponding orientational contribution $\Delta F_{or,ltX}$ has the following structure:

$$\Delta F_{or,ltX} \propto Q^X \left(\left\langle \prod_{l=1}^X \omega_{M-fold}(\hat{\mathbf{0}}, \check{\psi}(s_l)) \right\rangle - \left\langle \prod_{l=1}^X \omega_{SIAS}(\hat{\mathbf{0}}, \check{\psi}(s_l)) \right\rangle \right) .$$

Following the same reasoning as for the second order purely orientational term, it is clear that the lowest order M-specific contribution in this case is going to be proportional to $\eta^M \times \eta^M \times 1 = \eta^{2M}$ too. Because of the higher order prefactor Q^X , the resulting M-specific contribution is of higher order. As for the coupling terms, an argument similar to that for the second order contribution applies because the structure of the spatial contributions is essentially the same. Therefore, we can conclude that there are no contributions to ΔF that are of equal or lower order than the purely orientational contribution (D.14).

Note that considering (D.14) it is possible to argue that all the negative signs which appear in the final expression for ΔF_{or} are due to the replica limit. Evaluating the expectation value within the log-trace part and carrying out the integration over $\check{\varphi}$ within the gaussian contribution gives rise to positive contributions. Therefore, the only possible source of negative signs

D.3. LOWEST ORDER CONTRIBUTION TO ΔF

are the replica combinatorial factors that appear due to multiple occurrences of contributions when calculating the thermal average and the integral in the gaussian. In particular this result supports the hypothesis that the “wrong” sign which we encountered in the expression for ΔF_{4-fold} , (5.41), might be an artifact of the replica limit similar to the 2-fold case which was analyzed in section 5.4.3,

Appendix E

Hubbard-Stratonovich and mean-field approximation

In this Appendix we present some details on the reformulation of our original microscopic theory as a statistical field theory and on the saddle-point approximation. To this end, we consider only a simplified “one-component model” of our system with the replicated partition function

$$[Z^n] = \left\langle \exp (Na(|Q|^2 + \Re Q^* h)) \right\rangle . \quad (\text{E.1})$$

Here, the physical observable Q denotes

$$Q := \frac{1}{N} \sum_{i=1}^N \int_s e^{i\hat{\mathbf{k}}\mathbf{r}_i(s)} e^{i\tilde{m}\psi_i(s)} \quad (\text{E.2})$$

and h is introduced as an auxiliary. Its real part couples to the real part of Q and its imaginary part couples to the imaginary part of Q . Applying a HS transformation to the real and the imaginary part of Q separately, we obtain

$$[Z^n] = \frac{bN}{\pi} \int d\Re\Omega \, d\Im\Omega \quad (\text{E.3})$$

$$\left\langle \exp \left(-bN \left(|\Omega|^2 - 2\sqrt{\frac{a}{b}} \Re\{\Omega^* Q\} - \sqrt{\frac{a}{b}} \Re\{\Omega^* h\} \right) \right) \right\rangle .$$

The parameter b needs to be positive in order to ensure convergence of the integral, but apart from that it is arbitrary. The benefit of applying a HS transformation is that Q now appears *linearly* inside the exponential function. This allows to transform the original theory of N interacting particles into an

effective theory of a single particle in a fluctuating field:

$$\begin{aligned}
[Z^n] &= \frac{bN}{\pi} \int d\Re\Omega d\Im\Omega e^{-bN(|\Omega|^2 - \sqrt{\frac{a}{b}} \Re\{\Omega^* h\})} \times \\
&\quad \times \prod_{i=1}^N \left\langle \exp \left(2\sqrt{ab} \int_s \Re\{\Omega e^{i\hat{\mathbf{k}}\mathbf{r}_i(s)} e^{i\tilde{m}\check{\psi}_i(s)}\} \right) \right\rangle \\
&= \frac{bN}{\pi} \int d\Re\Omega d\Im\Omega e^{-bN(|\Omega|^2 - \sqrt{\frac{a}{b}} \Re\{\Omega^* h\})} \times \\
&\quad \times \left\langle \exp \left(2\sqrt{ab} \int_s \Re\{\Omega e^{i\hat{\mathbf{k}}\mathbf{r}(s)} e^{i\tilde{m}\check{\psi}(s)}\} \right) \right\rangle^N \\
&=: \frac{bN}{\pi} \int d\Re\Omega d\Im\Omega \exp(-N\mathcal{H}_{eff})
\end{aligned} \tag{E.4}$$

Here, we introduced the **effective Hamiltonian**

$$\mathcal{H}_{eff} = b|\Omega|^2 - \sqrt{ab} \Re\{\Omega^* h\} - \ln \left\langle \exp \left(2\sqrt{ab} \int_s \Re\{\Omega e^{i\hat{\mathbf{k}}\mathbf{r}(s)} e^{i\tilde{m}\check{\psi}(s)}\} \right) \right\rangle. \tag{E.5}$$

By means of h it is possible to derive an important relation between the field Ω and the physical observable Q . The logarithmic derivatives of (E.1) and of the last line of (E.4) with respect to real and imaginary part of the auxiliary field h need to be equal and give thus rise to the relations

$$\langle \Re\Omega \rangle_{\mathcal{H}_{eff}} = \sqrt{\frac{a}{b}} \int_s \left\langle \Re e^{i\hat{\mathbf{k}}\mathbf{r}(s)} e^{i\tilde{m}\check{\psi}(s)} \right\rangle^* \tag{E.6}$$

and

$$\langle \Im\Omega \rangle_{\mathcal{H}_{eff}} = \sqrt{\frac{a}{b}} \int_s \left\langle \Im e^{i\hat{\mathbf{k}}\mathbf{r}(s)} e^{i\tilde{m}\check{\psi}(s)} \right\rangle^*. \tag{E.7}$$

$\langle \cdot \rangle_{\mathcal{H}_{eff}}$ is supposed to denote an expectation value with respect to the effective Hamiltonian and $\langle \cdot \rangle^*$ denotes the corresponding average in the original microscopic formulation. By considering higher derivatives with respect to $\Re h$ and $\Im h$ it is easy to show that corresponding relations hold for all the cumulants of the distributions of Ω and Q .

So far, we have obtained a new formulation of our problem in terms of a statistical field theory. In order to make the problem analytically treatable we apply in the following the saddle-point approximation in lowest order [7]. This step gives rise to a theory on the mean-field level. The idea is to replace the highly complicated integral in the last line of (E.4) by the maximal value of its integrand in order to obtain the dominant contribution to $\ln[Z^n]$. We thus need to find the minimum of \mathcal{H}_{eff} with respect to Ω . A necessary condition

APPENDIX E. HUBBARD-STRATONOVICH AND MEAN-FIELD APPROXIMATION

for an extremum is stationarity, i.e.

$$\frac{\partial \mathcal{H}_{eff}}{\partial \Re \Omega} = \frac{\partial \mathcal{H}_{eff}}{\partial \Im \Omega} = 0 \quad (\text{E.8})$$

which gives rise to the self-consistency equation

$$\sqrt{\frac{b}{a}} \Omega = \frac{\left\langle e^{i\hat{\mathbf{k}}\hat{\mathbf{r}}(s)} e^{i\tilde{m}\check{\psi}(s)} \exp \left((2\sqrt{ab} \Omega \int_s \Re \{ e^{i\hat{\mathbf{k}}\hat{\mathbf{r}}(s)} e^{i\tilde{m}\check{\psi}(s)} \}) \right) \right\rangle}{\left\langle \exp \left(2\sqrt{ab} \Omega \int_s \Re \{ e^{i\hat{\mathbf{k}}\hat{\mathbf{r}}(s)} e^{i\tilde{m}\check{\psi}(s)} \} \right) \right\rangle}}. \quad (\text{E.9})$$

Note that we combined the equations for real and imaginary part for a more compact notation.

In principle, the resulting free energy should not depend on the positive but otherwise arbitrary parameter b that we introduced during the HS transformation. In order to show that this is indeed the case we introduce the new fields

$$\Re \Omega' := \sqrt{\frac{b}{a}} \Re \Omega \quad \text{and} \quad \Im \Omega' := \sqrt{\frac{b}{a}} \Im \Omega \quad , \quad (\text{E.10})$$

and the corresponding replica free energy is given by

$$\mathcal{F}' = a|\Omega|^2 - \ln \left\langle \exp \left(2a \int_s \Re \{ \Omega e^{i\hat{\mathbf{k}}\hat{\mathbf{r}}(s)} e^{i\tilde{m}\check{\psi}(s)} \} \right) \right\rangle. \quad (\text{E.11})$$

The redefined \mathcal{F}' does not depend on b and hence, the same is true for the corresponding saddle-point equations. However, the resulting saddle-point free energy \mathcal{F}_{SP} is unchanged.

The relations (E.6) and (E.7) on mean-field level and in terms of Ω' read consequently

$$\Re \Omega'_{SP} = \sqrt{\frac{a}{b}} \int_s \left\langle \Re \left\{ e^{i\hat{\mathbf{k}}\hat{\mathbf{r}}(s)} e^{i\tilde{m}\check{\psi}(s)} \right\} \right\rangle^* \quad (\text{E.12})$$

and

$$\Im \Omega'_{SP} = \sqrt{\frac{a}{b}} \int_s \left\langle \Im \left\{ e^{i\hat{\mathbf{k}}\hat{\mathbf{r}}(s)} e^{i\tilde{m}\check{\psi}(s)} \right\} \right\rangle^* . \quad (\text{E.13})$$

These new fields are related to disorder averaged expectation values of a physical observable.

Bibliography

- [1] In A. P. Young, editor, *Spin glasses and random fields*. World Scientific, 1998.
- [2] B. Alberts, D. Bray, J. Lewis, M. Raff, K. Roberts, and J. D. Watson. *Molecular Biology of the Cell*. Garland Publishing, New York, 1994.
- [3] K. R. Ayscough. *Curr. Opin. Cell Biol.*, 10:102, 1998.
- [4] S. J. Barsky and M. Plischke. *Phys. Rev. E*, 53:871, 1996.
- [5] J. R. Bartles. Parallel actin bundles and their multiple actin-bundling proteins. *Curr. Opin. Cell Biol.*, 12:72, 2000.
- [6] A. R. Bausch and K. Kroy. *Nature Phys.*, 2:231, 2006. and references therein.
- [7] C. M. Bender and S. A. Orszag. *Advanced Mathematical Methods for Scientists and Engineers, Asymptotic Methods and Perturbation Theory*. Springer, New York, 1999.
- [8] P. Benetatos. *private communication*.
- [9] P. Benetatos and A. Zippelius. *Phys. Rev. Lett.*, 99:198301, 2007.
- [10] K. Binder and A. P. Young. Spin glasses: Experimental facts, theoretical concepts, and open questions. *Rev. Mod. Phys.*, 58:801–976, 1986.
- [11] I. Borukhov, R. F. Bruinsma, W. M. Gelbart, and A. J. Liu. *Proc. Natl. Acad. Sci. USA*, 102:3673, 2005.
- [12] K. Broderix, M. Weigt, and A. Zippelius. Towards finite-dimensional gelation. *The European Physical Journal B*, 29:441–455, 2002.
- [13] R. F. Bruinsma. *Phys. Rev. E*, 63:061705, 2001.
- [14] R. T. Deam and S. F. Edwards. *Proc. Trans. R. Soc. Lon. Ser. A*, 280:317, 1976.

BIBLIOGRAPHY

- [15] Aleksandar Donev, Joshua Burton, Frank H. Stillinger, and Salvatore Torquato. Tetratic order in the phase behavior of a hard-rectangle system. *Phys. Rev. B*, 73:054109, 2006.
- [16] C. G. dos Remedios, D. Chhabra, M. Kekic, I. V. Dedova, M. Tsubakihara, D. A. Berry, and N. J. Nosworthy. Actin binding proteins: Regulation of cytoskeletal microfilaments. *Physiol. Rev.*, 83:433–473, 2003.
- [17] Viktor Dotsenko. *An Introduction to the Theory of Spin Glasses and Neural Networks*. World Scientific, Singapore, 1994.
- [18] O. Pelletier et al. *Phys. Rev. Lett.*, 91:148102, 2003.
- [19] P. Flory. *Principles of Polymer Chemistry*. Cornell University Press, 1981.
- [20] F Gittes, B Mickey, J Nettleton, and J Howard. Flexural rigidity of microtubules and actin filaments measured from thermal fluctuations in shape. *The Journal of Cell Biology*, 120(4):923–934, 1993.
- [21] P. M. Goldbart, H. E. Castillo, and A. Zippelius. *Adv. Phys.*, 45:393, 1996.
- [22] P. M. Goldbart, S. Mukhopadhyay, and A. Zippelius. *Phys. Rev. B*, 70:184201, 2004.
- [23] P. M. Goldbart and A. Zippelius. *Europhys. Lett*, 27:599, 1994.
- [24] C. Goodyear. *The application and uses of vulcanized gum-elastic*. Published for the author, New Haven, 1853.
- [25] N. Gronbech-Jensen, R. Mashl, R. Bruinsma, and W. Gelbart. *Phys. Rev. Lett.*, 78:2447, 1997.
- [26] B. I. Halperin and D. R. Nelson. *Phys. Rev. Lett.*, 41:121, 1978.
- [27] M. Huthmann, M. Rehkopf, A. Zippelius, and P. M. Goldbart. *Phys. Rev. E*, 54:3943, 1996.
- [28] P. A. Janmey. *Proc. Natl. Acad. Sci. USA*, 98:14745, 2001.
- [29] J. Kierfeld, T. Kuehne, and R. Lipowsky. *Phys. Rev. Lett.*, 95:38102, 2005.
- [30] H. Kleinert. *Path Integrals in Quantum Mechanics, Statistics, Polymer Physics, and Financial Markets*. World Scientific, Singapore, 2007.
- [31] O. Kratky and G. Porod. *Rec. Trav. Chim.*, 68:1106, 1949.

- [32] H. Lodish, A. Berk, S. L. Zipursky, P. Matsudaira, D. Baltimore, and J. Darnell. *Molecular Cell Biology*. W. H. Freeman and Company, New York, 1999.
- [33] X. Mao, P. M. Goldbart, X. Xing, and A. Zippelius. *Europhys. Lett.*, 80:26004, 2007.
- [34] Xiaoming Mao, Paul M. Goldbart, Xiangjun Xing, and Annette Zippelius. *Phys. Rev. E*, 80(3):031140, 2009.
- [35] N. D. Mermin and H. Wagner. *Phys. Rev. Lett.*, 17:1133, 1966.
- [36] M. Mézard, G. Parisi, and M. A. Virasoro. *Spin Glass Theory and Beyond*. World Scientific, Singapore, 1987.
- [37] V. Narayan, N. Menon, and S. Ramaswamy. *J. Stat. Mech.*, P01005:1742, 2006.
- [38] D. Nelson and J. Toner. *Phys. Rev. B*, 24:363, 1981.
- [39] D. R. Nelson. *Defects and Geometry in Condensed Matter Physics*. Cambridge University Press, Cambridge, 2002.
- [40] D. R. Nelson and B. I. Halperin. *Phys. Rev. B*, 19:2457, 1979.
- [41] D. R. Nelson, M. Rubenstein, and F. Spaepen. *Phil. Mag. A*, 46:105, 1982.
- [42] H. Nishimori. *Statistical Physics of Spin Glasses and Information Processing*. Oxford Science Publications, New York, 2001.
- [43] L. Onsager. *Ann. N.Y. Acad. Sci.*, 51:627, 1949.
- [44] A. Ott, M. Magnasco, A. Simon, and A. Libchaber. Measurement of the persistence length of polymerized actin using fluorescence microscopy. *Phys. Rev. E*, 48(3):R1642–R1645, 1993.
- [45] M. Plischke and S. J. Barsky. *Phys. Rev. E*, 58:3347, 1998.
- [46] C. Revenu, R. Athman, S. Robine, and D. Louvard. The co-workers of actin filaments: from cell structures to signals. *Nat. Rev. Mol. Cell Biol.*, 5:635, 2000.
- [47] C. Roos, A. Zippelius, and P. M. Goldbart. *Journal of Physics A*, 30:1967, 1997.
- [48] M. Rubinstein and R. H. Colby. *Polymer physics*. Oxford University Press, 2003.

BIBLIOGRAPHY

- [49] E. Sackmann. *Macromol. Chem. Phys.*, 195:7–28, 1994.
- [50] N. Saitô, K. Takahashi, and Y. Yunoki. *J. Phys. Soc. Jpn.*, 22:219, 1967.
- [51] T. M. Svitkina and G. G. Borisy. Arp2/3 complex and actin depolymerizing factor / cofilin in dendritic organization and treadmilling of actin filament array in lamellipodia. *J. Cell Biol.*, 145:1009, 1999.
- [52] J. X. Tang and P. A. Janmey. *J. Biol. Chem.*, 271:8556, 1996.
- [53] M. Tempel, G. Isenberg, and E. Sackmann. *Phys. Rev. E*, 54:1802–1810, 1996.
- [54] O. Theissen, A. Zippelius, and P. M. Goldbart. *Int. J. Mod. Phys. B*, 11:1945, 1996.
- [55] S. Ulrich, X. Mao, P. M. Goldbart, and A. Zippelius. *Europhys. Lett.*, 76:677, 2006.
- [56] S. Ulrich, A. Zippelius, and P. Benetatos. *Phys. Rev. E*, 81:021802, 2010.
- [57] J. A. C. Veerman and D. Frenkel. *Phys. Rev. A*, 42:5632, 1992.
- [58] S. J. Winder and K. R. Ayscough. *J. Cell Sci.*, 118:651, 2005.
- [59] K. W. Wojciechowski and D. Frenkel. Tetratic phase in the planar hard square system? *Comput. Methods Sci. Technol.*, 10:235, 2004.
- [60] X. Xing, S. Pfahl, S. Mukhopadhyay, P. M. Goldbart, and A. Zippelius. *Phys. Rev. E*, 77:051802, 2008.
- [61] K. Zhao, Ch. Harrison, D. Huse, W. B. Russel, and P. M. Chaikin. *Phys. Rev. E*, 46:40401(R), 2007.
- [62] A. G. Zilman and A. S. Safran. *Phys. Rev. E*, 66:51107, 2002.
- [63] A. G. Zilman and A. S. Safran. *Europhys. Lett.*, 63:139, 2003.

Danksagung

An dieser Stelle möchte ich mich bei denen bedanken, die mich bei der Verrichtung dieser Arbeit unterstützt und meine Promotionszeit in Göttingen bereichert haben.

Zuallererst gilt mein Dank Prof. Annette Zippelius. Zum einen möchte ich ihr dafür danken, dass sie mir die Möglichkeit eröffnet hat, an diesem faszinierenden und herausfordernden Thema zu arbeiten, zum anderen für die engagierte Betreuung und die vielen wertvollen Denkanstöße, die ich von ihr in den zahlreichen Diskussionen der letzten Jahre erhalten habe.

Weiterhin bedanke ich mich bei Dr. Panayotis Benetatos, dessen Tür mir immer offen stand. Von seiner Expertise auf dem Gebiet der biologischen Physik und seiner bemerkenswerten physikalischen Intuition habe ich sehr profitiert.

Herrn Prof. Reiner Kree danke ich herzlich dafür, dass er das Korreferat meiner Arbeit übernommen hat.

Dr. Timo Aspelmeier hat mich zu Beginn meiner Promotion bei der Arbeit an meinem ersten, leider nicht tragfähigen, Thema betreut. Für diese Unterstützung möchte ich mich vielmals bedanken, ebenso wie für die vielen nachfolgenden Diskussionen.

Hilfreiche Anregungen bei der Fertigstellung meiner Arbeit kamen von den Lektoren Jonathan Fish, Stephan Ulrich, Stephan Filor und Claus Heußinger, denen ich außerdem für die Korrektur von Rechtschreibfehlern und falschen Formulierungen dankbar bin.

Zuletzt möchte ich mich bei meinen Bürokollegen und allen Mitgliedern des Instituts für Theoretische Physik bedanken, die gemeinsam für eine anregende und freundschaftliche Arbeitsatmosphäre gesorgt haben.

Lebenslauf

Persönliche Daten

Name	Martin Kiemes
Adresse	Reinhäuser Landstr. 91 37083 Göttingen
Geburtsdatum	15. September 1977
Geburtsort	Lebach
Staatsangehörigkeit	deutsch

Ausbildung

Juni 1997	Abitur am Marie-Luise-Kaschnitz-Gymnasium, Völklingen
Juli 1997 - Apr. 1998	Wehrdienst beim Stabsmusikkorps der Bundeswehr, Siegburg
Okt. 1998 - Juli 1999	Studium der Musik mit der Fachrichtung "Künstlerische Instrumentalausbildung, Cello" an der Hochschule für Musik Köln, Abteilung Aachen
Okt. 1999 - Febr. 2006	Studium der Physik an der Ruprecht-Karls-Universität Heidelberg
Sept. 2003 - Aug. 2004	Studium an der Université de Paris 11, Orsay, als Erasmus-Stipendiat
Febr. 2006	Diplom in Physik Diplomarbeit am Institut für Theoretische Physik der Ruprecht-Karls-Universität Heidelberg bei Prof. Dr. Heinz Horner
Juni 2006 - Nov. 2010	Promotion am Institut für Theoretische Physik der Georg-August-Universität Göttingen bei Prof. Dr. Annette Zippelius

Göttingen, den 26. Oktober 2010